Die approbierte gedruckte Originalversion dieser Dissertation ist an der TU Wien Bibliothek verfügbar.
The approved original version of this doctoral thesis is available in print at TU Wien Bibliothek.

Dissertation

Optimisation of a FEEP thruster using simulation and beam diagnostics

---

Optimierung eines FEEP Triebwerks mittels Simulation und Strahldiagnostik

TU Wien
Institute of Applied Physics

By:
Nina Sarah Mühlich
Mat.Nr:
11902118

Supervisor:
Prof. Dr. Friedrich Aumayr, TU Wien
External Reviewers:
Prof. Dr. Hans J. Leiter, JLU Giessen
Prof. Dr. Martin Tajmar, TU Dresden

Vienna, August 2022

Die approbierte gedruckte Originalversion dieser Dissertation ist an der TU Wien Bibliothek verfügbar.
The approved original version of this doctoral thesis is available in print at TU Wien Bibliothek.

This work was supported with 50 % by FOTEC Forschungs- und Technologietransfer GmbH and with 50 % by the Austrian Research Promotion Agency (FFG) within the framework of the project "Optimisation of a FEEP thruster using simulation and beam diagnostics" (contract number: 874844).

Die approbierte gedruckte Originalversion dieser Dissertation ist an der TU Wien Bibliothek verfügbar.
The approved original version of this doctoral thesis is available in print at TU Wien Bibliothek.

Die approbierte gedruckte Originalversion dieser Dissertation ist an der TU Wien Bibliothek verfügbar.
The approved original version of this doctoral thesis is available in print at TU Wien Bibliothek.

Contents

1 Introduction 11
1.1 History of FEEP thruster technology . . . 11
1.2 Motivation . . . 12
1.3 Structure of the work . . . 13

2 IFM Nano Thruster performance studied by experiments and numerical simulations 19
2.1 Introduction . . . 19
2.2 Experimental setup . . . 22
2.2.1 Ion energy distribution . . . 22
2.2.2 Ion current density distribution . . . 23
2.3 Ion trajectory simulation model . . . 25
2.4 Comparison of experimental and simulation results . . . 28
2.4.1 Ion energy distribution . . . 29
2.4.2 Ion current density distribution . . . 31
2.5 Conclusion . . . 37
2.6 Acknowledgments . . . 37

3 Simultaneously measured direct and indirect thrust of a FEEP thruster using novel thrust balance and beam diagnostics 39
3.1 Introduction . . . 39
3.2 Analytical methods . . . 41
3.2.1 Direct thrust measurements . . . 41
3.2.2 Indirect thrust measurement . . . 41
3.3 Direct and indirect thrust measurement setup . . . 43
3.3.1 IFM Nano Thruster description . . . 43
3.3.2 Thrust balance setup . . . 43
3.3.3 Beam diagnostics setup . . . 47
3.4 Results . . . 48
3.4.1 Thrust balance results . . . 48
3.4.2 Beam diagnostics results . . . 50
3.4.3 Comparison of direct and indirect thrust measurement results . . . 52
3.5 Conclusion . . . 56
3.6 Acknowledgments . . . 56

Die approbierte gedruckte Originalversion dieser Dissertation ist an der TU Wien Bibliothek verfügbar.
The approved original version of this doctoral thesis is available in print at TU Wien Bibliothek.
TU Bibliothek Your knowledge hub WIEN

4 Performance improvements of IFM Nano Thruster with highly focused ion beam generated with a compact electrostatic lens module 57
4.1 Introduction . . . 57
4.2 IFM Nano Thruster . . . 59
4.2.1 Functional principle . . . 59
4.2.2 Performance characterisation . . . 60
4.3 Test setup . . . 61
4.3.1 Beam diagnostics . . . 61
4.3.2 Simulation model . . . 62
4.3.3 Focus electrode module . . . 64
4.4 Experimental performance measurements . . . 66
4.4.1 Determination of operation points . . . 66
4.4.2 Beam profile comparison . . . 68
4.4.3 Key beam properties comparison . . . 69
4.4.4 Performance comparison . . . 71
4.5 Conclusion . . . 74
4.6 Acknowledgments . . . 74

5 Conclusion and outlook 75

Die approbierte gedruckte Originalversion dieser Dissertation ist an der TU Wien Bibliothek verfügbar.
The approved original version of this doctoral thesis is available in print at TU Wien Bibliothek.
TU Bibliothek Your knowledge hub WIEN

Abstract

From the early 2000s until 2009 the AIT Austrian Institute of Technology GmbH (formerly Austrian Research Centers GmbH) and since 2010 FOTEC Forschungs- und Technologietransfer GmbH, the research subsidiary of the University of Applied Sciences Wiener Neustadt, have been developing the Field Emission Electric Propulsion (FEEP) technology, that allows to build thrusters working in the μN-thrust range. This makes these thrusters ideal for the precise control of a spacecraft. An example is the Indium FEEP Multiemitter (IFM) Nano Thruster developed by FOTEC and commercialised by ENPULSION, which is a thruster module especially designed for nano satellites (CubeSats). It is important to characterise and optimise the indium ion beam emitted by this thruster. In this way, a higher thrust can be achieved with the same amount of power and utilised propellant. Furthermore, by reducing the beam divergence angle, interactions with the spacecraft can be prevented. Due to such interactions, solar panels or electrical instruments on board the spacecraft could be damaged. So far, there are only a few studies on the structure and behaviour of the thruster beam.
Within the scope of the dissertation project, the beam and thrust properties of several laboratory versions of the IFM Nano Thrusters were characterised using a thrust balance and a self-developed beam diagnostics system. The developed beam diagnostics consists of 23 Digital Faraday Cups (DFC) on a rotatable semi-circular arm to measure the ion current density distribution and a Retarding Potential Analyser (RPA) to determine the kinetic energy distribution of the beam ions. A special feature of the FEEP thrusters is, that the thrust can be determined indirectly using the beam diagnostics. This was proven by simultaneous measurements with a thrust balance. An ion trajectory simulation model was developed and excellent agreement with the experimental results could be demonstrated. Subsequently, the model was used to optimise the beam properties. Thereby, different geometries of the thruster electrodes were simulated iteratively for different operating parameters. The most promising geometry resulted in a thrust optimisation of 30 %, a divergence angle reduction from 60 ° to 20 ° and a thrust vector stability improvement from $< 5\,^\circ$ to $< 0.9\,^\circ$. It is a modular focus system that can be mounted on an IFM Nano Thruster without increasing the complexity of the electronics or the required power. The so-called focus module was manufactured and measured again with the beam diagnostic system. The predictions of the simulation model were in excellent agreement with the experimental results. Therefore, the simulation model can be used in future to predict the performance of various FEEP thruster geometries.

Die approbierte gedruckte Originalversion dieser Dissertation ist an der TU Wien Bibliothek verfügbar.
The approved original version of this doctoral thesis is available in print at TU Wien Bibliothek.
TU Bibliothek Your knowledge hub WIEN

Die approbierte gedruckte Originalversion dieser Dissertation ist an der TU Wien Bibliothek verfügbar.
The approved original version of this doctoral thesis is available in print at TU Wien Bibliothek.

Zusammenfassung

Von Anfang der 2000er Jahre bis 2009 entwickelte die AIT Austrian Institute of Technology GmbH (vormals Austrian Research Centers GmbH) und ab 2010 die FOTEC Forschungs- und Technologietransfer GmbH, das Forschungsunternehmen der Fachhochschule Wiener Neustadt, die FEEP- (Field Emission Electric Propulsion) Technologie, die es ermöglicht Triebwerke zu bauen, die im μN-Schubbereich arbeiten. Damit eignen sich diese Triebwerke ideal für die präzise Steuerung eines Raumfahrzeugs. Ein Beispiel ist das von FOTEC entwickelte und von ENPULSION vertriebene Indium FEEP Multiemitter (IFM) Nano Triebwerk, ein speziell für Nanosatelliten (CubeSats) konzipiertes Triebwerksmodul. Es ist wichtig den vom Triebwerk emittierten Indium-Ionenstrahl zu charakterisieren und zu optimieren. Auf diese Weise kann ein höherer Schub bei gleicher Leistung und gleichem Treibstoff erreicht werden. Ferner können durch eine Reduzierung des Strahldivergenzwinkels Wechselwirkungen mit dem Raumfahrzeug vermieden werden. Aufgrund solcher Wechselwirkungen können Solarpaneele oder elektrische Instrumente an Bord des Raumfahrzugs beschädigt werden. Bisher gibt es nur wenige Untersuchungen zur Struktur und Verhalten des Triebwerkstrahls.
Im Rahmen des Dissertationsprojekts wurden die Strahl- und Schubeigenschaften mehrerer laborversionen der IFM Nano Triebwerke mit einer Schubwaage und einem eigens entwickelten Strahldiagnostiksystem charakterisiert. Zur entwickelten Strahldiagnostik gehören 23 Digitale Faraday Cups (DFC) an einem drehbaren Halbkreisarm zur Vermessung der Ionenstromdichteverteilung und ein Gegenfeldanalysator (RPA), zur Bestimmung der kinetischen Energieverteilung der Strahlionen. Eine Besonderheit der FEEP Triebwerke ist, dass der Schub indirekt über die Strahldiagnostik bestimmt werden kann. Dies wurde durch simultanes Messen mit einer Schubwaage bewiesen. Es wurde ein Ionentrajektorien-Simulationsmodell entwickelt und damit eine hervorragende Übereinstimmung mit den experimentellen Ergebnissen nachgewiesen. Anschließend wurde das Modell zur Optimierung der Strahleigenschaften verwendet. Dabei wurden unterschiedliche Geometrien der Triebwerkselektroden für verschiedene Betriebsparameter iterativ simuliert. Die vielversprechendste Geometrie führte zu einer Schuboptimierung von 30 %, einer Divergenzwinkelreduzierung von 60 ° auf 20 ° und einer Schubvektorstabilitätsverbesserung von $< 5\,^\circ$ auf $< 0.9\,^\circ$. Es handelt sich um ein modulares Fokussystem, welches auf ein IFM Nano Triebwerk aufgesetzt werden kann, ohne die Komplexität der Elektronik oder die benötigte Leistung zu erhöhen. Das sogenannte Fokusmodul wurde gefertigt und erneut mit dem Strahldiagnostiksystem vermessen. Die Vorhersagen des Simulationsmodells stimmten hervorragend mit den experimentellen Ergebnissen überein. Somit kann das Simulationsmodell in Zukunft zur Vorhersage der Performance verschiedener FEEP-Triebwerksgeometrien verwendet werden.

Die approbierte gedruckte Originalversion dieser Dissertation ist an der TU Wien Bibliothek verfügbar.
The approved original version of this doctoral thesis is available in print at TU Wien Bibliothek.
TU Bibliothek Your knowledge hub WIEN

Die approbierte gedruckte Originalversion dieser Dissertation ist an der TU Wien Bibliothek verfügbar.
The approved original version of this doctoral thesis is available in print at TU Wien Bibliothek.

1 Introduction

The Liquid Metal Ion Source (LMIS) technology is used in a wide range of application, such as microscopy, lithography or micro-machining [1]. Such an ion source consists of an emitter needle with tip size in the μm range that is wetted with liquid metal. A voltage difference in the kV-range is applied between the emitter and a nearby extractor electrode. Due to the strong electric fields, a so-called Taylor cone is formed on the needle tip, which creates a balance between the electrostatic field and liquid metal surface tension forces [2]. At the Taylor-cone tip, the strong fields cause field evaporation and field ionisation of the metal atoms. The ions are accelerated and focused with electrostatic lenses.

1.1 History of FEEP thruster technology

Research on LMIS technology began in the 1960s, including the geometry and behaviour of the Taylor cone at different emission currents and emitter voltages [2–13]. Due to the high velocity of the emitted metal ions and the resulting μN thrust, which can be adjusted precisely, the European Space Agency (ESA) started 1972 to investigate the use of LMIS technology as Field Emission Electric Propulsion (FEEP) for attitude and orbit control of spacecraft [14].
The Austrian Research Centers GmbH (today AIT Austrian Institute of Technology GmbH) developed their first LMIS in 1987. They designed capillary single needle type emitters operated with liquid indium and investigated their voltage-current characteristics, as well as mass and energy spectra [15]. First tests of an LMIS in space were carried out in 1991 during the AUSTROMIR-91 mission on the space station MIR [16]. In 1992, the technology was used as active spacecraft potential control (ASPOC) instrument EFD-iE on the Japanese GEOTAIL mission [16, 17]. The ion beam was focused by an electrostatic einzel lens to generate a maximum divergence half-angle of 15 °. Later, ASPOC instruments were also used for the missions Equator-S (1997), Cluster II (2000) [18], Double Star (2003) [19] and MMS (2015) [20]. The next generation of an ASPOC instrument (ASPOC-NG) is currently under development in collaboration between FOTEC and IWF (Insitut für Weltraumforschung) [21].
Following the successful operation of the ASPOC instrument on the GEOTAIL mission, the indium FEEP emitter was introduced 1997 as micro newton propulsion system [22, 23]. Under ESA funding, the micro thruster prototype was developed, characterised and endurance tested to be a candidate for drag-free missions like GOCE (Gravity Field and Steady-State Ocean Circulation Explorer), SMART-2 (LISA Pathfinder) or LISA (Laser Interferometer Space Antenna) [24–26]. An Indium FEEP micro thruster cluster

Die approbierte gedruckte Originalversion dieser Dissertation ist an der TU Wien Bibliothek verfügbar.
The approved original version of this doctoral thesis is available in print at TU Wien Bibliothek.
TU Bibliothek Your knowledge hub WIEN

was developed and qualified in cooperation with Astrium for the LISA Pathfinder mission [27–32]. Due to the required higher emitter current, the beam divergence increased to 60 °, why as usual for LMIS a focus system consisting of electrostatic lenses was developed [33, 34].
In 2008, the emitter technology was upgraded to an 28 needle crown-shaped Indium FEEP multiemitter (IFM) to achieve a thrust up to 1 mN [35–37]. Furthermore, a porous needle was developed instead of solid or capillary form. This allowed the fabrication of a sharp needle tip without losing the advantage of the capillary forces as passively propellant feeding. Also the beam focus system of a single needle emitter, was further developed for the IFM350, to be compliant with the requirements of ESAs Next Generation Gravity Mission (NGGM) where the FEEP technology was planned to be used as lateral and attitude control [38]. However, the IFM350 was not commercialised due to its disadvantageous size and mass. In 2010, all activities and IPRs of AIT Austrian Institute of Technology GmbH related to the FEEP technology were transferred to FOTEC.
In 2016, the IFM Nano Thruster was developed and tested which fits the dimensions of a CubeSat due to its miniaturised electronics based on COTS (Commercial Off-The-Shelf) components [39]. In addition, its modularity allows it to be clustered and thus used in a variety of applications, like main thruster for CubeSats or small satellites. In cooperation between FOTEC and its spin-out ENPULSION GmbH, founded in 2017, the first successful in-orbit demonstration of an IFM Nano Thruster took place in 2018 [40, 41]. To this day, the IFM Nano Thruster is being further developed in order to be able to offer different variations for specific requirements.

1.2 Motivation

In parallel to the IFM Nano Thruster, there are other electric propulsion (EP) technologies that have become successful in micro propulsion application (< 100 mN), which take on an increasingly important role in space propulsion [42]. In recent years many different electric micro propulsion systems have been demonstrated in orbit (IOD), as some examples presented in table 1.1. The technologies presented are all modular and can be adapted to the size of the satellite as required.
FEEP thrusters have many advantages compared to other EP technologies, such as low propellant consumption due to the high specific impulse I_{sp}. The solid form of the indium propellant and its passive supply by capillary forces is of particular advantage, since this eliminates the need for pressurised tanks and feeding systems. In addition, the reservoir can be kept small due to the high density of indium compared to other EP propellants. The miniaturised electronics consisting of COTS components also enables the thruster to be kept small and lightweight. For space applications, it is particularly important to keep the components of a subsystem as simple, light and small as possible. Besides these many advantages, the use of FEEP thrusters for highly complex scientific missions, for example, is limited due to the present beam divergence (IFM Nano: $\alpha_{div} \approx 60\,°$) and thrust vector stability (IFM Nano: $\alpha_{off} < 5\,°$). This could lead to in-

Die approbierte gedruckte Originalversion dieser Dissertation ist an der TU Wien Bibliothek verfügbar.
The approved original version of this doctoral thesis is available in print at TU Wien Bibliothek.

Table 1.1: Recent in orbit demonstrated electric micro propulsion thrusters.

Thruster	IFM Nano	NPT30-I2	REGULUS-50	NanoFEEP
				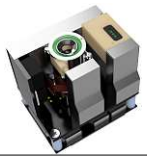
Company	Enpulsion	ThrustMe	T4i	Morpheus S.
Country	Austria	France	Italy	Germany
Type	FEEP	GIT	MEPT	FEEP
IOD	2018	2020	2021	2019
Thrust T [μN]	$1-350$	$300-1100$	$250-650$	$1-20$
I_{sp} [s]	<5000	<2400	<650	<8500
Power [W]	$8-40$	$35-65$	$30-60$	$0.2-3$
Propellent	Indium	Iodine	Iodine	Gallium
Mass [kg]	0.9	1.2	2.5	0.16
Volume [U]	1	1	1.5	1
Divergence α_{div} [°]	≈ 60 [43]	$10-15$	30	<48 [44]
T vector α_{off} [°]	<5 [45]	<1	-	<12[44]
REFs	[40, 46]	[47, 48]	[49, 50]	[51, 52]

teractions with the spacecraft or scientific instruments on board. Another disadvantage resulting from the beam divergence is the reduction of the thrust efficiency. In order to keep up with the competition, the beam properties have to be optimised.
One possibility to optimise these properties would be a focus electrode, as was already tried at the beginning of the FEEP evolution. As described in section 1.1, the focus system of the IFM350 thruster presented in 2013 was too complex to be commercialised. In order to design this focus system smaller, lighter and more efficient, simulation would be particularly suitable. Thereby, time and costs could be reduced and any geometry could be iteratively simulated. For example, COMSOL Mutiphysics could be used, to compute ion trajectories in electric fields including space charge effects. Before such a simulation could be set up, the behaviour and characteristics of a thruster have to be determined experimentally.

1.3 Structure of the work

This thesis is structured in a way, that the following chapters 2−4 correspond one-to-one to three scientific articles published by the PhD candidate as the main author (see details of involvement by the co-authors below) in peer-reviewed scientific journals:

Die approbierte gedruckte Originalversion dieser Dissertation ist an der TU Wien Bibliothek verfügbar.
The approved original version of this doctoral thesis is available in print at TU Wien Bibliothek.

1. Chapter 2: Nina Sarah Mühlich, Bernhard Seifert and Friedrich Aumayr, *IFM Nano Thruster performance studied by experiments and numerical simulations*, published in Journal of Physics D: Applied Physics (54 (2021) 095203), DOI: 10.1088/1361-6463/abc84c [43].

2. Chapter 3: Nina Sarah Mühlich, Joachim Gerger, Bernhard Seifert and Friedrich Aumayr, *Simultaneously measured direct and indirect thrust of a FEEP thruster using novel thrust balance and beam diagnostics*, published in Acta Astronautica (197 (2022) 107–114), DOI: 10.1016/j.actaastro.2022.05.009 [53].

3. Chapter 4: Nina Sarah Mühlich, Joachim Gerger, Bernhard Seifert and Friedrich Aumayr, *Performance improvements of IFM Nano Thruster with highly focused ion beam generated with a compact electrostatic lens module*, under review in Acta Astronautica (submitted on 19th of March 2022) [45].

All three papers are the sole result of the scientific work of the author of this PhD thesis. This author has set up and executed the described simulations, performed all the described experiments, did the data evaluation and drafted all three publications. After receiving comments from her co-authors, the author of this PhD thesis submitted all three manuscripts as first (main) and corresponding author, replied to referee comments and corrected the proofs. The co-authors were only involved in the planning of the work, gave some advice during the work, contributed to the discussion and read and commented on the manuscript before final submission.
The following describes the research plan and the connection between the individual articles. At the beginning of the work, the beam properties of a single emitting needle and the whole emitter crown of an IFM Nano Thruster laboratory model were investigated. Based on the results an ion trajectory simulation model was developed, which is presented in chapter 2 and published in [43]. For characterisation of the beam, the diagnostics system developed in 2018 was used, consisting of 23 Analogue Faraday Cups (AFC) [54] and one Retarding Potential Analyser (RPA) [55]. The RPA was designed and tested standalone as described in [55] and was used to measure the spatial energy distribution of the beam ions. In addition, the measuring device of the AFCs was optimised to enable the current resolution of a single emitting needle. Thereby, 1000 measurements were taken at each position, resulting in a measurement time of 1 hour for one beam profile scan. For both, RPA and AFC, a measurement and data evaluation software had to be prepared. The evaluation software computes the beam properties spatial ion current density distribution, beam divergence half-angle and thrust vector, as well as shift and widening of the ion energy distribution.
Using the diagnostics, the beam profile of a porous single emitting needle was measured two-dimensionally for the first time. The behaviour of the beam was analysed for different thruster settings, such as emitter current and electrode voltages. Special and novel findings have emerged about the behaviour of the beam and its density distribution. A circular beam structure with sharp edges was identified which differs from the previously known Gaussian distribution of a capillary emitter [56].

Die approbierte gedruckte Originalversion dieser Dissertation ist an der TU Wien Bibliothek verfügbar.
The approved original version of this doctoral thesis is available in print at TU Wien Bibliothek.
TU Bibliothek Your knowledge hub WIEN

The results of the experimental investigations and their findings were included in the development of an ion trajectory simulation model. The model was developed standalone and from scratch by the PhD candidate using COMSOL Multiphysics, where the ion trajectories are computed with the "Electric particle field interaction Multiphysics coupling" of the COMSOL particle tracing module as published in [57]. In order to match experiment and simulation precisely, the entire setup was implemented in the model, including boundaries of the vacuum facility, hemispherical diagnostics and the main geometrical parts of the IFM Nano Thruster. This includes, most prominently, the Taylor cone and its geometric behaviour depending on thruster parameters. The Taylor cone behaviour could be determined via an empirical equation, which could be determined on the basis of the experimental results. In addition, the density distribution with which the ions are initialised in the model was analysed and implemented on the basis of the experiment. Another special feature of the model is that is also provides parameters which are technically difficult to determine in an experiment, such as the space charge distribution generated by the ion trajectories. In this way, unexplained phenomena that occurred in the experiment could be explained with the model. In course of time, a total of three single emitting needles were experimentally characterised in detail and their results were integrated into the simulation model [45]. This enabled an upgrade to simulate an emitter current up to 300 μA per needle and with this the beam of an entire IFM Nano Thruster with 28 emitting needles. Thus, the distribution of the beam and its characteristics, including ion current density, beam divergence and thrust vector of an IFM Nano Thruster could be simulated for all measured operating points.
In the second part of the work a high degree of agreement between direct thrust balance measurements and indirect thrust measurements with an upgraded beam diagnostics was demonstrated, as presented in chapter 3 and published in [53]. The diagnostic system has been upgraded from analogue (AFC) to digital (DFC) Faraday cups, where the electronics is integrated in the head of each sensor [58]. Thus, an ion current density accuracy of 0.005 nA/cm^2 compared to 1 nA/cm^2 could be achieved and the measurement time of a beam scan could be drastically reduced. The idea for the Faraday cup optimisation and its design were developed in cooperation with input from TU Wien. A dedicated experiment using both systems, the available thrust balance and the new beam diagnostic system, was set up and an IFM Nano Thruster laboratory model was measured with both systems simultaneously. It was shown that the measured ion current density distribution of the DFCs could be converted into an indirect thrust. Direct and indirect thrust measurements for all thruster operation points could be measured to be consistent within 5 %. These results have shown that the thrust of a FEEP Thruster can be precisely determined by measuring its beam profile. Due to the excellent agreement with the simulation model, the model can be utilised to simulate the performance of an IFM Nano Thruster for any operation point.
In the third part of the work, the simulation model was used to develop a thruster geometry with improved beam divergence and thrust efficiency, which is presented in chapter 4 and published in [45]. The simulation model can be used to calculate the beam characteristics of any geometry without the need to manufacture and measure it

Die approbierte gedruckte Originalversion dieser Dissertation ist an der TU Wien Bibliothek verfügbar.
The approved original version of this doctoral thesis is available in print at TU Wien Bibliothek.
TU Bibliothek Your knowledge hub WIEN

Table 1.2: Performance of IFM Nano Thruster without and with attached focus module.

Thruster	T	I_{sp}	Power	Mass	Size	α_{div}	α_{off}
IFM Nano	$1-350\,\mu$N	5000 s	$8-40$ W	0.9 kg	1 U	$\approx 60\,^\circ$	$< 5\,^\circ$
Focus	$1-450\,\mu$N	6500 s	$8-40$ W	1.2 kg	1.5 U	$\approx 20\,^\circ$	$< 0.9\,^\circ$

experimentally. As a first step, requirements were defined for the optimised geometry. The design was supposed to be modular (100×100 mm) electrostatic lens system using the existing voltages of the emitter and extractor electrodes, so that the power consumption and the complexity of the electronics would not be increased.
In the simulation model, geometric and electrostatic parameters were varied iteratively in order to reduce the beam divergence angle. A trade-off was considered between the value of the optimisation and the size and weight of the focus module. A promising geometry was iterated between CAD model and simulation model in collaboration with the construction department of FOTEC to enable structural realisation. Particular consideration was given to durability and the position of the electrode connections. Subsequently, the final focus module was characterised in detail in the simulation model and predicted a beam divergence reduction of 40 ° and a thrust and specific impulse optimisation of 30 % [59]. A focusing electrode with the such optimised geometry was manufactured using available 3D printers. Experimental beam diagnostic measurements were performed on an IFM Nano Thruster laboratory model without and with attached focus module at same operation points. As predicted by the simulation model, the experiment demonstrated that the beam divergence was reduced from 60 ° to 20 ° and the thrust and specific impulse optimised by 30 % [60]. Furthermore, the thrust vector variation was reduced from $< 5\,^\circ$ to 0.9 °, whereby the mass and the size has increased only slightly. When comparing the results with Table 1.1 the performance improvements presented in Table 1.2 could be achieved by attaching the focus module on an IFM Nano Thruster. These results have shown that the simulation model can accurately predict the performance and beam characteristics of arbitrary FEEP thruster geometries.
The following papers and conference proceedings were also produced during the course of this PhD thesis in addition to the publications [43], [53] and [45]:

- Nina Sarah Mühlich, Emre Ceribas, Joachim Gerger, Bernhard Seifert and Friedrich Aumayr: *High-precision digital Faraday cups for FEEP Thrusters*, under review in Journal of Instrumentation (submitted on 27$^{\text{th}}$ April 2022) [58].

- Nina Sarah Mühlich, Joachim Gerger, Bernhard Seifert, David Krejci and Friedrich Aumayr: *Highly focused ion beam of a FEEP thruster generated with a compact electrostatic lens system*, IEPC-2022-189, presented at the 37$^{\text{th}}$ International Electric Propulsion Conference (IEPC), Boston, 06/2022 [60].

- Nina Sarah Mühlich, Joachim Gerger, Bernhard Seifert and Friedrich Aumayr: *Performance prediction of new FEEP thruster design verified with direct and in-*

Die approbierte gedruckte Originalversion dieser Dissertation ist an der TU Wien Bibliothek verfügbar.
The approved original version of this doctoral thesis is available in print at TU Wien Bibliothek.
TU Bibliothek Your knowledge hub WIEN

direct thrust measurements, SP2022-054, presented at the 8th Space Propulsion Conference, Estoril, 05/2022 [59].

- Nina Sarah Mühlich, Bernhard Seifert and Friedrich Aumayr: *Verification of simulation model based on beam diagnostics measurements of the IFM Nano Thruster*, IAC-21-C4.6.14, presented at the 72nd International Astronautical Concress, Dubai, 10/2021 [57].

- Nina Sarah Mühlich, Sebastian Keerl, Werner Engel, Emre Ceribas, Robert-Jan Koopmans: *Retarding Potential Analyser Development for Low Density FEEP Thruster Beam Diagnostics*, IEPC-2019-445, presented at the 36th International Electric Propulsion Conference, Vienna, 09/2019 [55].

Die approbierte gedruckte Originalversion dieser Dissertation ist an der TU Wien Bibliothek verfügbar.
The approved original version of this doctoral thesis is available in print at TU Wien Bibliothek.
TU Bibliothek Your knowledge hub WIEN

Die approbierte gedruckte Originalversion dieser Dissertation ist an der TU Wien Bibliothek verfügbar.
The approved original version of this doctoral thesis is available in print at TU Wien Bibliothek.

2 IFM Nano Thruster performance studied by experiments and numerical simulations

This chapter corresponds to the eponymous peer-review article published in Journal of Physics D: Applied Physics (54 (2021) 095203), DOI: 10.1088/1361-6463/abc84c.

Field emission electric propulsion (FEEP) thrusters are characterised by their low thrust range, which makes them ideal for a precise control of a spacecraft. Decisive for a precise control are the properties of the thruster ion beam, which includes the beam divergence angle and the thrust vector. The analysis of these properties is also necessary in order to be able to estimate the interactions of the beam with components of the spacecraft. Due to such interactions, solar panels or electrical instruments on board the spacecraft could be damaged by sputtering effects.
The spatial ion current density and energy distribution of a test crown emitter beam, with different specifications compared to the IFM Nano thruster, were examined experimentally with a diagnostics system, including Faraday cups (FC) and an retarding potential analyser (RPA). In addition to the analysis of the beam profile of an emitting crown, a single emitting needle was analysed. Based on these experimental analyses, an ion trajectory simulation model was developed to determine the theoretical ion current density distribution. This model includes the properties of a liquid metal ion source (LMIS), where the ion trajectories start from their point of origin, the so-called Taylor cone jet cap. The benchmark of the model shows that the thrust vector and divergence angle correspond to the experimental results and shows the identical calculations for different thruster parameters, like emission current and electrode voltages. The simulation allows optimisation of existing and novel thruster geometries in terms of performance, reliability and longevity.

2.1 Introduction

The Liquid metal ion source (LMIS) technology takes advantage of a Taylor cone, which is formed at a sharp needle tip, due to strong electric fields and liquid metal surface tension. The LMIS finds application for example in material preparation, microscopy or in ion beam lithography, furthermore, in space applications, like spacecraft potential control or propulsion systems [61]. The IFM (Indium FEEP Multiemitter) Nano Thruster, developed at FOTEC and commercialised by ENPULSION, is based on this ion thruster technology, where liquid indium is used as propellant [62]. The thruster

Die approbierte gedruckte Originalversion dieser Dissertation ist an der TU Wien Bibliothek verfügbar.
The approved original version of this doctoral thesis is available in print at TU Wien Bibliothek.

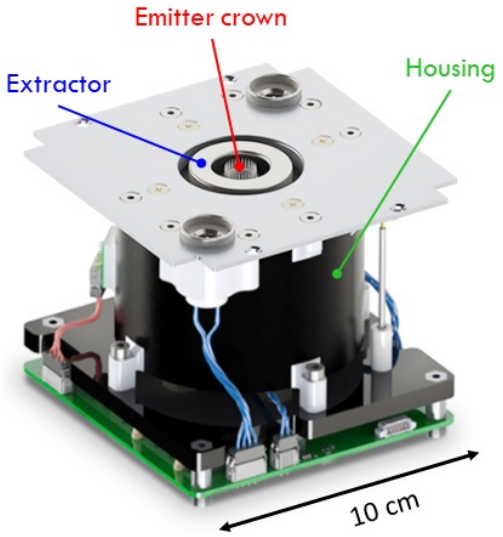

Figure 2.1: IFM Nano Thruster with its main components emitter crown, extractor and housing.

emitter consists of a porous tungsten crown composed of 28 needles, wetted with liquid indium. Additional main components are the ring extractor and the housing structure as represented in Figure 2.1.
Research on the LMIS technology started in the early 1960s, where Taylor [2] analysed the shape of a liquid cone. He calculated that the cone has a half angle of 49.3 ° at the static equilibrium between the electric field forces and the liquid metal surface tension. Based on the schematic drawing in Figure 2.2, the cone structure is explained. The Taylor cone half angle θ_{T} is material independent [2] and also independent of the tip radius r_{tip} [3]. Gomer developed one of the first theories on liquid metal ion sources [4]. He has shown that the space charge at the Taylor cone apex has a great influence on the cone shape even at low ion emission currents. Kingham and Swanson developed a theory to describe the Taylor cone shape including liquid flow and space charge effects [5], which was improved by Ljepojevic in 1992 [6]. In 1994 Praprotnik [7] did experimental measurements and Kingham and Ljepojevic did theoretical calculations on the Taylor cone half angle and the jet length in dependence of the emission current. Praprotnik observed the dynamic behaviour of an LMIS for the first time in-situ, at a tungsten tip coated with liquid indium in a high-voltage electron microscope during emission. He found out that there is a linear dependency of the Taylor cone half angle θ_{T} on the ion emission current I_{em} due to the change of the field strength

$$\begin{aligned} \theta_{\mathrm{T}} &= \theta_{\mathrm{T}_0} - \frac{d\theta}{dI_{\mathrm{em}}} \cdot I_{\mathrm{em}}, \\ \text{with } \theta_{\mathrm{T}_0} = 51.1\,^\circ \text{ and } \frac{d\theta}{dI_{\mathrm{em}}} &= 0.298\,\frac{^\circ}{\mu\mathrm{A}}. \end{aligned} \tag{2.1.1}$$

Die approbierte gedruckte Originalversion dieser Dissertation ist an der TU Wien Bibliothek verfügbar.
The approved original version of this doctoral thesis is available in print at TU Wien Bibliothek.

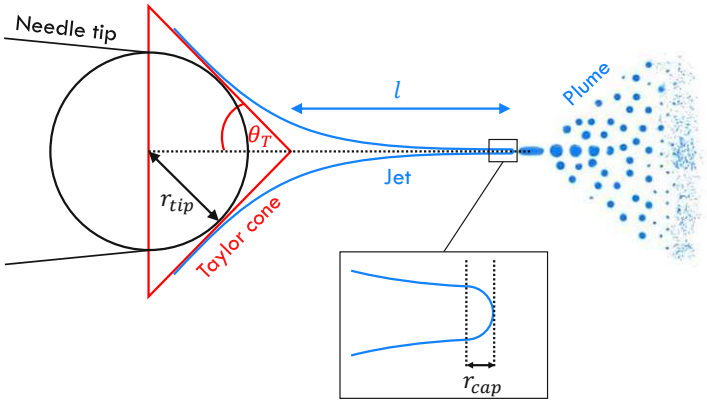

Figure 2.2: Schematic drawing of a Taylor cone formed on a needle tip including radius of jet cap.

For emission currents $I_{\mathrm{em}} > 10\,\mu\mathrm{A}$ an extension of the Taylor cone jet occurs. The jet length increases under the influence of the electrostatic field to provide an equilibrium between the electric field forces and the liquid metal surface tension [8], [9]. Mair and Forbes [10] analysed a linear dependence of the jet length to the emission current

$$l \approx \frac{2}{3\pi\gamma}\sqrt{\frac{m}{2e}\cdot V_{\mathrm{em}}}\cdot I_{\mathrm{em}}, \tag{2.1.2}$$

where γ is the surface tension, e/m the charge to mass ratio of the ions and V_{em} the emitter voltage. Mair also described that the increasing jet length with increasing emission current is part of the reason for microdroplet emission [8]. Another consequence of increasing emission current, is the increasing probability that multi Taylor cones are formed at one needle tip [7].

In 1989 Hornsey did analysis of the energy distribution of a gallium LMIS [11]. He observed that an increasing emission current leads to an energy broadening. One reason for the broadening effect is because of the longitudinal Taylor cone jet oscillation in the GHz range. These oscillation amplitudes are small ($\approx$10 % of the jet length) and do not influence the emitted current. The energy spectrum results from ions emitted at different phases of the Taylor cone jet oscillation. Hornsey also described the energy distribution as almost Gaussian and he assumed that the Taylor cone shape has a direct influence on the energy spread of the emitted ions. In addition, the energy broadening occurs because of Coulomb interactions of the ions in the beam, which is known as Boersch effect [12]. Mair [13] measured an increase of the energy broadening ($5 - 35\,\mathrm{eV}$) and a decrease of the energy shift ($\sim 5\,\mathrm{eV}$) with increasing emission current ($1 - 50\,\mu\mathrm{A}$).
Beam diagnostics measurements of a capillary single needle indium FEEP thruster, the predecessor of the IFM Nano Thruster, were done in the early 2000s. These measurements were carried out with wire probes and a Langmuir probe [26], [63]. Tajmar et. al. observed that the shape of the beam is similar to a cosine distribution at lower thrust

Die approbierte gedruckte Originalversion dieser Dissertation ist an der TU Wien Bibliothek verfügbar.
The approved original version of this doctoral thesis is available in print at TU Wien Bibliothek.

values and closer to a Gaussian distribution at higher thrust values. Based on these measurements Vasiljevich did numerical simulations of ion trajectories and calculated the beam divergence. Here the ions started at 50 μm distance from the needle tip [64]. The analysis of the thruster beam shape and behaviour is of considerable interest in order to increase the thrust efficiency and avoid interactions with spacecraft components. In this paper, a detailed analysis of a test crown emitter ion beam with simulation and experimental methods will be presented. Thereby, the properties of an entire emitting crown and a single emitting needle will be analysed. The beam properties of experimental and simulation results will be compared. On the one hand, the shape of the ion current density profile including divergence angle will be analysed and on the other hand the ion energy distribution including energy shifting and broadening.

2.2 Experimental setup

The thruster used for this analysis is a research model from FOTEC. The structure and emitter of this model is similar to the IFM Nano Thruster, but differs with regards to the emitter specifications such as needle shape. For analysing the test crown emitter beam, a beam diagnostics system was developed at FOTEC in 2018 [55], [54]. The diagnostics system is located in FOTEC's largest vacuum facility LIFET4, which has a length of 3 m and a diameter of 2.2 m. The diagnostics consists of a remotely controlled semi-circle rotating arm equipped with 23 Faraday cups (FC) and an RPA as shown in Figure 2.3 (left). The cups are arranged at different intervals, 4 °, 8 ° and 10 ° in peripheral direction. At the centre of the arm a horizontal curved extension is located, equipped with an retarding potential analyser (RPA) at the $\phi = -10\,^\circ$ position. The diagnostics arm can be rotated stepwise from $-80\,^\circ$ to $+80\,^\circ$ in a distance of 95 cm around the thruster emitter centre point. All measurements were performed at a vacuum facility pressure of $2 \cdot 10^{-7}$ mbar.

2.2.1 Ion energy distribution

The RPA was used to analyse the ion energy distribution of the test crown emitter beam. It consists of four grid electrodes and a collector. The first grid is grounded and sets up a potential gradient against subsequent grids. Due to the negative potential (−30 V) of the second grid electrons cannot enter from outside and influence the collector signal. At the retarding electrode a positive voltage V_{ret} is swept from 0 V up to 10 kV to discriminate between ions of different energies. Only ions with an energy higher than eV_{ret} can pass through the retarding electrode and reach the collector. The suppressor is a second negative electrode (−35 V) to prevent secondary electrons, which are generated by ion bombardment from reaching the collector. This electrode provides a higher resolution of the detected ion current. The last part of the RPA stack is the ion collector, which measures current with respect to the retarding electrode voltage. A more detailed description can be found in [55]. Figure 2.4 represents an RPA measurement at the thruster emission current of 37 μA and emitter voltage of 6 kV with 1 of 28 needles firing at RPA

Die approbierte gedruckte Originalversion dieser Dissertation ist an der TU Wien Bibliothek verfügbar.
The approved original version of this doctoral thesis is available in print at TU Wien Bibliothek.
TU Bibliothek Your knowledge hub WIEN

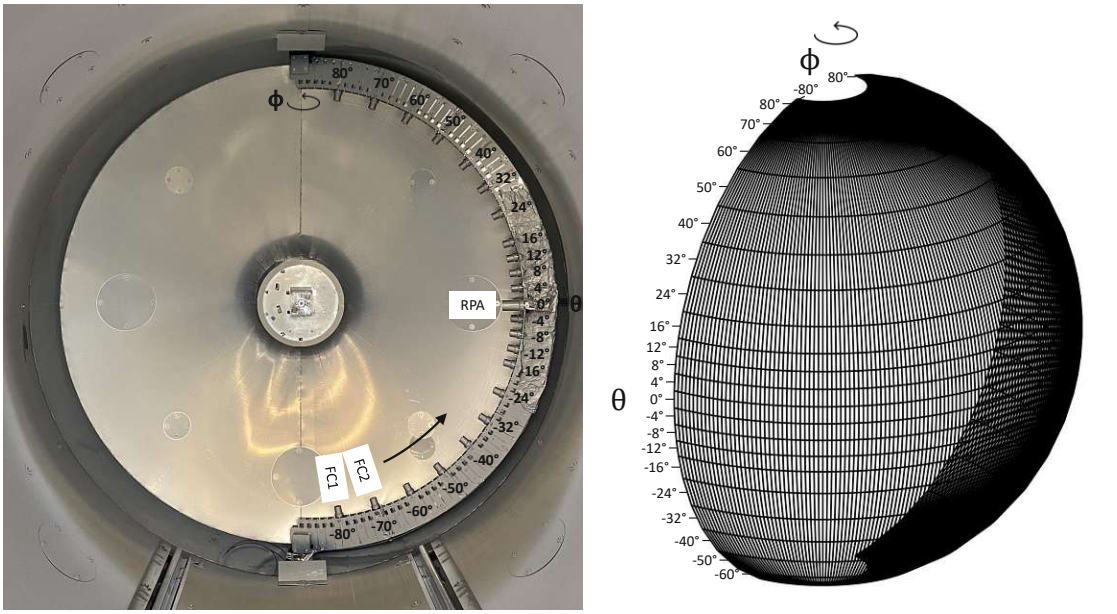

Figure 2.3: Movable beam diagnostics arm equipped with 23 Faraday cups (FC) and an Retarding potential analyser (RPA) in vacuum facility LIFET4 with test crown emitter in the semi-circle center (left). Experimental mesh resulting from the position of the Faraday cups and the 1° step size of the diagnostics arm (right).

position $\phi = 0\,°$. The measured ion current distribution during the voltage sweep at the retarding electrode is indicated in blue. The energy distribution $f(eV_{\mathrm{ret}})$ represented in red, results from the derivation of the ion current distribution [65]:

$$f\left(eV_{\mathrm{ret}}\right) \propto -\frac{dI_{\mathrm{c}}}{dV_{\mathrm{ret}}}, \tag{2.2.1}$$

where e is the elementary charge, I_{c} is the total ion current at the collector and V_{ret} is the bias voltage of the retarding electrode.
To be able to compute the derivative of the ion current density in Figure 2.4, the Savitzky-Golay filter was applied with a window size of 20 and a polynomial order of 2. The ion energy distribution is characterised with a Gaussian fit, as Hornsey [11] described. This enables the energy shift and the width of the distribution to be analysed. In Figure 2.4 it can be seen, that the energy is distributed around 6 kV, matching the applied thruster emitter voltage with a shift of +82 eV. This energy shift is expected and will be explained in section 2.4.1.

2.2.2 Ion current density distribution

The Faraday cups were used to map the ion current density distribution of the test crown emitter beam. During the ion current density measurements, the arm was moved from

Die approbierte gedruckte Originalversion dieser Dissertation ist an der TU Wien Bibliothek verfügbar.
The approved original version of this doctoral thesis is available in print at TU Wien Bibliothek.

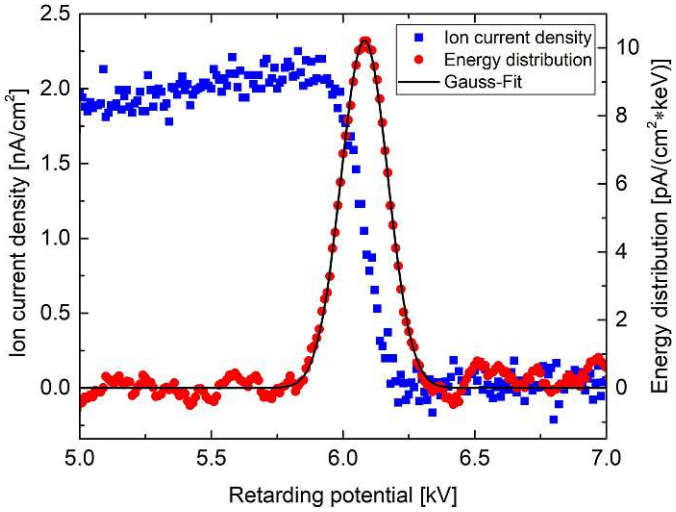

Figure 2.4: Retarding potential analyser measurement at thruster emission current 37 μA and emitter voltage 6 kV with 1 of 28 needles firing at RPA position $\phi = 0°$C.

$-80\,°$ to $+80\,°$ in steps of $1\,°$. From this step size and the arrangement of the Faraday cups, the mesh results in Figure 2.3 (right). Thereby, r is the constant distance of 95 cm of the Faraday cups, ϕ is the diagnostics arm position and θ is the Faraday cup position. Each cell is filled with the density measured in its centre.
The Faraday cup repeller electrode was biased negatively (-15 V) to prevent thermionic electrons or slow charge exchange ions from entering the cup and to recapture secondary electrons that are released by ion bombardment. With a frequency of 1.5 kHz the Faraday cup collector current was measured successively[1]. In order to reduce the noise of the measurement signal it was measured 1000 times for a single needle emitter and 10 times for the emitting crown. This results in a measurement time of the complete scan of 1 h for the single needle and 15 min for the crown emitter. During this period, the profile remained stable and no thermal drift was noticeable, which was verified by multiple measurements.
The data was collected on the virtual hemisphere, which is visualised in Figure 2.5 as a projection onto a 2D plane. The Figure shows an example of the ion current density distribution at a thruster emission current of 37 μA and an emitter voltage of 6 kV with 1 of 28 needles firing. The density profile shows a plateau with sharp edges. Within the region bounded by the dashed circle, 95 % of the total ion current is measured, which corresponds to the beam divergence angle. This is an common definition of the beam divergence angle to compare electric propulsion thrusters [66]. The cross in the centre of the circle indicates the thrust vector.

[1] A/D converter not able to measure all channels simultaneously

Die approbierte gedruckte Originalversion dieser Dissertation ist an der TU Wien Bibliothek verfügbar.
The approved original version of this doctoral thesis is available in print at TU Wien Bibliothek.

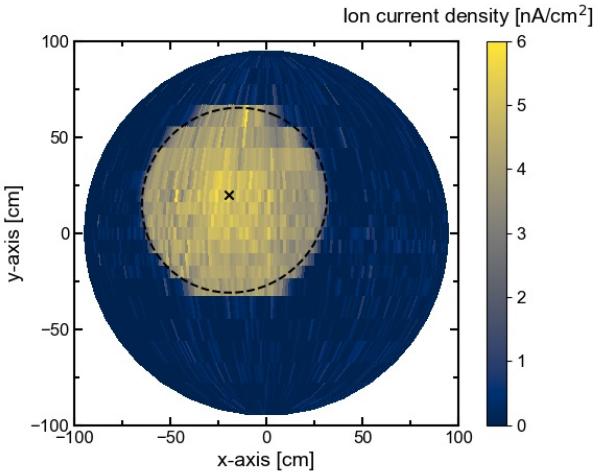

Figure 2.5: Ion current density measurement of 23 Faraday cups at thruster emission current 37 μA and emitter voltage 6 kV with 1 of 28 needles firing.

2.3 Ion trajectory simulation model

For calculating the ion beam trajectories, a simulation model was set up with COMSOL Multiphysics. The system consisting of the test crown emitter geometry and detector sphere is located inside a vacuum cylinder as shown in Figure 2.6. The ion trajectory colour represents the particles kinetic energy, where an emitter voltage of 2 kV and an extractor voltage of −8.8 kV is applied. The particles are accelerated up to 7 kV and subsequently decelerated back to their initial potential of 2 kV. A half sphere with 95 cm radius having the emitter needles in the centre, represents the detector, where the properties of the simulated ions are recorded.
The simulation model setup was carried out based on low emission currents, to reduce the complexity of the dynamics occurring at the tip of an LMIS. For lower emission currents ($< 10\,\mu$A) the following can be assumed:

- No Taylor cone jet extension exists [7].
- No microdroplet emission occurs [67], [68].
- No current fluctuations and no multiple Taylor cones on the needle tip appear [69].

An ion trajectory analysis was carried out, which includes an iteration procedure between calculating the electric field and the resulting space charge due to the ion trajectories. The main part of the simulation model is the inlet of the ions, which represents the radius of the Taylor cone jet cap r_{jet}, as indicated in orange in Figure 2.7. Kingham and Swanson described the shape of the Taylor cone jet cap as a hemispherical cap [5], which is why the jet cap in the simulation model has a curvature radius of r_{cap} The physical diameter of the jet is around 5 nm, but the effective ion optical diameter is

Die approbierte gedruckte Originalversion dieser Dissertation ist an der TU Wien Bibliothek verfügbar.
The approved original version of this doctoral thesis is available in print at TU Wien Bibliothek.

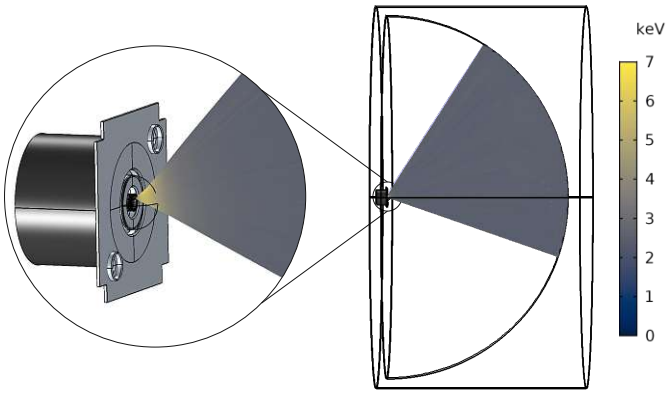

Figure 2.6: Ion trajectory simulation model located in a vacuum cylinder, including the thruster geometry and a detector sphere to analyse beam properties.

around 50 nm because of Coulomb interactions between the emitted ions [1]. Typically, the test crown emitter needle tips have a radius r_{tip} between 1 μm to 10 μm [70]. The tip of the needle, which was used for the measurements presented in this paper was scanned with an electron microscope (Figure 2.7) and an radius of 2 μm was estimated. This shape was taken over to the simulation geometry of the needle and is indicated in red. As described in the introduction, the Taylor cone half angle is independent of the needle tip radius, which means that the beam divergence angle is not affected. According to [7], the Taylor cone half angle, as well es the Taylor cone jet length are linear depending on the emission current (equations 2.1.1 and 2.1.2). This dependency was simplified by only changing the Taylor cone half angle linearly, which is why the following pre-factors in equation 2.3.1 differ from equation 2.1.1. With this, the following function emerged by a calibration for the simulation model:

$$\begin{aligned} \theta_{\text{T}} &= \theta_{\text{T}_0} - \frac{d\theta}{dI_{\text{em}}} \cdot I_{\text{em}}, \\ \text{with } \theta_{\text{T}_0} = 28.7992\,^\circ \text{ and } \frac{d\theta}{dI_{\text{em}}} &= 0.4216\,\frac{^\circ}{\mu\text{A}}. \end{aligned} \tag{2.3.1}$$

The calibration of this equation was based on two experimental measuring points, point 1: $I_{\text{em}} = 9\,\mu$A, $V_{\text{em}} = 2\,$kV and point 2: $I_{\text{em}} = 37\,\mu$A, $V_{\text{em}} = 2\,$kV, which will be explained in section 2.4.2.1. All simulation results are based on this equation 2.3.1.
For calculating the ion trajectories, the COMSOL particle tracing module was used. Here a Lagrangian description of a problem by solving ordinary differential equations using Newton's law of motion is applied [71]. Thereby, Newton's law of motion is solved with the indium ions particle mass m_{ion} and forces acting on the particles $\vec{F}$. The forces are composed on the one hand of the external electric field $\vec{F} = q\vec{E}$ which is computed with the finite element method. On the other hand, it is composed of the space charge density by solving the Poisson equation.
This calculation is carried out by the particle-field interaction, which is a mesh depended

Die approbierte gedruckte Originalversion dieser Dissertation ist an der TU Wien Bibliothek verfügbar.
The approved original version of this doctoral thesis is available in print at TU Wien Bibliothek.
TU Bibliothek Your knowledge hub WIEN

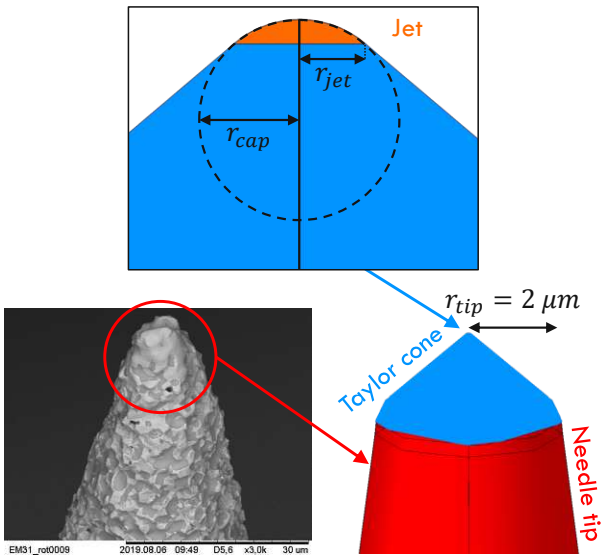

Figure 2.7: SEM picture of the utilised porous tungsten needle which was used in this work, compared to the modelled needle with Taylor cone and jet.

iteration process. The emitter current is given, which results in particles (super-particles) which represents a number of charged particles per unit time. The space charge density $\rho(\vec{r})$ is assigned to the mesh elements the super-particle passed. This means, there are no direct interactions between the ions, but the ion trajectories are influenced by the electric field of particles of previous iterations. A quadratic Lagrangian shape function is used to define the variation of the electric field in each element. The calculation alternates between electric field and particle trajectories with a certain number of iterations, including the previous solutions.
The indium ions are initialised with a density distribution accordingly to the spherical surface at the Taylor cone jet:

$$\rho = -\frac{1}{(1.3 \cdot r_{\text{jet}})^2} \cdot \left(x^2 + y^2\right) + 1, \tag{2.3.2}$$

where $r_{\text{jet}} = r_{\text{cap}} \cdot \cos(\theta_T)$ is the radius of the inlet surface. A pre-factor of 1.3 was chosen to prevent that zero particles start at the edge of the jet surface. The number of 1 was added to shift the parabolic distribution with the result that maximum density is reached in the centre of the surface. To match experiment and simulation, equation 2.3.2 was used for all simulation results. The ions start with zero kinetic energy and potential energy corresponding to the emitter voltage V_{em}. For this reason, a high space charge density is formed in the area of the inlet. Therefore, the mesh elements in the area of the jet, have a supporting role. At the inlet surface a mesh consisting of triangles with side length of $0.5 - 10$ nm is used as represented in Figure 2.8. Around the inlet a sphere composite of tetrahedrons is located (tip mesh). The next larger mesh (beam mesh) has the shape of a cone, because the ions spread in this area. Compared to previous

Die approbierte gedruckte Originalversion dieser Dissertation ist an der TU Wien Bibliothek verfügbar.
The approved original version of this doctoral thesis is available in print at TU Wien Bibliothek.
TU Bibliothek Your knowledge hub WIEN

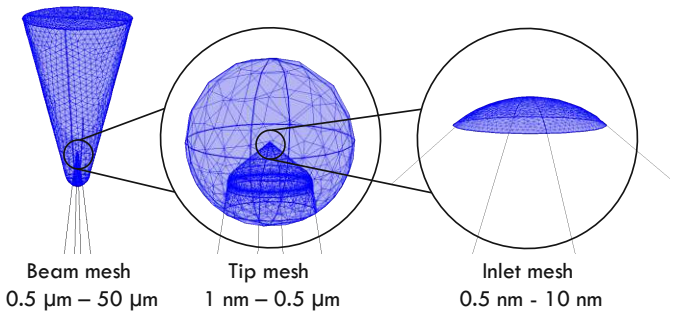

Figure 2.8: Mesh structure of needles and Taylor cone, consisting of beam mesh, tip mesh and inlet mesh.

Table 2.1: Experimental and numerical parameters of the simulation model.

	Parameter	**Size**
Experimental	Emitter current I_{em}	$9 - 37\,\mu$A per needle
	Emitter voltage V_{em}	$2 - 7\,$kV
	Extractor voltage V_{ex}	$-(1.5 - 8.9)\,$kV
Geometrical	TC half angle θ_{T}	$28.7992\,^\circ - 0.4216\,\frac{^\circ}{\mu\mathrm{A}} \cdot I_{\mathrm{em}}$
	TC jet cap curv. rad. r_{cap}	$50\,$nm
	Needle tip radius r_{tip}	$2\,\mu$m
Numerical	Mesh size	$0.5\,\mathrm{nm} - 20\,\mathrm{mm}$
	Timestep tolerance	$3 \cdot 10^{-8}\,\mu$s
	Number of particles	10^5
	Number of iterations	3

simulation models (e.g. [64]), the space charge density at the point of origin is included.

Table 2.1 shows the experimental, geometric and numerical parameters used in the simulation model. The listed numerical parameters were converged when setting up the simulation model in order to get the best possible accordance with the experiment. Timesteps are defined with a given tolerance by the time depended solver. With this, the solver can adjust the size of the steps according to the change in the field strength.

2.4 Comparison of experimental and simulation results

The beam properties of the test crown emitter were measured in a distance of 95 cm, both by experimental measurements and simulations. Thereby, the energy and the ion current density distribution were analysed.

Die approbierte gedruckte Originalversion dieser Dissertation ist an der TU Wien Bibliothek verfügbar.
The approved original version of this doctoral thesis is available in print at TU Wien Bibliothek.

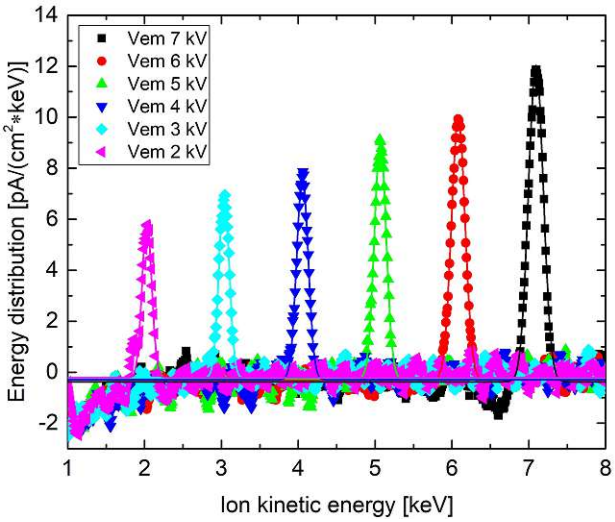

Figure 2.9: Experimental ion energy distribution for a single needle firing fitted with a Gaussian distribution for an emitter current of I_{em} 37 μA and different emitter voltages V_{em}.

2.4.1 Ion energy distribution

The energy distributions during the experimental investigations were measured for one needle firing with an emission current of 37 μA at different emitter voltages, varying from 2 to 7 kV, as shown in Figure 2.9. The higher the emitter voltage V_{em}, the higher is the number of collected ions. With higher V_{em} at constant emission current, the beam divergence angle decreases and the ion current density of the beam profile increases. This leads to an increased number of ions reaching the RPA collector at $\phi = 0\,°$, $\theta = 0\,°$. Furthermore, the higher V_{em} the more widened is the energy distribution and the more it is shifted to higher energies. The measurement points are fitted with a Gaussian distribution. The detailed results are given in Table 2.2. Δx_{c} indicates the shift of the energy distribution centre and ΔE the full width at half maximum (FWHM) of the Gaussian distributions.
In the V_{em} range of 2 kV to 7 kV an energy shift variation of 62 eV and a broadening of 80 eV is observed. The centre of the Gaussian distribution x_{c} in Table 2.2 is about 1.3 % higher than the applied thruster emitter voltage V_{em}. One explanation for this energy shift and broadening is a potential dimple in the centre of the RPA retarding electrode grid apertures, as represented in Figure 2.10. The colour scale shows the electric potential within the vacuum area and the grid with a retarding potential of 7 kV is represented in white. The percentage distribution of the potential stays the same for different applied retarding voltages. This creates a maximum potential dimple of 4.2 %, through which the ions with lower energy can pass. Another explanation of the energy shift was described by Knauer [72], where the Coulomb potential in front of the Taylor cone increases the energy of the ions.

Die approbierte gedruckte Originalversion dieser Dissertation ist an der TU Wien Bibliothek verfügbar.
The approved original version of this doctoral thesis is available in print at TU Wien Bibliothek.
TU Bibliothek Your knowledge hub WIEN

Table 2.2: Experimental Gaussian fit results for 37 μA emission current at different emitter voltages V_{em}.

Thruster electrodes		Energy distribution	
V_{em} [kV]	V_{ex} [kV]	centre Δx_c [eV]	FWHM ΔE [eV]
7	−2.6	+92	228
6	−3.8	+82	210
5	−5.1	+67	183
4	−6.4	+54	177
3	−7.6	+35	158
2	−8.8	+30	148

Table 2.3: Experimental Gaussian fit results for 6 kV emission voltage at different emission currents per needle I_{em}.

Thruster electrodes		Energy distribution	
$I_{em_{needle}}$ [μA]	V_{ex} [kV]	centre Δx_c [eV]	FWHM ΔE [eV]
148	−10.2	+51	204
111	−8.4	+57	202
74	−6.1	+58	178
37	−3.5	+67	164

When looking at the width of energy distribution in Table 2.2 an increasing energy broadening ΔE with increasing emitter voltage V_{em} is determined. Hornsey stated that the energy distribution results from ions emitted at different phases of the longitudinal Taylor cone jet oscillation [11]. Considering equation 2.1.2, the jet length increases with V_{em} and thus also ΔE, which explains the energy broadening trend with V_{em}.
The ions starting from the needle tip have besides their main longitudinal also transversal components of motion, which are very low compared to the longitudinal movement. Because of the high space charge density at the tip an energy redistribution takes place, which leads to an energy broadening effect of ≈ 5 eV for currents $< 2\,\mu$A [12]. For higher currents the broadening increases rapidly [1].
Table 2.3 shows the experimental Gaussian fit results for 6 kV emitter voltage and different emission currents. In the I_{em} range from 37 μA to 148 μA an energy shift of 16 eV and a FWHM variation of 40 eV is determined. A similar behaviour as measured by Mair [13] is observed. An increasing emission current leads to an increase of the energy broadening and a decrease of the energy shift. Additionally, the ratio of emission current to FWHM goes also into a saturation.
With increasing current, the productions of droplets increase. Droplets are produced very close to the Taylor cone [73]. If a droplet decays due to ion bombardment close to

Die approbierte gedruckte Originalversion dieser Dissertation ist an der TU Wien Bibliothek verfügbar.
The approved original version of this doctoral thesis is available in print at TU Wien Bibliothek.
TU Bibliothek Your knowledge hub WIEN

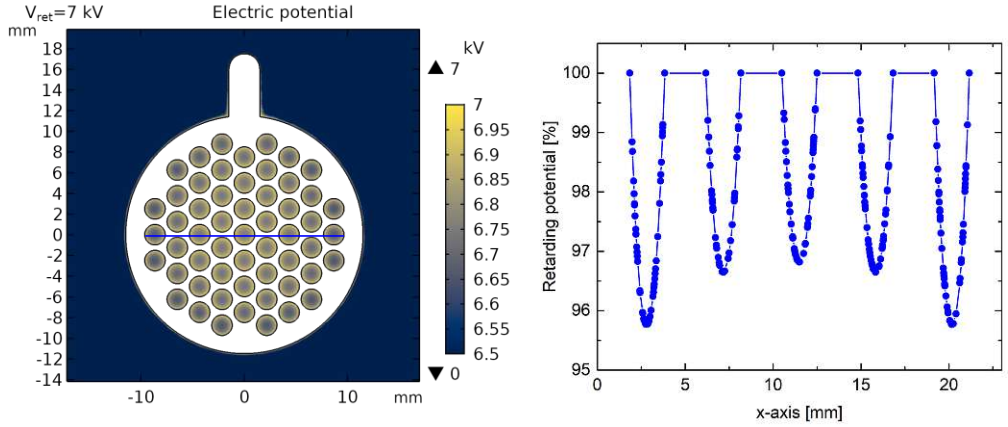

Figure 2.10: Potential distribution of the RPA retarding grid electrode with applied voltage V_{ret} of 7 kV (left) and procedural potential distribution in a cut through an aperture row (right).

the tip, the energy distribution is broadened and there are more ions with lower energy. In the simulation model the ions have the same kinetic energy as the emitter voltage with a numerical distribution of 1 %. The effects responsible for energy broadening and shifting are not fully covered with the developed simulation model.

2.4.2 Ion current density distribution

In this section the experimental and simulated beam profiles of one emitting needle and an emitter crown are compared. Thereby, the behaviour for different thruster emission current and electrode potential ranges are discussed. For higher emission currents microdroplet emission takes place, which is why this emission range was not covered by the simulation model. The following investigations were carried out for emitter voltages of $2 - 7$ kV. An emission current of 1 mA was used for the crown. For the single needle measurements the emission current was scaled down ($\frac{1}{27}$ mA), which consequently does not correspond to the emission current of an entire crown.

2.4.2.1 Emission of a single needle

The first beam profile analyses were carried out on a single emitting needle. This needle was located in the top left of the crown as shown in Figure 2.11 (a) left. The corresponding beam profile on the right side shows a shift to the top-left according to the needle position. Here the experimental measured ion current density distribution at an emission current of 9 μA is presented. It is characterised by a circular distribution with a sharp edge.
The corresponding beam profile resulting from the simulation model is represented in Figure 2.11 (b). A circular distribution with a shift to the top left and sharp edges is also observed. When comparing the ion current density from the simulation model

Die approbierte gedruckte Originalversion dieser Dissertation ist an der TU Wien Bibliothek verfügbar.
The approved original version of this doctoral thesis is available in print at TU Wien Bibliothek.

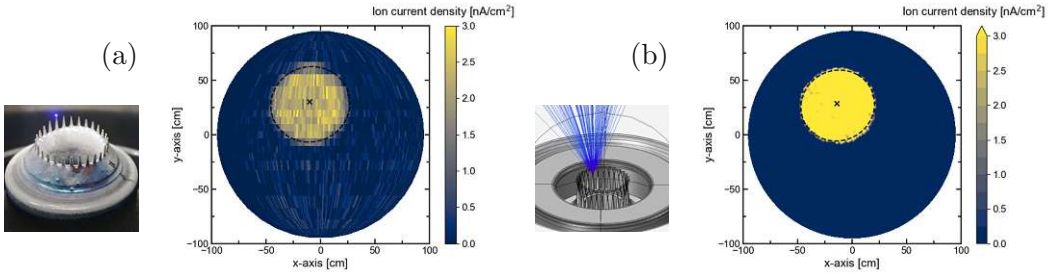

Figure 2.11: Beam profile of one emitting needle with $I_{em} = 9\,\mu A$, $V_{em} = 6\,kV$ and $V_{ex} = 3.9\,kV$ ((a): experiment, (b): simulation).

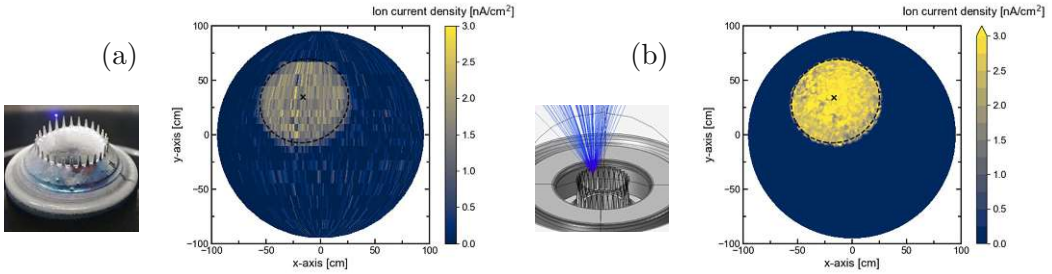

Figure 2.12: Beam profile of one emitting needle with $I_{em} = 9\,\mu A$, $V_{em} = 2\,kV$ and $V_{ex} = 8.8\,kV$ ((a): experiment, (b): simulation).

(Figure 2.11 (b)) to the experimental results (Figure 2.11 (a)), an overall higher density is determined. In the experiment the resolution is affected by the geometry of the Faraday cups and with this by sputtering effects occurring at the entrance aperture. Ions hitting the negative graphite repeller electrode, release electrons (electron emission yield $\approx 0.5 - 2$), of which 40 % will be registered inside the cup and 60 % will leave the cup[1]. These secondary electrons reduce the measured current, whereby in the simulation model no electrons are included.

The profiles of experiment and simulation show similar behaviour for different thruster parameters. This is shown when comparing Figure 2.11 with Figure 2.12. In both Figures the same emission current of $9\,\mu A$ is applied, but different electrode potentials. The lower the emitter voltage and with this the larger the extractor voltage, the more the beam is widened. The divergence angle increases by a factor of 1.04 ± 0.06, while the extractor voltage drops by a factor of $-(1.30 \pm 0.27)$. This experimental trend is reproduced with the simulation model with almost perfect agreement.

In order to analyse the structure of the ion current density distribution more precisely, a cut through the beam profiles for different emitter voltages and an emission current of $37\,\mu A$ is represented in Figure 2.13, for both experiment and simulation. Since with an emission current of $37\,\mu A$ the thrust vector is located at $\theta = 8\,°$, the cut through the beam profiles is at this angle. A steep increase occurs at $\sim -50\,°$ and a steep decrease

[1] Determined by separate simulation not shown.

Die approbierte gedruckte Originalversion dieser Dissertation ist an der TU Wien Bibliothek verfügbar.
The approved original version of this doctoral thesis is available in print at TU Wien Bibliothek.

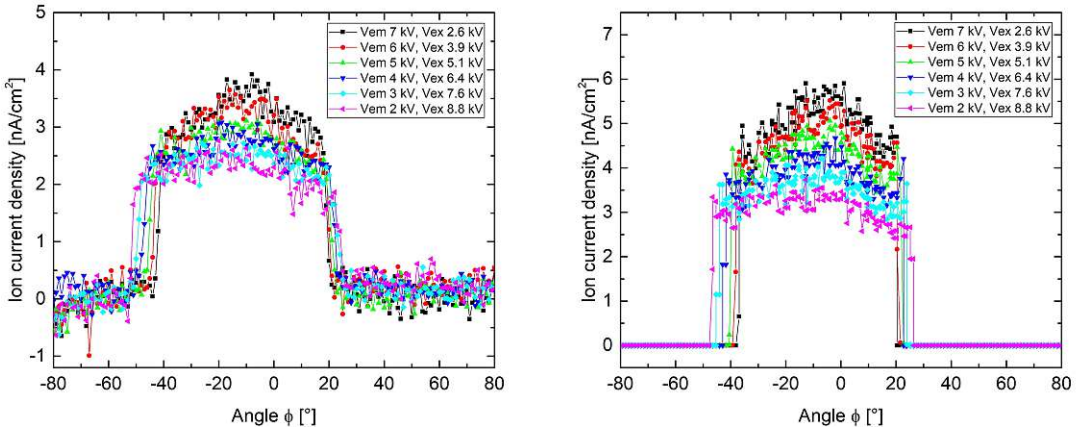

Figure 2.13: Angular ion current density distribution at $\theta = 8\,^\circ$ for one of 28 needles firing at 37 μA emission current and different emitter and extractor voltages, for experiment (left) and simulation (right).

at $\sim 20\,^\circ$. The density within the plateaus increases towards the centre. The higher the extractor voltage V_{ex} the more the profile is expanded and is directed towards the nearest surface of the extractor electrode ($-\phi$). This becomes distinct due to the increased distance between the profiles at the rise on the left side compared to the relegation on the right side. The density of the plateau increases towards the centre for both experiment and simulation. Thereby, the amount of the rise depends on the emitter voltage, which confirms that the beam is more focused with a higher emitter voltage. While the shape of simulated and measured profile shows excellent agreement, the absolute value differs by a factor of 1.4. This is probably due to secondary electrons as discussed above.
Compared to the measurements of Tajmar [26], no cosine distribution for one emitting needle is observed. Swanson [74] measured also that the angular ion current density distribution is rather flat near the 0 degree axis. In Tajmar's measurements a wire probe was used, which has no acceptance angle compared to the here used Faraday cups, which have an acceptance angle of $46\,^\circ$. Therefore, it is possible to resolve the sharp profile edges.
In order to investigate the behaviour of the beam profiles in more detail, the divergence angle α_{div} was analysed for different thruster parameters. The divergence angle is the opening angle of the beam cone around the thrust vector, which contains 95 % of the total current density. In Figure 2.14, the experimental and simulated divergence angle is plotted against the emitter voltage for different emission currents. There is a close to linear dependency of emission current to divergence angle as well as of emitter voltage to divergence angle. This is determined in both cases, for simulation and experiment. This means, the higher the emitter voltage (lower extractor voltage respectively) and the lower the emission current, the more focused is the ion beam. The effect, $\alpha_{\mathrm{div}} \propto V_{\mathrm{ex}}$, occurs because with higher extraction voltage the ion trajectories are pulled outwards towards the extractor. The second effect, $\alpha_{\mathrm{div}} \propto I_{\mathrm{em}}$, is explained with the Coulomb

Die approbierte gedruckte Originalversion dieser Dissertation ist an der TU Wien Bibliothek verfügbar.
The approved original version of this doctoral thesis is available in print at TU Wien Bibliothek.

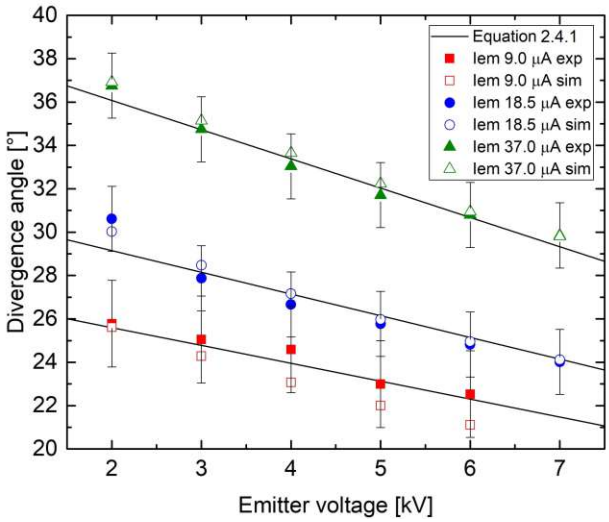

Figure 2.14: Divergence angle α_{div} as a function of the emitter voltage for one needle emitting with different currents and experiment and simulation in comparison.

potential in front of the Taylor cone, which occurs by the beam itself. Due to the small emitting area, a high current density occurs in front of the Taylor cone. This leads to Coulomb interactions of the ions and with this to an increasing space charge. The Coulomb potential formed in front of the tip is influenced by the Taylor cone shape and with this by the emitted current. The higher the emitted current, the higher is the Coulomb potential, as shown in Figure 2.15. Furthermore, the Taylor cone angle decreases, which has an influence on the shape of the Coulomb potential, which fans out. At the same time, this leads to a deflection of the ion trajectories, which causes a broadening and defocusing of the beam.
From the experimental results shown in Figure 2.14 the following empirical equation can be established for one emitting needle:

$$\begin{aligned} \alpha_{\text{div}}[^\circ] &= 23.547 + 0.411 \cdot I_{\text{em}}\,[\mu\text{A}] \\ &+ (-0.657 - 0.019 \cdot I_{\text{em}}\,[\mu\text{A}]) \cdot V_{\text{em}}\,[\text{kV}]. \end{aligned} \tag{2.4.1}$$

The divergence angle α_{div} can be determined with the input parameters emission current I_{em} and emitter voltage V_{em} in the range below 37 μA and 7 kV. This angle is independent of the location of the Taylor cone on the needle tip.

2.4.2.2 Emission of an emitter crown

In order to investigate the behaviour of the entire thruster ion beam, diagnostic measurements were carried out on an emitting crown. One of the 28 needles emitted weakly due to manufacturing reasons, which was located on the left side of the crown, as marked in Figure 2.16 (a) left. The corresponding beam profile on the right side shows a slight

Die approbierte gedruckte Originalversion dieser Dissertation ist an der TU Wien Bibliothek verfügbar.
The approved original version of this doctoral thesis is available in print at TU Wien Bibliothek.

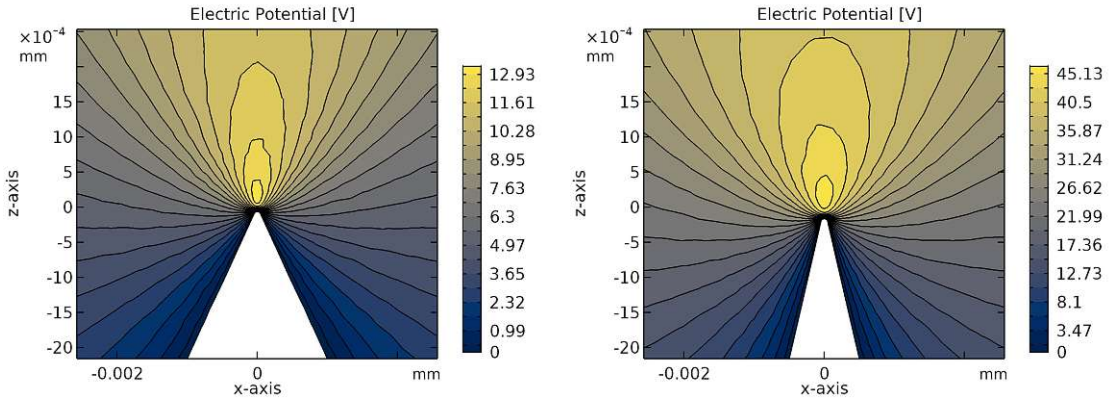

Figure 2.15: Coulomb potential caused by the beam particles in front of the Taylor cone for 9 μA (left) and 37 μA (right) emission current.

shift to the right due to the weakly emitting needle. Here the experimental measured ion current density distribution at an emission current of 1 mA is presented. In comparison to the single-needle profile, no sharp edges can be observed due to the overlapping of the individual circular profiles. The corresponding beam profile resulting from the simulation model is represented in Figure 2.16 (b). Here as well, an overall higher current in the simulation than in the experiment was measured, which can again be explained by the limitation of the Faraday cups. The profiles show a similar shape with increasing ion current density towards the centre. The experimental beam divergence angle in Figure 2.16 is 63 ° compared to 49 ° in the simulation. The simulation model is idealised, which means, every Taylor cone has the same shape and is directed exactly vertically upwards. In addition, in the simulation model, the same current value of $\frac{1}{27}$ mA is emitted from each needle tip. This cannot be influenced in the experiment, where only regulation of the entire emission current is possible. This implies that some needles emit less and some higher currents.

In order to analyse the structure of the ion current distribution more precisely, a cut through the beam profiles at $\theta = 0\,^\circ$ for different emitter voltages is represented in Figure 2.17 for both experiment and simulation. The results can be compared with the results of one emitting needle in Figure 2.13 (left), because of the same emitted current of 37 μA on average per needle. The lower the emitter voltage and the higher the extractor voltage respectively, the more the beam profile flattens which leads to a defocussing effect. This is the same trend as analysed for the single emitter. In comparison to other electric propulsion thrusters, the beam profile cannot be described with a Gaussian distribution. For higher emitter voltages it is a conical distribution with a distinctive tip in the profile centre. With decreasing voltage, this tip is getting flatter. The simulation results in Figure 2.17 (right) show the same behaviour but an overall more focused beam profile than in the experiment.

Die approbierte gedruckte Originalversion dieser Dissertation ist an der TU Wien Bibliothek verfügbar.
The approved original version of this doctoral thesis is available in print at TU Wien Bibliothek.

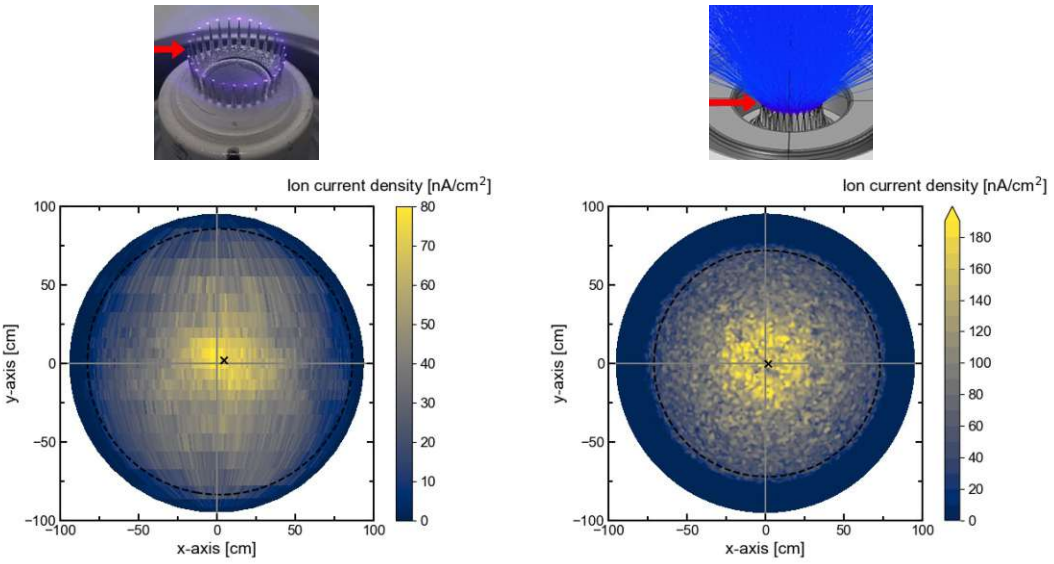

(a) (b)

Figure 2.16: Ion current density distribution for 27 of 28 needles emitting with 1 mA current and 6 kV emitter voltage ((a): experiment with $\alpha_{\text{div}} = 63°$ and $\alpha_{\text{off}} = 3°$, (b): simulation with $\alpha_{\text{div}} = 49\,°$ and $\alpha_{\text{off}} = 1\,°$).

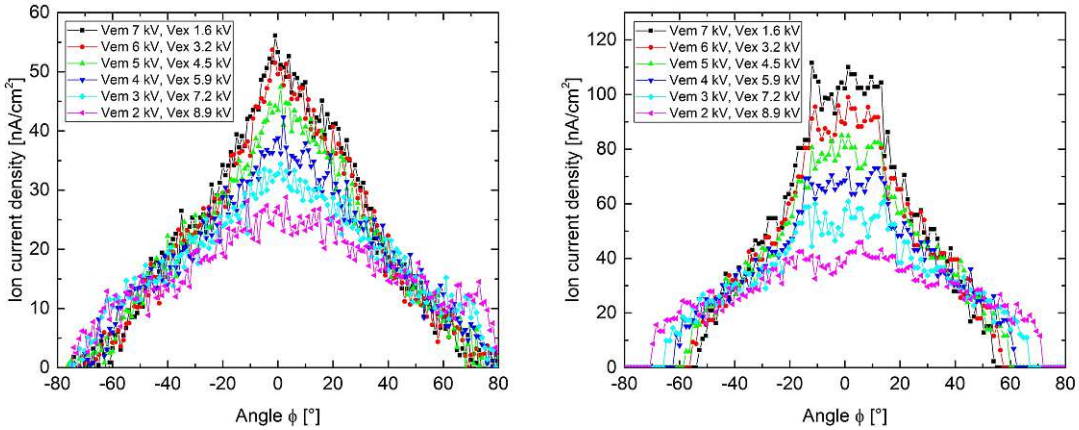

Figure 2.17: Angular ion current density distribution at $\theta = 0\,°$ for 27 of 28 needles firing at 1 mA emission current at different emitter and extractor voltages for experiment (left) and simulation (right.

Die approbierte gedruckte Originalversion dieser Dissertation ist an der TU Wien Bibliothek verfügbar.
The approved original version of this doctoral thesis is available in print at TU Wien Bibliothek.

2.5 Conclusion

Our detailed analysis of a test crown emitter beam provides an overview of the beam profile behaviour for a single emitting needle and an entire emitting crown in different emission regimes. Beam profile and ion energy distributions measurements were carried out. It shall be noted that the emitter used in this work was manufactured to different specification than the IFM Nano Thruster. The experimental energy distribution measurements have shown, that with increasing emission current, an increase of the energy broadening occurs.
The COMSOL Multiphysics particle tracing module was used to simulate the ion beam trajectories. As an input parameter, the linear dependency of the Taylor cone angle on the emission current was included in the model. The model was calibrated using two experimental measurement points. Based on this, all other values were calculated without fitting. In the model, the space charge was calculated based on the slow ions in front of the nanometre-sized Taylor cone jet, so that the ions can start from their point of origin. The beam profile including divergence angle and density distribution of a single emitting needle can be simulated in a low emission current area. Experiment and simulation have shown a linear dependence of the divergence angle on the emission current and on the thruster electrode voltages. With increasing emission current and also with increasing extractor voltage the divergence angle increases, which leads to a defocusing effect of the beam. Hereby the simulation model has shown that the inclusion of space charge and with this the Coulomb interaction plays an important role for the ion trajectory calculation. The model has access to parameters that are hard to determine experimentally, e.g. the space charge and Coulomb potential due to the ion beam itself. Due to the excellent benchmark of the model, it will be used in the near future to optimise the focusing of the thruster beam by adjusting the extraction geometry.

2.6 Acknowledgments

This chapter is the result of research projects funded by the Austrian Research Promotion Agency (FFG) under the contract 874844 and the European Space Agency (ESA) under the contracts 4000127152/19NL/HB and 4000116898 /16/NL/EM.

Die approbierte gedruckte Originalversion dieser Dissertation ist an der TU Wien Bibliothek verfügbar.
The approved original version of this doctoral thesis is available in print at TU Wien Bibliothek.
TU Bibliothek Your knowledge hub WIEN

Die approbierte gedruckte Originalversion dieser Dissertation ist an der TU Wien Bibliothek verfügbar.
The approved original version of this doctoral thesis is available in print at TU Wien Bibliothek.

3 Simultaneously measured direct and indirect thrust of a FEEP thruster using novel thrust balance and beam diagnostics

This chapter corresponds to the eponymous peer-review article published in Acta Astronautica (197 (2022) 107–114), DOI: 10.1016/j.actaastro.2022.05.009.

For the characterisation of an electric propulsion system, the determination of the thrust has a crucial role. The thrust of an Indium FEEP Multiemitter (IFM) Nano Thruster laboratory model is measured directly with a thrust balance and indirectly via beam diagnostics. Both measurements are carried out simultaneously to enable mutual verification with high accuracy. The novel mN-torsion thrust balance by FOTEC resolves six different thrust magnitudes, ranging from $10\,\mu N$ *to* $1\,N$*. It is based on the so-called force-feedback method using a voice coil actuator to determine the thrust, which leads to an accuracy of better than* $2\,\%$*. The indirect thrust measurements were performed with a high-precision beam diagnostics system by FOTEC. A semi-circular diagnostics arm equipped with* 23 *digital Faraday cups is used to measure the ion current density distribution of the entire beam. The thrust results of both systems show an agreement with a deviation less than* $5\,\%$ *for thruster operation points ranging from* 50 *to* $450\,\mu N$*. This proves that the performance of a FEEP thruster can be characterised very precisely by indirect trust measurements.*

3.1 Introduction

Field emission electric propulsion (FEEP) thrusters are playing an increasingly important role in the space sector, especially the Indium FEEP Multiemitter (IFM) Nano Thruster. The IFM Nano Thruster, shown in Figure 3.1, was developed at the research company FOTEC and commercialised by the space tech company ENPULSION, both located in Austria. FEEPs have a wide range of application areas, like as CubeSat propulsion or for science and Earth observation missions [41, 75]. Thereby, they are used for drag free and fine attitude control or as a clustered version as main propulsion system of a spacecraft, which includes station keeping, orbital raising and drag compensation. In order to be able to comply with the requirements of the different application areas, a performance characterisation of the thruster is necessary.
Direct and indirect thrust measurements are commonly used methods to analyse the performance of an electric propulsion (EP) thruster. The thrust of different EP tech-

Die approbierte gedruckte Originalversion dieser Dissertation ist an der TU Wien Bibliothek verfügbar.
The approved original version of this doctoral thesis is available in print at TU Wien Bibliothek.

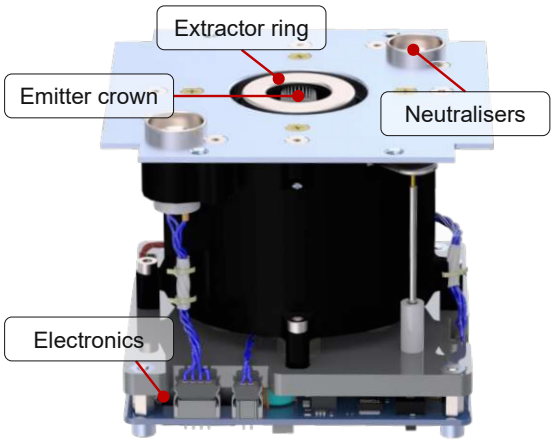

Figure 3.1: Drawing of an IFM Nano Thruster with indicated main components.

nologies can be determined directly using a thrust balance. For this purpose, typically pendulum balances are used [47, 76–82], such as a horizontal μN torsion balance developed by FOTEC in 2013 [83, 84]. This balance is especially suitable for high voltage ($< 20\,\mathrm{kV}$) and high current ($< 3\,\mathrm{A}$) electric propulsion systems. Since 2013, it has received several upgrades, to be able to cover a thrust range over several orders of magnitude with high accuracy. This was achieved by converting the deflection measurement into a force-feedback mode, which is also known as steady state null balance [85].
Alternatively, the thrust of an ion thruster can be determined indirectly from its beam properties. For this purpose, certain key parameters are required, like beam shape, ion energy distribution and fraction of multiply charged particles. When calculating the thrust, it is of elementary importance how precisely these parameters can be determined. For ion thrusters, these parameters are usually distribution functions, depending on the operation point. In addition, they are influenced by chamber effects, which distorts the calculated thrust. Due to these two effects direct thrust measurements are usually preferred in order to qualify an EP thruster.
However, in this paper it will be shown that for FEEP thrusters the parameters can be determined precisely leading to an accurate indirect thrust calculation. In order to prevent influences on the beam, like charge exchange effects or beam widening, a sufficiently large high vacuum facility is used. Another advantage of indirect measurement is the access to other key parameters that play an important role in the characterisation of an EP thruster. This includes the beam divergence angle, which is required to analyse the spacecraft-beam interaction. Furthermore, the thrust vector alignment can be computed, which is particularly important for a precise spacecraft attitude control.
Direct thrust measurements in combination with full beam diagnostics measurements are rarely done. In this process, many inaccuracies could arise when comparing the results of the two separate systems. In this paper, both, indirect and direct thrust measurements methods are performed simultaneously at an IFM Nano Thruster laboratory model. For the direct thrust measurements, the newly developed mN-torsion pendulum thrust bal-

Die approbierte gedruckte Originalversion dieser Dissertation ist an der TU Wien Bibliothek verfügbar.
The approved original version of this doctoral thesis is available in print at TU Wien Bibliothek.
TU Bibliothek Your knowledge hub WIEN

ance is used, which is presented the first time in this configuration. The indirect thrust measurements are carried out with an upgraded digital beam diagnostics system [58]. It is shown that the results of the direct and indirect thrust measurements have a high level of agreement. This allows to verify the data obtained from both systems at the same time and helps to reduce measurement uncertainties.
With this knowledge, the electrostatic beam simulation model developed in 2020 can predict the thrust of any new FEEP thruster geometry [43].

3.2 Analytical methods

3.2.1 Direct thrust measurements

For direct thrust measurements of an EP thruster pendulum thrust balances are typically used. Thereby, the produced thrust can be computed from the deflection of the balance arm. However, there is also a second possibility in which the balance arm is held stationary in the centre, which is known as steady state null balance or force compensation method. For the presented thrust balance, this is done through a so-called voice coil actuator (VCA), which uses Lorentz forces to generate actuation. A schematic drawing of the used VCA is shown in Figure 3.2. It consists of an axially magnetised cylindrical permanent magnet and a moving coil, which is located in a ferromagnetic cylinder. The applied current generates a magnetic field which exerts a force on the permanent magnet. The generated force T is proportional to the applied current I:

$$T = I \int dl \times B = f \cdot k \cdot I + b\,[\mathrm{N}], \tag{3.2.1}$$

where l represents the geometry of the solenoid and B the magnetic flux in the permanent magnetic field. A conversion factor of $f = 3.89\,\mathrm{N/A}$ is specified by the VCA supplier to convert the applied current into a force. The gain-factor k and the offset b are determined by the calibration procedure of the VCA. For calibration, the VCA permanent magnet is placed on a weight scale. The coil is positioned with a stamp at a minimum distance exactly above the magnet. A current is applied to the coil, which is increased successively. At the same time the mass change on the weight scale is measured and can be converted into force. In this way, a calibration fit-curve can be created to determine the parameters k and b, as will be shown in section 3.4.1.

3.2.2 Indirect thrust measurement

The thrust produced by an ion thruster can also be calculated from its beam properties, known as indirect thrust measurement:

$$T = I_{\mathrm{em}} \cdot \sqrt{\frac{2m \cdot \eta_\nu \cdot V_{\mathrm{em}}}{e}} \cdot \alpha \cdot \gamma, \tag{3.2.2}$$

where I_{em} is the emitter current, m/e the mass to charge ratio and V_{em} the emitter voltage. The thrust correction factors are η_ν acceleration efficiency, γ divergence efficiency

Die approbierte gedruckte Originalversion dieser Dissertation ist an der TU Wien Bibliothek verfügbar.
The approved original version of this doctoral thesis is available in print at TU Wien Bibliothek.
TU Bibliothek Your knowledge hub WIEN

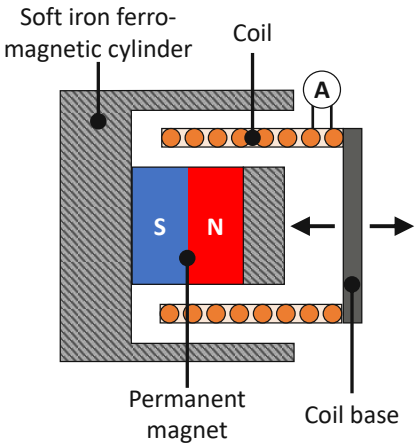

Figure 3.2: Schematic drawing of the used voice coil actuator (VCA), consisting of a permanent magnet and a coil driven by a current-controlled power supply (A).

and α multiply charged species term [66].
The α factor considers the fraction of multiple charged ions, which are commonly observed in electric thrusters [66]. Fehringer did magnetic mass spectrometry investigations of a needle type FEEP thruster, which was the predecessor of the IFM Nano Thruster [23]. He analysed that single charged indium ions make up 98 % of the total emitted current. Other electric thruster types produce a larger number of multiple charged ions, such as a High Efficiency Multistage Plasma Thruster (HEMPT) ion beam consists with 60 % of doubly and triply charged ions [86].
The correction factor η_ν includes the ion acceleration efficiency. This efficiency was observed with a retarding potential analyser (RPA) [43, 55]. Thereby, it was analysed that the energy of the ions corresponds exactly to the emitter voltage V_{em}, independent of the spatial angle. In the case of Hall Effect Thrusters (HET), there is a spread in beam energies produced in the thruster [66, 87]. Or for example for HEMP thrusters the ion energy varies dependent on the plume angle [88].
The divergence efficiency coefficient γ includes the cosine loss effects on the beam current I_{em} due to the divergence of the beam. For this the spatial ion current density distribution over the entire beam has to be integrated:

$$\gamma = \frac{1}{I_{\mathrm{em}}} \cdot \sum_{ij} I_{ij} \cdot \cos\theta_i \cdot \cos\phi_j, \tag{3.2.3}$$

where θ and ϕ are the spherical coordinates of a hemisphere in front of the beam. The current density I is typically measured with Faraday cups. A large vacuum facility is particularly suitable for measuring the beam with highest precision. For example, the beam can be influenced by the potentials of the facility walls. Furthermore, a high pumping rate is beneficial, as this reduces the charge exchange effects of wall reflected species that could distort the current measurement of the Faraday cups.

Die approbierte gedruckte Originalversion dieser Dissertation ist an der TU Wien Bibliothek verfügbar.
The approved original version of this doctoral thesis is available in print at TU Wien Bibliothek.
TU Bibliothek Your knowledge hub WIEN

In summary, the IFM Nano Thruster has a mono-energetic, singly-ionised beam ($\alpha = 1$ and η_ν=1). Therefore, only the divergence efficiency γ has to be considered for the indirect thrust computation. This efficiency is analysed with the high precision beam diagnostics system.

3.3 Direct and indirect thrust measurement setup

Two different thrust measurement setups were used at the same time, located in FOTEC's large vacuum facility as shown in Figure 3.3. Therefore, no setup change between the measurements is carried out, which avoids air cycles or system conversions that could lead to inaccuracies. The vacuum facility has a length of 3 m, a diameter of 2.2 m and reaches during nominal thruster operation a pressure of $2 \cdot 10^{-7}$ mbar. In this test setup, both the direct and the indirect thrust of an IFM Nano Thruster test module are to be determined simultaneously. The thruster is located on the mN-thrust balance, which is protected by a shield against back sputtering. A semi-circular diagnostics arm equipped with 23 Faraday cups is used to measure the ion current density distribution of the thruster beam in 1 m distance. The thrust balance is mounted in such a way that the thruster emitter is exactly centred in the semi-circle of the diagnostics arm. A sketch of both combined setups is shown in Figure 3.4. Both measurement setups are described separately in the following subsections.

3.3.1 IFM Nano Thruster description

The IFM Nano Thruster is based on the field emission principle, where ions are emitted from a liquid metal by means of strong electric fields [84]. A schematic drawing of the IFM Nano Thruster is shown in Figure 3.5. The core of the thruster is a porous tungsten crown with 1 cm diameter consisting of 28 needles, wetted with liquid indium. Each of these needles acts as a separate ion emission source, where the term 'multiemitter' is originated. This configuration results in a higher achievable total emission current. A positive high voltage is applied to the crown emitter and a negative high voltage at the ring-shaped extractor. Due to the strong electric fields at the needle tips, ions are produced and accelerated. The ions are accelerated along the electric field, which produces the thrust. For the experimental tests performed in this paper, a laboratory model of the IFM Nano Thruster was used.

3.3.2 Thrust balance setup

A schematic drawing of FOTEC's novel mN-thrust balance is shown in Figure 3.6. It consists of an horizontal 80 cm long arm suspended by two spring bearings in the centre, which ensures frictionless deflection of the arm. The pivot frame is retaining the spring bearings ensuring low thermal drift, high reproducibility and ultra-low noise levels. On the right balance table, the IFM Nano Thruster test module is located and on the left side the counterweight with equal mass. This ensures cancellation of the overall torque and prevents bearings from absorbing shear forces. The total capacity of the thrust

Die approbierte gedruckte Originalversion dieser Dissertation ist an der TU Wien Bibliothek verfügbar.
The approved original version of this doctoral thesis is available in print at TU Wien Bibliothek.
TU Bibliothek Your knowledge hub WIEN

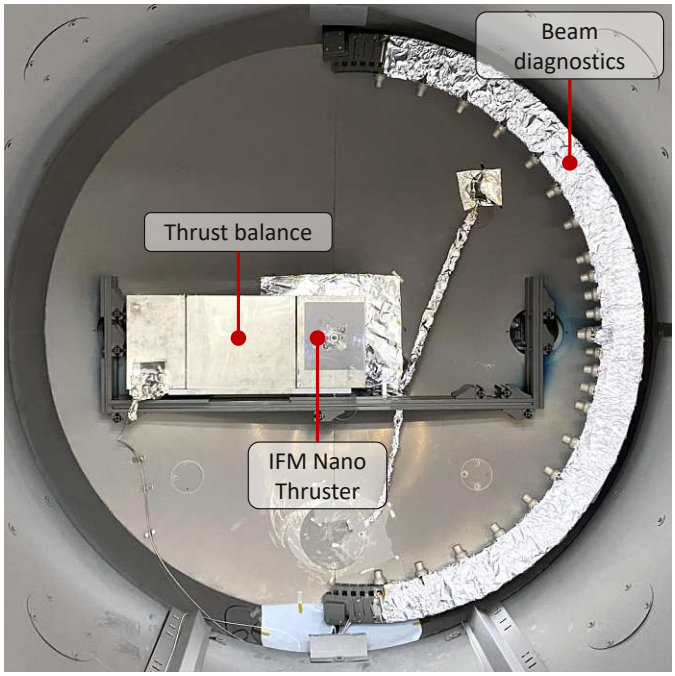

Figure 3.3: Combined test setup with IFM Nano Thruster test module mounted on mN-thrust balance and semi-circular beam diagnostics arm equipped with 23 Faraday cups.

balance is 15 kg on each table.
An optical displacement sensor measures the distance between the sensor and the mirror mounted on the arm. The thrust balance is operated in force-feedback mode, where the arm is kept in its centre position. This is realised with the main voice coil actuator (VCA), which is located underneath the counterweight table. The VCA permanent magnet is mounted on the balance arm and the voice coil is mounted on a support in front of the arm. This avoids current supply connections to the balance arm. The VCA compensates the force generated by the thruster, which allows the computation of the generated thrust, as described in section 3.2.1. A software-based control loop is used to control the force actuator. Depending on the thrust transients, thrust level and thruster mass, the PID controller values can be adjusted for improved results, such as faster response, low overshoot or low noise [89]. A second auxiliary VCA is used to test the balance with a known force. Thereby, the auxiliary VCA simulates a thrust by applying a test force. This allows a direct verification and calibration of the thrust balance. The VCAs are located behind the balance arm, to ensure that for both the force vector points in the same direction and can therefore be compared more accurately.
The thrust balance is equipped with a magnetic damping system. It consists of an eddy current brake to reduce measurement noise and long-lasting oscillations caused by an over- or undershoot. The damping rate can be varied by shifting the damping system along the arm, which is particularly suitable for pulsed thrusters. For the character-

Die approbierte gedruckte Originalversion dieser Dissertation ist an der TU Wien Bibliothek verfügbar.
The approved original version of this doctoral thesis is available in print at TU Wien Bibliothek.

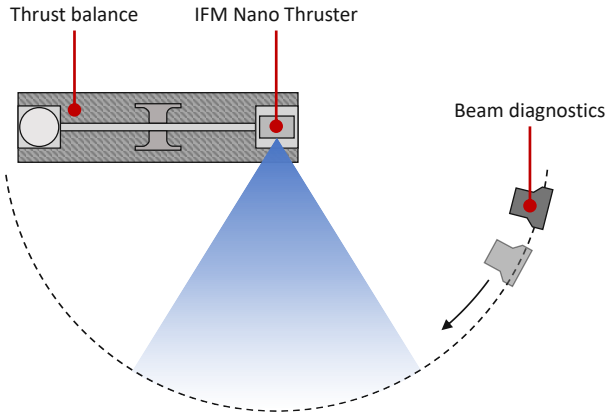

Figure 3.4: Top view sketch of combined setup with IFM Nano Thruster attached on thrust balance combined with beam diagnostics.

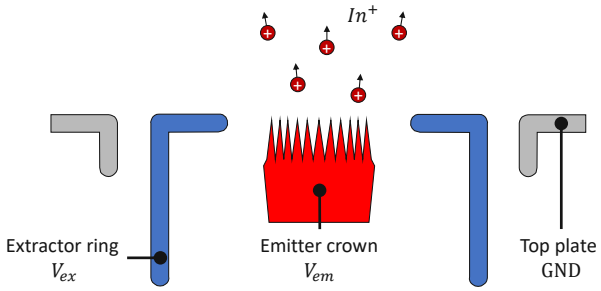

Figure 3.5: IFM Nano Thruster simplified as schematic drawing with positive emitter and negative extractor electrode.

isation of continuous electric propulsion systems such as FEEP, Hall or gridded ion thrusters the low response rate has no influence on the results. Alternatively, a software based damping system can be used, which was developed for the new thrust balance. During this test, only the software based damping system is used.
Standard electrical feed-troughs (F/T) cannot be used to supply or read out the thruster. Thin cables could heat up at higher currents and generate a phantom force. This common effect is mitigated by using a conductive liquid to connect the lead wires on the movable part of the balance with the electrical connections outside the test facility.
The thrust balance is also equipped with a gas propellant system, so that it can also be used for other thruster types with gas supply. Special tube holder and ultra-flexible tubes ensures minimal influence of thrust measurement accuracy. Since the IFM Nano Thruster includes a solid indium propellant tank, no gas feeding system is used during this test. The mN-thrust balance key specifications are shown in Table 3.1. The balance has a variable measurement range up to 1 N, where six different thrust ranges can be

Die approbierte gedruckte Originalversion dieser Dissertation ist an der TU Wien Bibliothek verfügbar.
The approved original version of this doctoral thesis is available in print at TU Wien Bibliothek.
TU Bibliothek Your knowledge hub WIEN

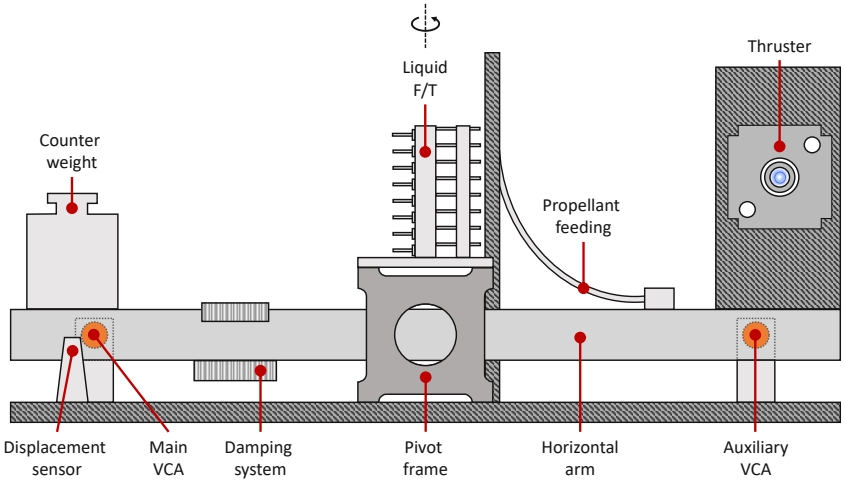

Figure 3.6: Schematic drawing of FOTEC's novel mN-thrust balance.

Table 3.1: mN-thrust balance key specifications.

Parameter	Size
Thrust range	$0 - 1\,\mathrm{N}$
Measurement ranges	$< 0.01, 0.1, 1, 10, 100, 1000\,[\mathrm{mN}]$
Accuracy	$2\,\%$ of measurement range
Noise floor	$15\,\mu\mathrm{N}$ RMS
Sensitivity	$1.66\,\mu\mathrm{N}/\mu\mathrm{m}$
Dimensions	$800 \times 200 \times 374\,\mathrm{mm}$ (L × W × H)
Max. load	$15\,\mathrm{kg}$

used, making it suitable for a variety of thruster types. The VCA controller support different current ranges and the most suitable is automatically selected by the firmware. The measurement accuracy is the difference between the measured and the commanded thrust. Error propagation has shown that the VCAs have the major contribution to the accuracy, which results in $2\,\%$ of the respective measurement range.
The resolution is defined as the smallest measurable difference between two thrust inputs. In practice, the resolution is limited by the noise floor of the thrust measurement [85]. The noise floor is the same for all measurement ranges with $15\,\mu$N RMS (also shown in section 3.4.1).
Typically, the sensitivity s is also given for a thrust balance, which is described as the deflection of the balance arm x for a given applied force F: $s = dx/dF = r^2/D$. Since the mN-thrust balance is operated in the force-feedback mode where the arm is stationary in the centre, the sensitivity is here defined by a combination of the spring constant D and the arm length r. A Philtec DMS D64 is used as an optical displacement sensor.

Die approbierte gedruckte Originalversion dieser Dissertation ist an der TU Wien Bibliothek verfügbar.
The approved original version of this doctoral thesis is available in print at TU Wien Bibliothek.

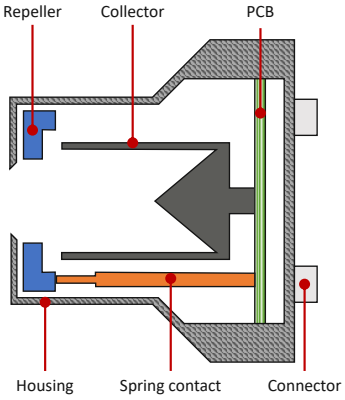

Figure 3.7: Schematic drawing of a digital Faraday cup.

Table 3.2: Digital Faraday cup system key specifications.

Parameter	Size
Current density range	$< 3.8\,\mu A/cm^2$
Accuracy	$\pm\ 5\,pA/cm^2$
Sampling frequency	$7 - 3520\,Hz$
Horizontal resolution	$> 0.1\,^\circ$
Vertical resolution	$4 - 12\,^\circ$
Repeller	$-80 - 0\,V$

It has an accuracy of $\pm 1\,\mu m$ in the far field, which corresponds to $1.6\,\mu N$ and is included in the balance accuracy.

3.3.3 Beam diagnostics setup

In 2021 FOTEC developed an upgraded beam diagnostics system for high spatial resolution of an ion beam in polar and azimuthal direction [58]. The diagnostics system consists of 23 digital Faraday cups (DFC) and one retarding potential analyser (RPA). These are mounted on the semi-circular diagnostics arm as shown in Figure 3.3. With the Faraday cup system, the ion or electron current density distribution of a particle beam can be measured. The entire measuring electronics is located in the head of the DFC. This allows high precision measurements of the beam current density, since signal interference due to cable length or movement of the diagnostics arm can be eliminated. Furthermore, the DFCs automatically switch between different current ranges. Thus, the optimal resolution is achieved for thrusters of different power ranges and current densities. In Figure 3.7 a schematic drawing of a digital Faraday cup can be seen. In the geometric design, the widening of the beam is considered, which means the entrance

Die approbierte gedruckte Originalversion dieser Dissertation ist an der TU Wien Bibliothek verfügbar.
The approved original version of this doctoral thesis is available in print at TU Wien Bibliothek.

aperture has the smallest diameter. Sputtering effects in the area of the entrance aperture are reduced by a bevelling structure. A cup-shaped collector measures the current caused by impinging ions or electrons. In addition, the cup has a conical structure to trap secondary electrons. The negative biased repeller electrode prevents ambient electrons or slow charge exchange ions from entering the cup. These slow ions are attracted to the orifice and do not contribute to the measured current. Furthermore, secondary electrons triggered by ion bombardment are prevented from leaving the cup. Other Faraday cup studies for FEEP thrusters came to a similar geometric design [90] or also feature built-in electronics for signal processing [88]. A major advantage compared to other beam diagnostics systems is that the measurement and control electronics is integrated in the head of the DFC on a printed circuit board (PCB). For the application of FEEP thrusters, the structure of the DFC insulators considers the deposition of indium, which could lead to conductive connections.
The 23 DFCs are attached to the semi-circular diagnostics arm with different spacings to have a higher resolution in the beam centre. The key specifications of the DFC system are presented in Table 3.2. All DFCs are triggered to sample and convert the signal at the same time the rotation in 1 ° steps from −80 ° to 80 ° in 90 cm distance around the thruster. With this the measured ion current density is mapped on a spherical surface mesh [43]. Typical beam properties can be analysed from the 3D measurement data. This includes total beam current and the thrust vector. Furthermore, the divergence half-cone angle can be computed, defined as angle from the thrust vector which contains 95 % of the total beam current.

3.4 Results

The IFM Nano Thruster test module was operated at different operation points by varying the emitter current I_{em}, emitter voltage V_{em} and extractor voltage V_{ex}. At every operation point direct thrust measurements were performed for 5 mins and an average value was formed. A beam diagnostics scan was carried out afterwards which took $\sim$ 20 mins. Previous analyses have shown that the beam remains stable over time, which is also shown in section 3.4.2. Therefore, measurements were made with a higher resolution [43]. The measurements of the two systems were performed successively for each point, so that the direct thrust measurement is not disturbed by the movement of the diagnostics arm. In the following, the respective results of the two systems are shown and compared thereafter.

3.4.1 Thrust balance results

Before starting with the thrust balance measurements the two voice coil actuators (VCA) were calibrated with the procedure described in section 3.2.1. The recorded calibration curve for the thrust measurement range ¡1 mN is shown in Figure 3.8. The measured weight force is plotted against the applied voice coil current. From the linear fit of the data points a gain factor of $k = 4.0397/3.89 = 1.0385$ and an offset of $b = 5.325 \cdot 10^{-7}$ N

Die approbierte gedruckte Originalversion dieser Dissertation ist an der TU Wien Bibliothek verfügbar.
The approved original version of this doctoral thesis is available in print at TU Wien Bibliothek.
TU Bibliothek Your knowledge hub WIEN

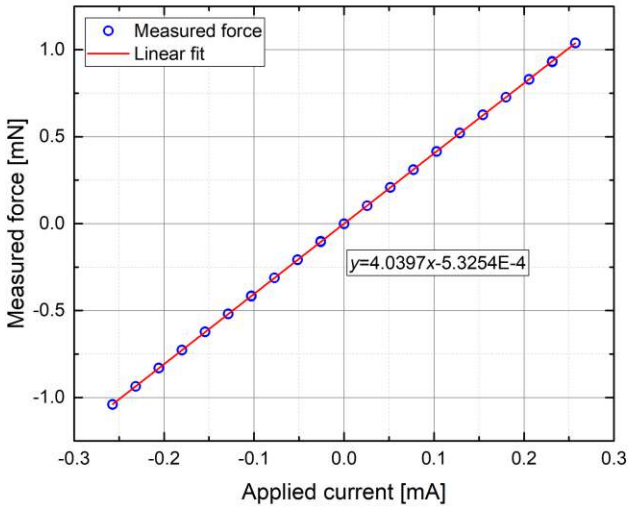

Figure 3.8: Voice coil actuator (main) calibration curve for < 1 mN thrust range with linear fit-function.

could be observed. These parameters are used as input parameters for the VCA firmware, which uses equation 3.2.1. With this the required VCA current to compensate the force of the thruster can be computed into direct thrust. Subsequently the parameters were verified in the same setup, by repeating the thrust measurement using the software with the identified calibration factors. A maximum peak-to-peak deviation of 10 μN and an RMS of 5 μN were achieved, which is within the expected accuracy of the thrust balance.

The two calibrated VCAs were installed on the mN-thrust balance in the test setup described in section 3.3.2. Next step was the verification of the VCAs calibration data. For this purpose, a test force is applied using the auxiliary VCA. At the same time, the main VCA counteracts the applied force of the auxiliary VCA with a certain current. With the current and the previously identified calibration factors the required thrust is computed using equation 3.2.1 . The two results are compared with each other, which can be seen in Figure 3.9. The red curve shows the applied thrust of the auxiliary VCA and the blue curve the measured thrust with the main VCA. The following forces were applied in succession: 0, 1000, 500, 400, 250, 100, 50, 20, 0 μN. It can be identified that the main VCA reacts immediately to the applied force without overshooting. The comparison between commanded and measured thrust results in a deviation of $< 20\,\mu$N ($\approx$2 %), which describes the accuracy of the thrust balance. The noise floor corresponds to the RMS of 15 μN and can be reduced by longer measurement time.

Direct thrust measurements of an IFM Nano Thruster test module were performed using the mN-thrust balance including the two calibrated and verified VCAs. The measurement data was recorded for every thruster operation point for 5 mins with 0.05 s sample interval. An average value was formed over 100 data points. Both results can be seen in Figure 3.10. This series of measurements was taken at a constant thruster emitter current of 3.5 mA, which corresponds to the nominal operation of an IFM Nano

Die approbierte gedruckte Originalversion dieser Dissertation ist an der TU Wien Bibliothek verfügbar.
The approved original version of this doctoral thesis is available in print at TU Wien Bibliothek.
TU Bibliothek Your knowledge hub WIEN

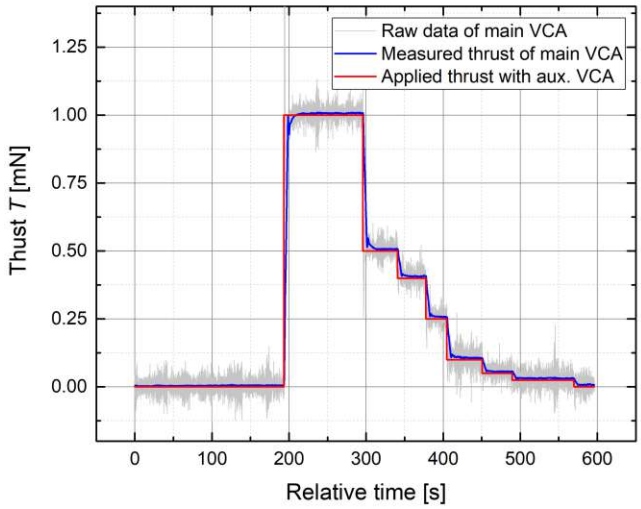

Figure 3.9: Thrust balance verification at $< 1\,\mathrm{mN}$ thrust range, installed on mN-thrust balance.

Thruster. In order to vary the thrust, the emitter voltage was gradually reduced from 10 kV down to 3 kV. Further measurements were carried out at constant emitter voltage as well as at constant extractor voltage. The results are presented and compared with the beam diagnostics results in section 3.4.3.

3.4.2 Beam diagnostics results

Beam diagnostics measurements of an IFM Nano Thruster test module were performed with the system described in section 3.3.3. The diagnostics arm was moved in steps of $1\,^\circ$ from $-80\,^\circ$ to $80\,^\circ$ around the thruster and 10 data points were recorded at each position. The spherical data recorded with the semi-circular diagnostics arm can be projected into Cartesian coordinates to visualise the beam profile. The beam properties are calculated on the basis of the three-dimensional data and are displayed visually in the projected beam profile. Figure 3.11 (left) shows a beam profile measured at an minimum thruster emission current of $I_{\mathrm{em}} = 5\,\mu\mathrm{A}$. This value lies outside the usual operation of an IFM Nano Thruster. It is shown to demonstrate the high resolution of the DFC system, where a maximum ion current density of $\sim 2\,\mathrm{nA/cm^2}$ was measured. It shows the profile of a single emitting needle located in the upper part of the emitter crown. The beam diagnostics analysis software indicates the computed thrust vector with a cross. The divergence half-angle α_{div} is represented with a dashed circle.

Figure 3.11 (right) shows a beam profile measured at a nominal thruster emission current of $I_{\mathrm{em}} = 3.5\,\mathrm{mA}$. A maximum ion current density current of $\sim 200\,\mathrm{nA/cm^2}$ was measured. Here the individual beamlets coming from the 28 emitting needles can be diagnosed. With this the beam divergence angle of the whole beam profile ($\alpha_{\mathrm{div}} = 69\,^\circ$) consisting of 28 single beamlets is larger than of a single emitting needle ($\alpha_{\mathrm{div}} = 17\,^\circ$)

Die approbierte gedruckte Originalversion dieser Dissertation ist an der TU Wien Bibliothek verfügbar.
The approved original version of this doctoral thesis is available in print at TU Wien Bibliothek.

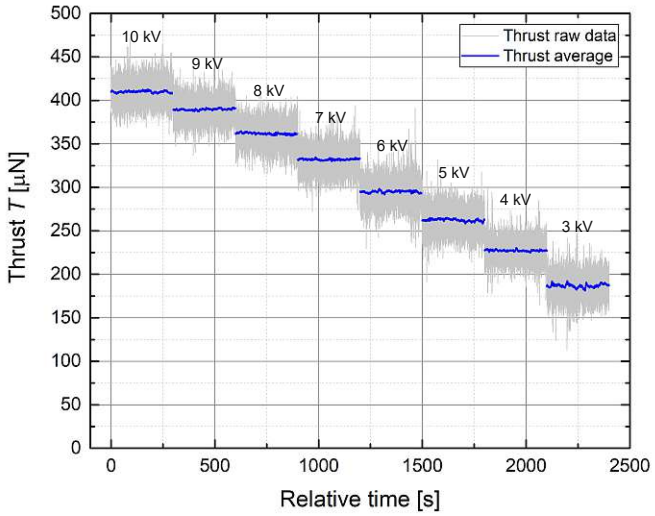

Figure 3.10: Direct thrust measurement at constant emitter current $I_{em} = 3.5\,\text{mA}$ and stepwise variation of emitter voltage V_{em} from 10 down to 3 kV.

in Figure 3.11 (left).
Figure 3.12 shows the time-dependent beam stability of an IFM Nano Thruster laboratory model with a measuring interval of 1.5 hours. Thereby, the beam divergence angle varies by less than 0.07 °.
According to section 3.2.2, the divergence coefficient γ is necessary to compute the indirect thrust. The divergence angle is related to the γ-coefficient, which is why it is examined in more detail. In Figure 3.13 the computed divergence angles α_{div} for different emitter current I_{em} values are shown. The red data points show the divergence angle at constant emitter voltage and the blue data points at constant extractor voltage. The emitter needles require a certain field strength to ignite. For this reason, with increasing emitter current the number of emitting needles increases which in turn increases the divergence angle. Furthermore, the space charge in front of the emitter increases with higher emission current, which leads to a beam widening. When comparing the two data series, a larger increase is noticeable for V_{em} constant in the range between 0.5 to 4 mA. In this series, a higher emitter current is achieved by increasing the negative extractor voltage. By increasing the negative voltage, the positive ions are drawn outwards and the beam expands, which explains the increased divergence angle.
The total beam current I_{tot} was calculated by integrating the current density of the entire beam profile and compared with the beam emission current I_{em}. The deviation between I_{tot} and I_{em} is always below 0.2 mA. In terms of percentage, the deviation decreases with increasing current, which is shown in Figure 3.14. In the nominal ion emission operating range of the IFM Nano Thruster ($2 - 4\,\text{mA}$), the deviation is always $< 5\,\%$. For lower emission currents the integration becomes less accurate over the entire beam profile. Thereby it has to be considered, that the set emitter current has an error between $6 - 150\,\mu\text{A}$. Consequently, a deviation of 24 % results for 25 μA emission

Die approbierte gedruckte Originalversion dieser Dissertation ist an der TU Wien Bibliothek verfügbar.
The approved original version of this doctoral thesis is available in print at TU Wien Bibliothek.
TU Bibliothek Your knowledge hub WIEN

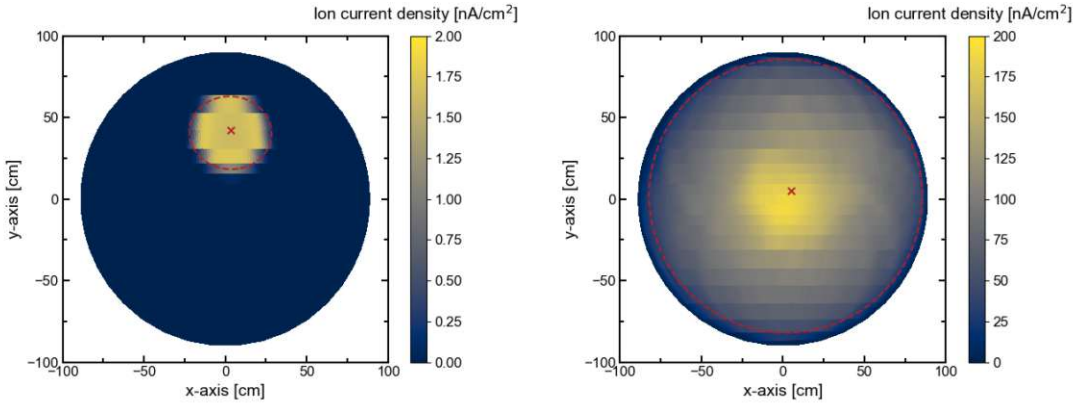

Figure 3.11: Example of beam profiles at IFM Nano Thruster emission current of $I_{em} = 5\,\mu A$ (left) and $I_{em} = 3.5\,mA$ (right).

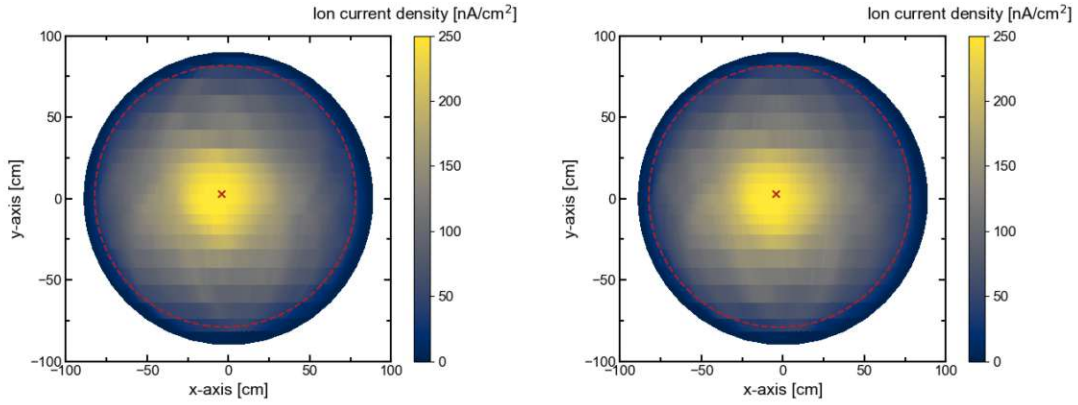

Figure 3.12: Example of beam profile stability over time with measurement interval of 1.5 h at IFM Nano Thruster emission current of $I_{em} = 3\,mA$.

current.
For the indirect thrust calculation, the γ-coefficient is calculated with equation 3.2.3 from the beam diagnostics data. With this the thrust can be computed according to equation 3.2.2.

3.4.3 Comparison of direct and indirect thrust measurement results

The direct and indirect thrust measurement results of sections 3.4.1 and 3.4.2 are compared in the following. Figure 3.15 shows thrust measurement comparison during a thruster emitter voltage sweep at constant emitter current of 3.5 mA. Both data series show a thrust increase with increased emitter voltage. According to equation 3.2.2 the thrust is proportional to the square root of the emitter voltage V_{em}. On average of all data points the measured direct thrust is $\sim 8.5\,\mu N$ larger than the indirect thrust, which

Die approbierte gedruckte Originalversion dieser Dissertation ist an der TU Wien Bibliothek verfügbar.
The approved original version of this doctoral thesis is available in print at TU Wien Bibliothek.

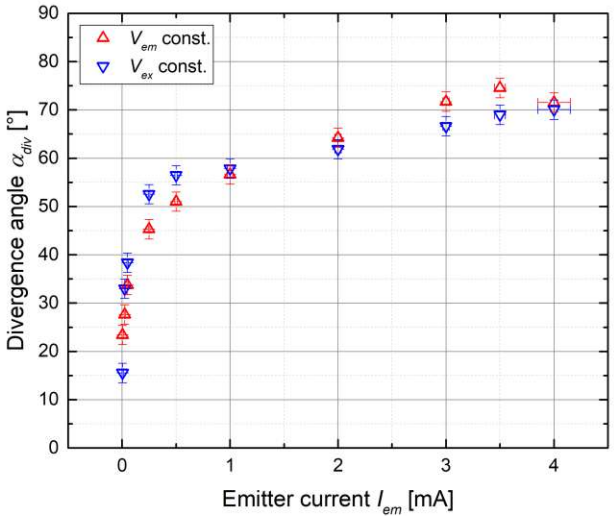

Figure 3.13: Measured divergence angle for different thruster emission currents at constant emitter voltage (red) and constant extractor voltage (blue).

corresponds to $\sim 2.8\,\%$. This inaccuracy can be explained mainly with the vertical inaccuracy of the beam diagnostics system, as the digital Faraday cups are positioned at a certain distance, as described in section 3.3.3. In future, the diagnostics system will be upgraded by using a DFC array to increase the vertical resolution. However, the beam diagnostics results are all within the accuracy range of the thrust balance ($< 20\,\mu$N). In addition to the emitter voltage sweep, an emitter current sweep was carried out as can be seen in Figure 3.16. Thereby, once the emitter voltage was kept constant and afterwards the extractor voltage. All four data series show an increase in thrust with an increase in current. According to equation 3.2.2 the thrust is proportional to the emitter current. However, the V_{ex} constant data series has a stronger thrust increase than the V_{em} constant series. This behaviour has two causes. For the data series V_{ex} constant, the emitter voltage V_{em} had to be increased to achieve a higher current. However, this value is also included in the thrust equation 3.2.2 and therefore leads to an additional thrust increase. In the data series with V_{em} constant, V_{em} has no influence on the thrust change. However, there is no linear increase in thrust with current, because the curve flattens with increased emitter current. This can be explained with the γ-coefficient, which directly depends on the divergence angle. As presented in section 3.4.2, the divergence angle increases with increasing current. Due to the widening of the beam, the cosine losses increase and thus the value of the γ-coefficient decreases.
When comparing the direct and indirect measurement results, a minimally larger value for the direct measurement is again noticeable. In the nominal emitter current range ($2 - 4\,$mA) of the laboratory IFM Nano Thruster version, in average a deviation of $\sim 4.4\,\mu$N ($\sim 1.6\,\%$) can be observed for the V_{em} constant values between direct and indirect thrust. The V_{ex} constant values have in average an increased deviation of $\sim 15.2\,\mu$N ($\sim 4.3\,\%$) in the nominal operation range. The increased deviation can be explained

Die approbierte gedruckte Originalversion dieser Dissertation ist an der TU Wien Bibliothek verfügbar.
The approved original version of this doctoral thesis is available in print at TU Wien Bibliothek.
TU Bibliothek Your knowledge hub WIEN

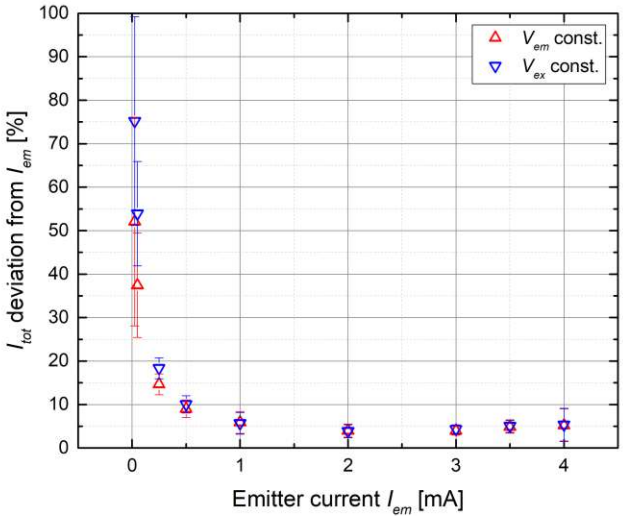

Figure 3.14: Deviation of integrated total current I_{tot} from the thruster emitter current I_{em}.

by increased current fluctuations that were detected during the test of the V_{ex} constant data series. For lower currents, the percentage deviation increases for both measurement series. This can again be explained with the vertical inaccuracy of the beam diagnostics system. Another explanation is the increased deviation of the integrated total beam current with lower emission current as described in section 3.4.2. However, all beam diagnostics values are again within the error range of the thrust balance.

Die approbierte gedruckte Originalversion dieser Dissertation ist an der TU Wien Bibliothek verfügbar.
The approved original version of this doctoral thesis is available in print at TU Wien Bibliothek.

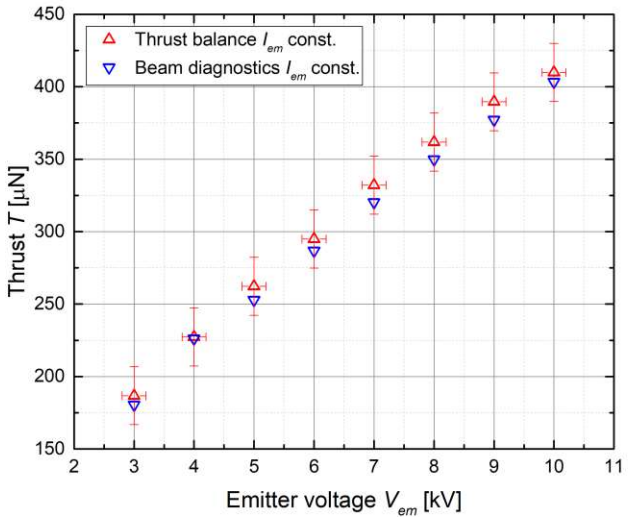

Figure 3.15: Comparison of direct (red) and indirect (blue) thrust measurements at constant thruster emitter current $I_{\mathrm{em}} = 3.5\,\mathrm{mA}$ and different emitter voltages.

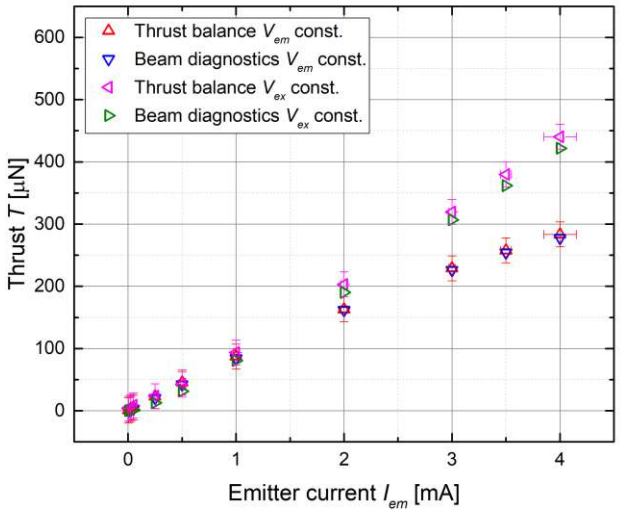

Figure 3.16: Comparison of direct and indirect thrust measurements at constant thruster emitter voltage $V_{\mathrm{em}} = 5\,\mathrm{kV}$ (red and blue) and constant extractor voltage $V_{\mathrm{ex}} = -5\,\mathrm{kV}$ (magenta ad green) at different emitter currents I_{em}.

Die approbierte gedruckte Originalversion dieser Dissertation ist an der TU Wien Bibliothek verfügbar.
The approved original version of this doctoral thesis is available in print at TU Wien Bibliothek.

3.5 Conclusion

The newly developed high-precision mN-thrust balance was presented, which achieves an accuracy of less than 2 % at six different thrust magnitudes, ranging from 10 μN to 1 N. The high accuracy is achieved by using voice coil actuators, which take advantage of the linear dependence of an applied current on the executed force. At the same time as the direct thrust measurements, indirect measurements were performed with our beam diagnostics system on an IFM Nano Thruster test module. By using both systems simultaneously, inaccuracies due to air cycles or system conversions could be prevented. The comparison of both systems has shown that they agree with an inaccuracy of less than 5 % for a thrust ranging from 50 to 450 μN. The results confirm the reliability of indirect thrust measurements for FEEP thrusters. These findings will be used in our verified electrostatic beam simulation model. This enables the thrust prediction of any new FEEP thruster geometry.

3.6 Acknowledgments

This chapter is the result of research projects funded by the European Space Agency (ESA) under the contract 4000127152/19NL/HB and the Austrian Research Promotion Agency (FFG) under the contracts 874844 and 884120.

Die approbierte gedruckte Originalversion dieser Dissertation ist an der TU Wien Bibliothek verfügbar.
The approved original version of this doctoral thesis is available in print at TU Wien Bibliothek.
TU Bibliothek Your knowledge hub WIEN

4 Performance improvements of IFM Nano Thruster with highly focused ion beam generated with a compact electrostatic lens module

This chapter corresponds to the eponymous peer-review article under review in Acta Astronautica.

The requirements for electric propulsion systems suitable for scientific missions are becoming increasingly stringent. This includes, in particular, the reduction of the beam divergence and the alignment accuracy of the thrust vector. Therefore, a modular electrostatic lens module has been developed by using an ion trajectory simulation model which considers the ion produced space charge. The focus module can be mounted on an IFM Nano Thruster with equal side length of 100 *mm and it works for the entire operation envelope without increasing the electronics complexity. Experimental beam diagnostics measurements and performance analyses are carried out on an IFM Nano Thruster laboratory model with and without attached focus module. The results show an improvement in thrust and specific impulse of up to* 30 *%. In addition, the beam divergence half-angle is drastically reduced down to* $< 20\,^\circ$ *half-angle and a high thrust vector accuracy of* $< 0.9\,^\circ$ *is achieved. In addition, the focus module significantly reduces the droplet contamination angle. With this design evolution, the IFM Nano Thruster is becoming a suitable candidate for highly complex scientific missions, such as NGGM.*

4.1 Introduction

Early 2018 the first spacecraft equipped with an IFM Nano Thruster was launched. The thruster has been developed by the research company FOTEC and is commercialised by the space tech company ENPULSION [40, 41]. Since then, over 80 IFM Nano Thrusters have been brought into space [91] and the need for electric propulsion constantly increases [92]. The IFM Nano Thruster, shown in Figure 4.1 (centre) can be used for a variety of applications, such as attitude control, station-keeping, formation flight, deorbiting or orbit raising. It is characterised by its compact and modular design suitable for CubeSats (1U). Depending on mission requirements, any number of thrusters can be clustered in various configurations. Due to this wide range of applications, it was desirable to develop an add-on focus module, in order to further increase the thruster's performance. This optimisation should include a reduction of beam divergence and an

Die approbierte gedruckte Originalversion dieser Dissertation ist an der TU Wien Bibliothek verfügbar.
The approved original version of this doctoral thesis is available in print at TU Wien Bibliothek.

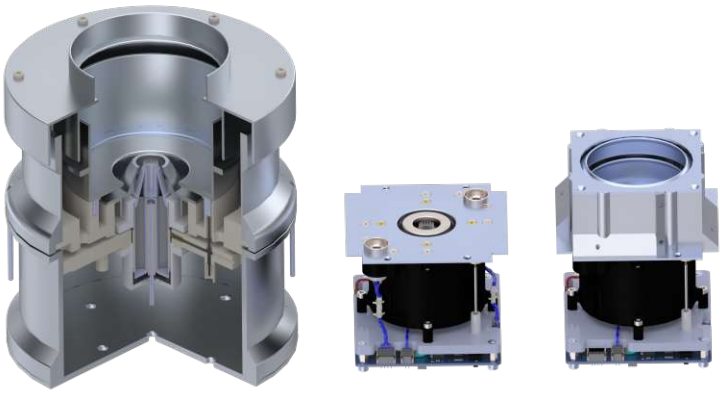

Figure 4.1: Evolution of FEEP thruster systems from IFM 350 (left), IFM Nano (centre) and the IFM Nano with attached focus module (right).

optimisation of thrust vector stability. With this, the focus module increases the range of achieving thrust and specific impulse and it prevents damage of spacecraft components. Electrostatic lenses are suitable for focusing a beam of charged particles [1]. For the development of electrostatic lenses, numerical ion trajectory simulation models are particularly suitable, in which a quick parameter variation can be performed [33, 43, 64, 93, 94]. A first focus system design for a single needle FEEP thruster was developed at the Austrian Research Center (ARC) in 2005, which was the predecessor of FOTEC. During the design phase it was identified, that a L-shape is appropriate for bending highly divergent ion trajectories [33]. The design resulted in a reduced beam divergence for emission currents up to 300 μA [33]. This geometry is also used for similar ion beam focus systems [93]. Since that time, the single needle emitters have evolved into multiemitters consisting of 28 needles. The shape of the corresponding focus system was similar to the single needle focus system. However, the system has been enlarged, resulting in a bulky and heavy structure with a diameter of 180 mm and 80 mm height [38]. This propulsion system is known as IFM 350 thruster shown in Figure 4.1 (left).
In this paper, the focus principle of the IFM 350 is transferred to an add-on module for the significantly smaller IFM Nano Thruster in order to be able to comply with the compact modular design. With a reduction of the focus system, challenges occur, such as an increased space charge. These effects were taken into account by the use of a verified simulation model during the focus module development process [43]. An IFM Nano Thruster laboratory model is experimentally tested with and without attached developed focus module, shown in Figure 4.1 (right), using FOTEC's high-precision beam diagnostics system [58]. Under the use of the accurate indirect thrust measurements demonstrated in [53], the performance for different thruster operating points is analysed. With the results presented on beam divergence and thrust vector stability, the thruster is a promising candidate for scientific missions, such as ESA's Next Generation Gravity Mission (NGGM) [75, 95].

Die approbierte gedruckte Originalversion dieser Dissertation ist an der TU Wien Bibliothek verfügbar.
The approved original version of this doctoral thesis is available in print at TU Wien Bibliothek.
TU Bibliothek Your knowledge hub WIEN

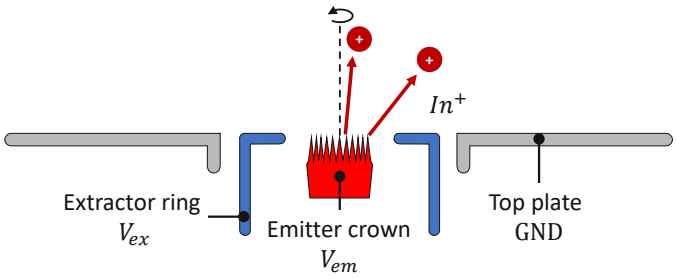

Figure 4.2: IFM Nano Thruster electrode geometry and working principle.

4.2 IFM Nano Thruster

4.2.1 Functional principle

The IFM Nano Thruster is based on decades of development of FEEP technology. The main component of the thruster is a porous tungsten crown consisting of 28 needles wetted with liquid indium. High field strengths are achieved at the needle tips due to the high potential gradient between the emitter crown and the extractor electrode, shown in the schematic drawing in Figure 4.2. With this, a so-called Taylor cone builds up on the needle tips from which ions are extracted and accelerated. Due to the use of the capillary forces of liquid metal, no pressurised tanks are required for the propellant storage and feeding. With this method, a compact design of $100 \times 100 \times 82.5\,\text{mm}$ is achieved.
The IFM Nano Thruster is equipped with two thermionic neutralisers, consisting of negatively biased filaments [62]. An electron current corresponding to the ion emission is released in order to prevent a negative charging of the spacecraft.
There are several effects that lead to a defocusing of the thruster ion beam. One of the major source of defocusing is the ion beam's own space charge [96]. Indium ions are released without initial velocity from the nm-sized Taylor cone tip. Due to the slow movement of the ions out of the emitting area, a space charge distribution is formed in front of the Taylor cone tip due to the particle's own charge. The space charge increases the potential in front of the tip, which leads to a widening of the ion beam. The higher the emitter current, the larger the space charge and the greater the beam divergence. At a certain emission current, the potential reaches a size where the ions cannot pass through.
The electrons released by the neutraliser are directed towards the positive space charge in front of the thruster generated by the ion beam. This lowers the positive coulomb potential, which counteracts the beam widening, meaning that the beam is focused using a neutraliser.
It is also known, that the Taylor cone geometry changes with the emission current [7], which is also considered in the simulation model, which will be explained in section 4.3.2.
Another defocusing effect comes from the ring-shaped extractor geometry. The emitted ions are accelerated in the direction of the extractor electrode, which leads to an increased

Die approbierte gedruckte Originalversion dieser Dissertation ist an der TU Wien Bibliothek verfügbar.
The approved original version of this doctoral thesis is available in print at TU Wien Bibliothek.
TU Bibliothek Your knowledge hub WIEN

divergence of the whole beam.
These defocusing effects can be reduced by means of an electrostatic lens system.

4.2.2 Performance characterisation

The performance of an electric propulsion system is defined by several parameters, such as thrust, specific impulse and required power. Thrust balances are typically used to determine the thrust directly. Another possibility is the indirect thrust determination by means of beam diagnostics, which works for a FEEP thruster with a high degree of accuracy [53]. Thereby, the thrust T can by calculated with

$$T = I_{\mathrm{em}} \cdot \sqrt{\frac{2m \cdot V_{\mathrm{em}}}{e}} \cdot \gamma, \tag{4.2.1}$$

where I_{em} is the emitter current, m/e the mass to charge ratio of the emitted ions, V_{em} the emitter voltage and γ the divergence efficiency. The γ-coefficient considers the beam divergence by including the cosine losses. Typically, the IFM Nano Thruster achieves a thrust ranging from $10 - 350\,\mu$N.
The specific impulse indicates how efficiently the propellant is used:

$$I_{\mathrm{sp}} = \frac{1}{g_0} \cdot \sqrt{\frac{2e \cdot V_{\mathrm{em}}}{m}} \cdot \eta_m \cdot \gamma, \tag{4.2.2}$$

where g_0 is the gravitational acceleration and η_m is the mass efficiency. Tajmar et al. established a model that describes the dependence of the mass efficiency on the emitter current [97]. With increasing emitter current the mass efficiency decreases. Compared to other electric thruster types, the IFM Nano Thruster is characterised by its high specific impulse ($2000 - 6000\,$s), which is achieved through the high particle velocity determined by V_{em}.
The propulsion system consumes a power of $8 - 40\,$W, which is composed of neutraliser consumption, heater power and PPU losses (max. 6 W) as well as beam power ($I_{\mathrm{em}} \cdot V_{\mathrm{em}}$). The power-to-thrust ratio PTR is another parameter for the performance characterisation of an electric thruster. For a FEEP thruster, the PTR depends on the emitter voltage and the divergence efficiency:

$$PTR = \frac{1}{\gamma} \cdot \sqrt{\frac{e \cdot V_{\mathrm{em}}}{2m}}. \tag{4.2.3}$$

In addition, the thruster is characterised by the properties of its crown emitter. Emitter crowns are available with different impedances, which define the emission current for a certain voltage applied [62]. Low impedance emitters are suitable for higher thrusts at lower system power. High impedance emitters require an increased power for higher thrusts, but achieve a higher specific impulse.

Die approbierte gedruckte Originalversion dieser Dissertation ist an der TU Wien Bibliothek verfügbar.
The approved original version of this doctoral thesis is available in print at TU Wien Bibliothek.
TU Bibliothek Your knowledge hub WIEN

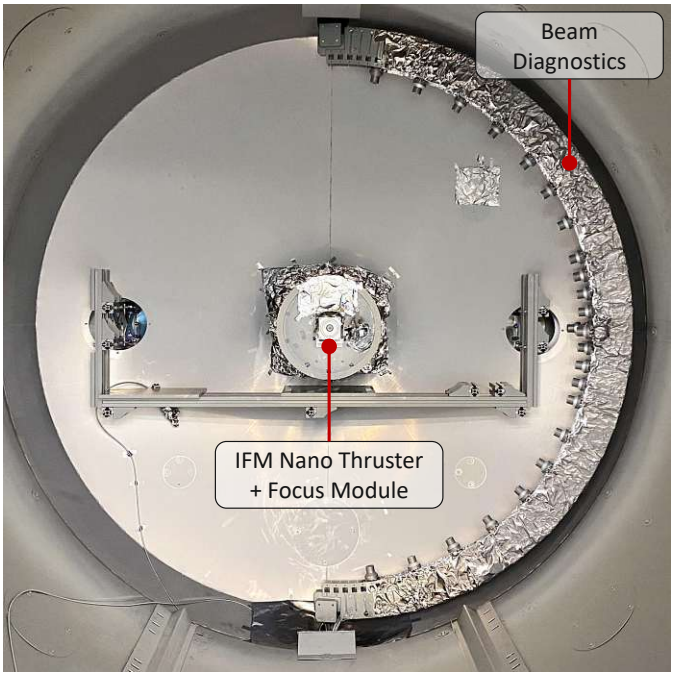

Figure 4.3: Test setup of IFM Nano Thruster with attached focus module and rotatable semi-circular beam diagnostics arm equipped with 23 digital Faraday cups.

4.3 Test setup

4.3.1 Beam diagnostics

The high precision beam diagnostics system [58] is used to analyse the beam properties of the IFM Nano Thruster laboratory model with and without attached focus module. The beam diagnostics system, shown in Figure 4.3, is located in FOTEC's large vacuum facility with a length of 3 m and 2.2 m diameter. Due to the sufficient size of the facility, no noticeable influences on the beam are expected, like charge exchange effects or beam widening due to the facility wall potential. The facility is grounded as well as the thruster housing to reduce the influence of the beam. Due to the low beam density of an IFM Nano Thruster ($\approx 10^{10}\,/\mathrm{m}^3$ [58]) no neutraliser was used.
The thruster is located in the centre of the rotatable semi-circular diagnostics arm which is equipped with 23 digital Faraday cups (DFCs). In order to obtain a higher resolution of the beam centre, the DFCs are positioned at lower spacing near the geometric centre axis. During a beam scan, the diagnostics arm moves from $-80\,^\circ$ to $+80\,^\circ$ in $1\,^\circ$ steps at a distance of 90 cm from the emitter crown. The diagnostics system measures the ion current density distribution of the entire beam, from which the main beam properties can be calculated [43, 53, 58]. This includes the thrust vector and the divergence half-angle, which describes the half-cone angle from the thrust vector that contains 95 % of

Die approbierte gedruckte Originalversion dieser Dissertation ist an der TU Wien Bibliothek verfügbar.
The approved original version of this doctoral thesis is available in print at TU Wien Bibliothek.

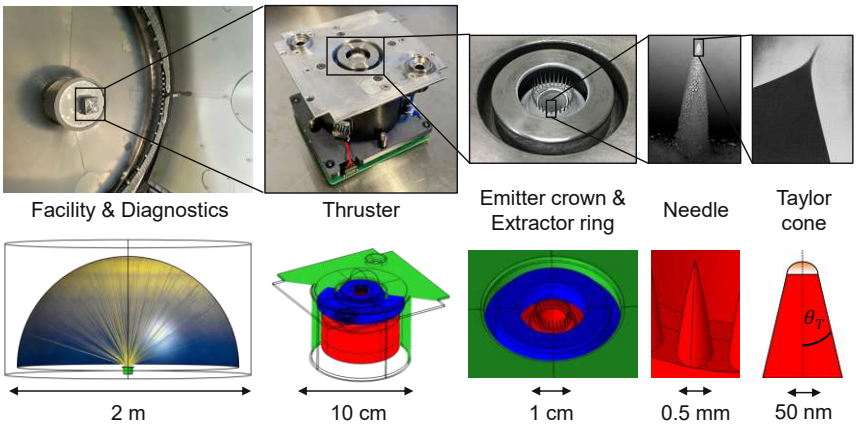

Figure 4.4: Experimental setup (top) and implementation in COMSOL ion trajectory simulation model (bottom)[2].

the total beam current. Furthermore, the generated thrust and specific impulse can be computed from the beam profile with high accuracy using equations 4.2.1 and 4.2.2 [53].

4.3.2 Simulation model

When developing an electrostatic lens system, there is a large number of possible combinations. An ion trajectory simulation model is suitable for finding the optimal combination with iterative analysis. The model, which is published in [43, 57], was set up in COMSOL Multiphysics using the AC/DC and the particle tracing modules. It is based on the experimental setup described in section 4.3.1, whereby the test facility including diagnostics system and the IFM Nano Thruster geometry is implemented, as can be seen in Figure 4.4. The indium ions are initialised at the nm-sized Taylor cone tip (indicated in orange in Figure 4.4) and their trajectories are computed numerically with the electric particle field interaction Multiphysics coupling. The particles ion current density distribution is detected on a half-sphere at a distance of 90 cm diameter, which corresponds to the curved beam diagnostics arm of the experiment. Based on the ion current density distribution, the performance parameters of the thruster can be identically calculated as in the experiment. The model computes the space charge density due to the particle movement through the mesh elements. Furthermore, it considers the change of the Taylor cone geometry according to the emission current by a calibration curve. The Taylor cone geometry is described by the half-cone angle and the jet length, by which the cone is extended. In the model both properties are combined in one parameter θ_T, which is also indicated in the Taylor cone geometry in Figure 4.4.
The first calibration of the model in [43, 57] is based on the experimental results of a single emitting needle located in the crown emitter EM1. In order to obtain a single needle, the tips of the remaining 27 needles are cut off at the very tip to minimally influ-

[2]Taylor cone picture by Praprotnik [7]

Die approbierte gedruckte Originalversion dieser Dissertation ist an der TU Wien Bibliothek verfügbar.
The approved original version of this doctoral thesis is available in print at TU Wien Bibliothek.

Table 4.1: Experimentally determined single needle beam profiles including divergence half-angle of three different emitters EM1−EM3 at emitter current $I_{\mathrm{em}} = 10\,\mu\mathrm{A}$.

	EM1	EM2	EM3
Position / $I_{\mathrm{em}} = 10\,\mu\mathrm{A}$	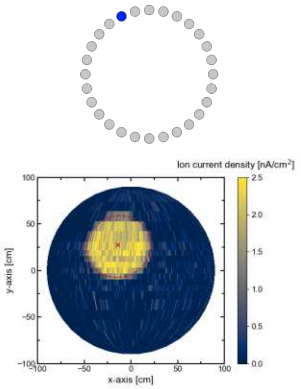	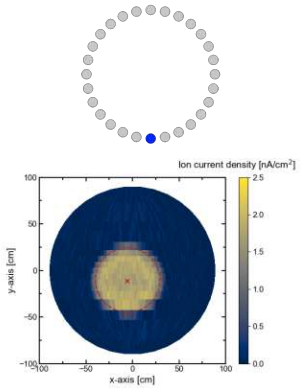	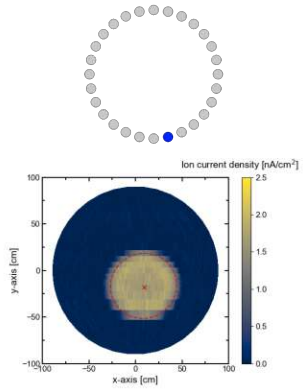
	$\alpha_{\mathrm{div}} = 23.0\,^\circ$	$\alpha_{\mathrm{div}} = 23.1\,^\circ$	$\alpha_{\mathrm{div}} = 23.7\,^\circ$

ence the electric field. In Table 4.1 the position of the remaining needle inside the crown emitter and the measured ion current density distribution at emission current of $10\,\mu\mathrm{A}$ is shown. Based on the distribution, a divergence half-angle of $23\,^\circ$ can be computed for EM1. Further results of the EM1 divergence half-angle depending on the emission current are shown in green in Figure 4.5. Measurements were only performed for low emission currents ($< 40\,\mu\mathrm{A}$). The data points show a linear distribution, from which the Taylor cone geometry θ_T was calibrated in [43]

However, the IFM Nano Thruster nominally emits $125\,\mu\mathrm{A}$ per needle. The model was therefore further enhanced on the basis of two additional emitters EM2 and EM3, which is presented the first time within this article. The beam profiles at $10\,\mu\mathrm{A}$ are shown in comparison to EM1 in Table 4.1. All three profiles have a divergence half-angle of approx. $23 - 24\,^\circ$. It has to be noted that the utilised emitters are laboratory models used for scientific research.

The divergence half-angle results for EM2 and EM3 at higher emission currents are also presented in Figure 4.5. From $0-70\,\mu\mathrm{A}$ the emitters show a linear slope of the divergence half-angle with increasing emission current. From approx. $70\,\mu\mathrm{A}$, the measurement data saturates and the divergence half-angle increases only slightly. Using the new experimental measurement data of EM2 and EM3, a second calibration curve was established that covers the entire IFM Nano Thruster emission range ($< 150\,\mu\mathrm{A}$ per needle) and above. The Taylor cone geometry is thus described with the following updated formula:

$$\theta_T\,[^\circ] = 0.473 + 37.023 \cdot e^{-0.065 \cdot I_{em}\,[\mu A]}, \tag{4.3.1}$$

Die approbierte gedruckte Originalversion dieser Dissertation ist an der TU Wien Bibliothek verfügbar.
The approved original version of this doctoral thesis is available in print at TU Wien Bibliothek.

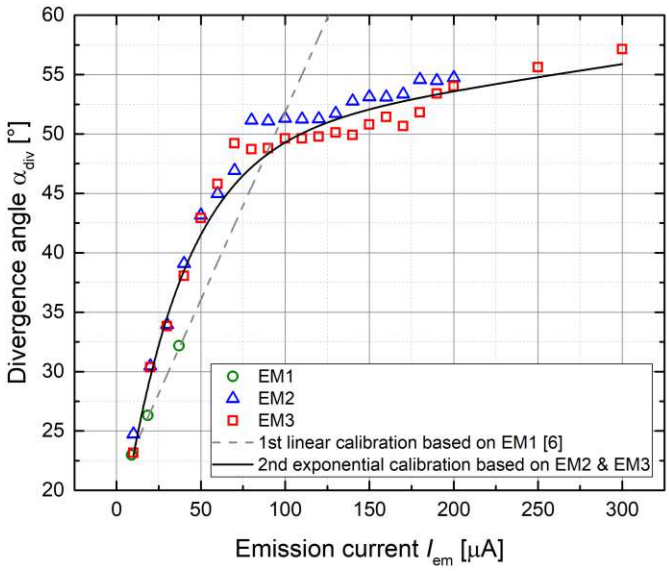

Figure 4.5: Experimental divergence half-angle of three different emitters; derived first linear calibration for simulation model based on EM1 and second exponential calibration based on EM2 and EM3.

with emitter current I_{em} per needle. More information on simulation model calibration and convergence analysis can be found in [43, 57].

4.3.3 Focus electrode module

The developed focus electrode is a stand-alone module that can be attached onto an IFM Nano Thruster and complies with the side length of 100 mm. In order to be able to use the IFM Nano Thruster electronics, the module is supplied with already available potentials.

The ion trajectory simulation model described in section 4.3.2 was used to develop the focus module. Thereby, geometric and electrostatic parameters were iteratively varied which ultimately led to the design shown in Figure 4.6. The focus module consists of two axial symmetric electrostatic lenses and an electrode shield. It is a typical tube lens consisting of a positive (converging) and a negative (diverging) lens. The converging lens is called focus electrode at potential V_{fe} and the diverging lens is called protection electrode at potential V_{pe}. Based on the previous focus electrode designs, a rotation-symmetrical L-shape is used for the focus electrode, which guides the most divergent beam portions and turns them in direction of the thruster axis [33, 38, 64, 98]. It is at the same potential as the emitter crown ($V_{fe} = V_{em}$). Due to the use of equal potentials, the system can also be classified as an einzel lens.

The protection electrode is at the same negative potential as the extractor ($V_{pe} = V_{ex}$) and is used to create a negative potential in front of the focus electrode. This prevents ambient electrons and electrons released by the neutraliser from entering the focus

Die approbierte gedruckte Originalversion dieser Dissertation ist an der TU Wien Bibliothek verfügbar.
The approved original version of this doctoral thesis is available in print at TU Wien Bibliothek.

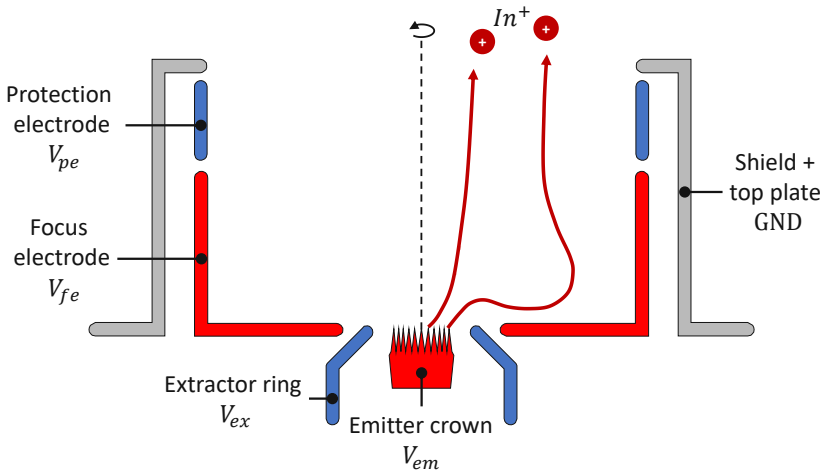

Figure 4.6: IFM Nano Thruster electrode geometry with attached focus module.

module, which in-turn protects the system from heating up. In addition, the negative potential leads to a further focusing effect. Since $V_{fe} > V_{pe}$, the ions are accelerated while passing through the module. Their velocity is lower in the area of V_{fe} than in the area of V_{pe}, which however leads to a greater focusing than defocusing effect. The grounded shield and top plate are used to shield the high voltage electrodes. Furthermore, it provides a hard limit for Indium droplets.
During the development process it was analysed that the aspect ratio of the electrodes is of particular importance. A higher beam focus is achieved by lengthening the tube lenses, which however increase the weight and complexity. Furthermore, it leads to an increased space charge, which may lead to ions trajectories that intersect the extractor electrode.
Further adjustments were carried out in the transfer of the simulation design to a mechanical design. A new extractor geometry was designed to ensure sufficient space for the focus electrode. In addition, the module is equipped with a labyrinth structure to prevent indium droplets from generating a conductive layer on internal insulators. The focus module is attached by replacing the IFM Nano top plate including extractor electrode.

The ion trajectories simulated with the COMSOL Multiphysics simulation model are shown in Figure 4.7 for the IFM Nano Thruster compared with attached focus module. The colour of the trajectories indicates the kinetic energy of the ions. The IFM Nano Thruster laboratory model, in close-up view shown in Figure 4.8 (left), is supplied with two external high-voltage power supplies. In order to test different potential configurations and measure the current at each electrode, two additional high-voltage power supplies are used to supply the focus module, shown in Figure 4.8 (right).
The two IFM Nano Thruster neutralisers were not in operation during the test, since only the pure impact of the focus module had to be investigated. As explained in section 4.2.1 the neutralisers would lead to an additional focus effect.

Die approbierte gedruckte Originalversion dieser Dissertation ist an der TU Wien Bibliothek verfügbar.
The approved original version of this doctoral thesis is available in print at TU Wien Bibliothek.
TU Bibliothek Your knowledge hub WIEN

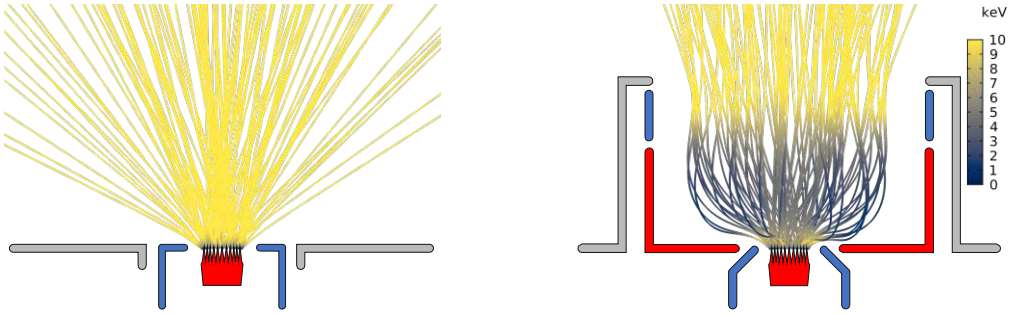

Figure 4.7: Simulated ion trajectories of IFM Nano Thruster (left) and with attached focus module (right).

Figure 4.8: Close-up view of IFM Nano Thruster laboratory model (left) and with attached focus module (right).

4.4 Experimental performance measurements

Beam profile measurements were carried out using the setup described in section 4.3.1. First, the required voltages at extractor and protection electrode are identified, along the with the total emitted current. In addition, the spherical and 1D beam profile of the IFM Nano Thruster model with and without attached focus module are shown and the key beam properties are analysed. Afterwards, performance analyses are carried out for both systems, including thrust, specific impulse and beam power.

4.4.1 Determination of operation points

As described in section 4.3.3, when a tube lens is lengthened, the space charge can become significant enough to cause ions to be accelerated back towards the extractor electrode. Thus, the ions would not be able to leave the focus module and would not be registered on the diagnostic system. Therefore, the emitted current I_{em} is compared with the measured total beam current I_{tot}, which is computed by integrating the ion current density on the half-sphere detector surface. The measured total currents for

Die approbierte gedruckte Originalversion dieser Dissertation ist an der TU Wien Bibliothek verfügbar.
The approved original version of this doctoral thesis is available in print at TU Wien Bibliothek.

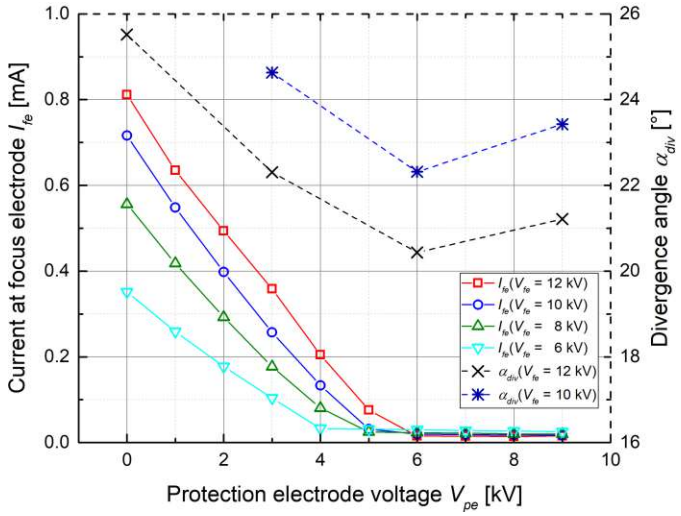

Figure 4.9: Measured current at focus electrode I_{fe} at a voltage sweep at the protection electrode V_{pe} for different focus electrode voltages $V_{\mathrm{fe}} = V_{\mathrm{em}}$.

both configurations show a maximum variation of 0.2 mA from the emitted current. All deviations are smaller than the experimentally determined accuracy of $< 5\,\%$ of the diagnostics system [53].

In Figure 4.9 it is analysed which negative voltage is required at the protection electrode to prevent electrons from outside entering the focus module. For this purpose, a voltage sweep was carried out at the protection electrode V_{pe} and the current at the focus electrode I_{fe} was measured at the same time. The sweep was performed for different focus electrode voltages $V_{\mathrm{fe}} = V_{\mathrm{em}}$. The higher the voltage at the focus electrode, the higher is the measured current I_{fe}. This means that the higher V_{fe}, the more electrons are attracted. All measurements show that no significant current is measured at the focus electrode above a negative voltage at the protection electrode of $V_{\mathrm{pe}} = -6\,\mathrm{kV}$. Furthermore, in Figure 4.9 the divergence half-angle was observed for different protection electrode voltages and two different focus electrode voltages. For both focus voltages the divergence half-angle reaches a minimum at $-6\,\mathrm{kV}$. Due to these two reasons, $-6\,\mathrm{kV}$ is applied to the protection electrode for all measurements.

The required extractor voltage to emit a certain current with and without attached focus module is compared in Figure 4.10. The emitter voltage respectively the focus electrode voltage was kept constant ($V_{\mathrm{em}} = V_{\mathrm{fe}} = \mathrm{const.}$) for each measurement series. The higher the current to be emitted, the higher the required extractor voltage. When a lower emitter voltage is applied, a correspondingly higher extractor voltage is required. When comparing the required extractor voltage with and without focus for $V_{\mathrm{em}} = 10\,\mathrm{kV}$, it can be identified that the value is similar with maximum deviation of 0.7 kV. With lower emitter voltages, a higher extractor voltage is required when using the focus module. However, with a higher emitter voltage, a lower extractor voltage is required by using

Die approbierte gedruckte Originalversion dieser Dissertation ist an der TU Wien Bibliothek verfügbar.
The approved original version of this doctoral thesis is available in print at TU Wien Bibliothek.

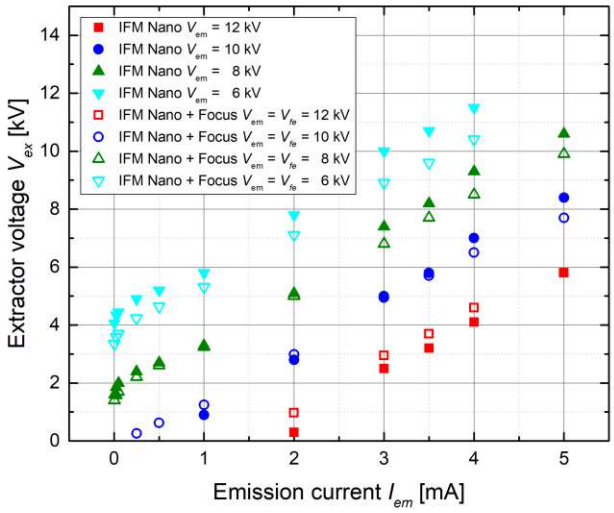

Figure 4.10: Required extractor voltage V_{ex} to achieve a certain emitter current I_{em} for different emitter electrode voltages V_{em} with and without attached focus module.

the focus module. This means that there are no significant differences in required power when using the focus module.

4.4.2 Beam profile comparison

In order to visualise the beam profiles, the spherically recorded measurement data is projected on Cartesian coordinates. An example of the IFM Nano Thruster test model beam profile at nominal emitter current of 3.5 mA can be seen in Figure 4.11 (left). The calculated thrust vector is indicated with a cross and the divergence half-angle with a dashed circle. In this case the calculated thrust vector misalignment is 2.6 ° from the thruster geometric centre. The divergence half-angle amounts to 59.7 °. When comparing the beam profile at the same thruster operation point ($I_{\mathrm{em}} = 3.5\,\mathrm{mA}$, $V_{\mathrm{em}} = 12\,\mathrm{kV}$) with attached focus module, as shown in Figure 4.11 (right) a drastic reduction of the divergence half-angle by $\approx 40\,°$ is achieved. The thrust vector misalignment reduces to 0.2 ° and the divergence half-angle to 20.3 °. The profile shows a circular distribution with sharp edges.

In order to be able to examine the structure of the profiles more precisely, the angular ion current density distribution of a horizontal cut through the profiles of Figure 4.11 is shown in Figure 4.12. The beam profile of the IFM Nano Thruster laboratory module shows a symmetrical distribution, without sharp edges since the individual circular single needle profiles are overlapping. The beam profile generated with the focus module has a steep increase at $-23\,°$ and a steep decrease at $+23\,°$. A parabolic structure ranges from $-13\,°$ to $+13\,°$, which fades into sharp spikes at $-18\,°$ and $+18\,°$. The spikes originate from the ion trajectories that were least affected by the focus module, which

Die approbierte gedruckte Originalversion dieser Dissertation ist an der TU Wien Bibliothek verfügbar.
The approved original version of this doctoral thesis is available in print at TU Wien Bibliothek.
TU Bibliothek Your knowledge hub WIEN

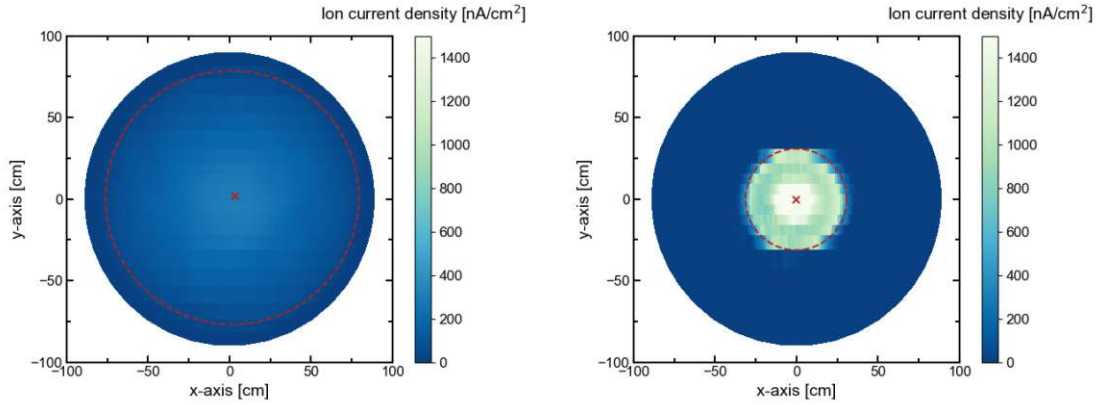

Figure 4.11: Beam profile of IFM Nano Thruster laboratory model (left) and with attached focus module (right) at emitter current of $I_{em} = 3.5\,\text{mA}$ and emitter voltage of $V_{em} = 12\,\text{kV}$.

was identified with the ion trajectory simulation model. The maximum ion current density in the centre of the profile with attached focus module is six times higher than without. This is due to the fact that the total current is distributed over a significantly smaller area.

4.4.3 Key beam properties comparison

The beam properties shown visually in the beam profiles of section 4.4.2 are analysed in more detail by varying the emitter current and voltage. Figure 4.13 shows the divergence half-angle as a function of the emitter current for different emitter voltages. The filled data points represent the results of the beam produced by the IFM Nano Thruster laboratory model. With increasing emitter current the divergence half-angle increases due to the increased space charge in front of the needle tips, which is described in section 4.2.1. Furthermore, the divergence half-angle increases with lower emitter voltage and higher extractor voltage respectively. This can be explained with the ring-shaped extractor geometry, which leads to a widening of the beam, also described in section 4.2.1. Overall, the divergence half-angle ranges from 59 ° to 71 ° for the IFM Nano Thruster laboratory model.

When comparing the results with the unfilled data points of the attached focus module a similar behaviour can be observed which can be attributed to the same explanations. For all operating points, the focus module leads to a reduction of the beam divergence by $41 \pm 2.3\,°$. With the use of the focus module, the divergence half-angle ranges from 19 ° to 27 °. In conclusion, the most focused beam is achieved by applying a high emitter voltage and low emitter current.

A further divergence half-angle investigation was carried out in Figure 4.14 at constant emitter current $I_{em} = 3.5\,\text{mA}$ for different emitter voltages. When comparing the results of the IFM Nano Thruster test module with and without attached focus module, it is

Die approbierte gedruckte Originalversion dieser Dissertation ist an der TU Wien Bibliothek verfügbar.
The approved original version of this doctoral thesis is available in print at TU Wien Bibliothek.

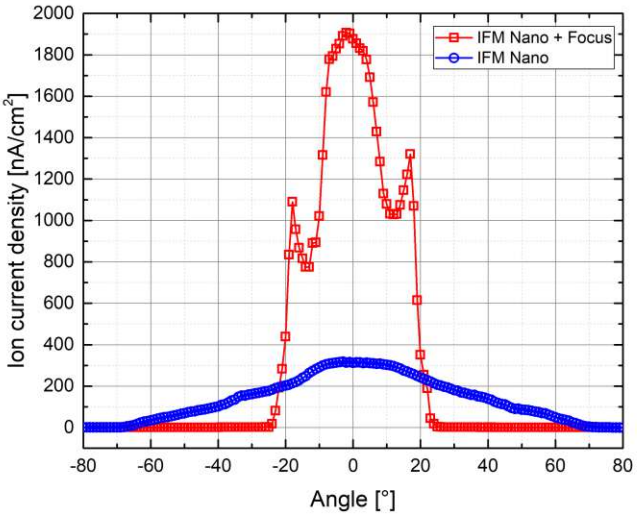

Figure 4.12: Angular ion current density distribution at horizontal cut through spherical beam profile for IFM Nano Thruster with and without attached focus module at $I_{em} = 3.5\,\text{mA}$ and $V_{em} = 12\,\text{kV}$.

noticeable that the divergence half-angle decreases linearly with the emitter voltage in both cases. The slope without focus module ($m = -1.7$) is larger than that with focus module ($m = -1.1$), calculated for data points from $6 - 12\,\text{kV}$. The lower slope is caused by the fact that the focus module counteracts the extractor beam widening effect. When looking at the divergence half-angle with attached focus module, it is noticeable that at the lowest emitter voltage $V_{em} = 5\,\text{kV}$ a re-focusing occurs. As shown in Figure 4.6, the most divergent trajectories are most affected by the focus module. This could be an explanation for the more efficiently focusing at the lowest beam power in Figure 4.14. In the future, it will be investigated in more detail what occurs at even lower emitter voltages, since then the thruster can be operated with minimum power.

The thrust vector direction can be described with the off-axis angle, which is the angle between the thrust vector and the thruster geometrical centre axis. In Figure 4.15 the measured off-axis angle as function of the emitter current for different emitter voltages can be seen. The off-axis angle varies from $2.2\,^\circ$ to $4.4\,^\circ$. This deviation from $0\,^\circ$ can be explained by a slight misalignment between emitter crown and extractor ring during the assembly of the thruster laboratory model. The unfilled data points obtained with the attached focus module show an angle which is always smaller than $0.9\,^\circ$. This is also the case when emission from some needles ceases at a lower current or if the current is not equally balanced between the needles. This means that the focus module realigns the beam with the geometrical axis of the thruster and therefore compensates slight mechanical inaccuracies during thruster assembly.

Die approbierte gedruckte Originalversion dieser Dissertation ist an der TU Wien Bibliothek verfügbar.
The approved original version of this doctoral thesis is available in print at TU Wien Bibliothek.
TU Bibliothek Your knowledge hub WIEN

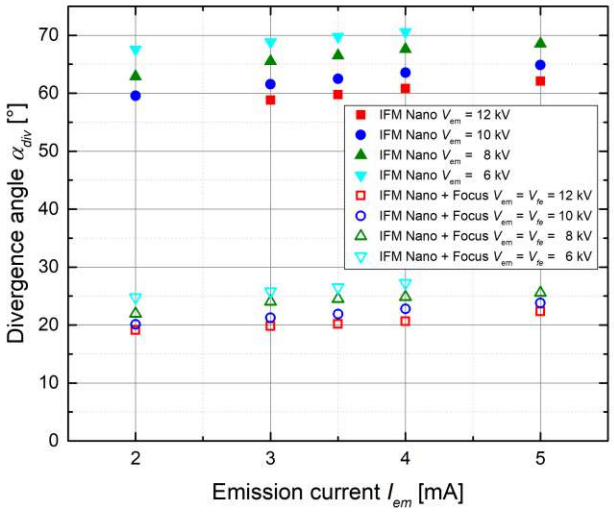

Figure 4.13: Divergence half-angle α_{div} as a function of the emitter current I_{em} for different emitter voltages V_{em} for IFM Nano Thruster with and without attached focus module.

4.4.4 Performance comparison

The performance of an electric propulsion thruster is typically described by a performance map shown in Figure 4.16 created for the IFM Nano Thruster laboratory model and with attached focus module. Thrust computations were carried out using equation 4.2.1 with the divergence efficiency γ calculated from the beam diagnostics measurements. The specific impulse was computed with equation 4.2.2 using the described mass efficiency model for a tip radius of 2 μm and also the γ-coefficient from the beam measurements. The performance map was generated by varying the emitter current I_{em} and the electrode voltages of emitter V_{em} and extractor V_{ex}. The focus electrode voltage again corresponds to the emitter voltage $V_{\mathrm{fe}} = V_{\mathrm{em}}$ and the protection electrode was constantly at -6 kV.
When comparing the performance map of the IFM Nano Thruster test model and the focus module in Figure 4.16, it is obvious that the performance covers a wider area by using equal beam power. The thrust range increase up to 815 μN compared to 665 μN and the specific impulse ranges from $3600 - 10300$ s compared to $2700 - 8000$ s. Both parameters improve by the same percentage, since voltage and current are included in equations 4.2.1 and 4.2.2 in the same ratio, whereby in equation 4.2.2 the current is included in the mass efficiency. Both the thrust and the specific impulse increase by up to 32 %. Furthermore, the required power to reach a certain thrust PTR decreases with the focus module. When looking at the nominal operation point (cyan) at 35 W it can also be seen that a higher thrust and specific impulse can be achieved. Customised operation is enabled in the entire area of the performance map depending on the available beam power.

Die approbierte gedruckte Originalversion dieser Dissertation ist an der TU Wien Bibliothek verfügbar.
The approved original version of this doctoral thesis is available in print at TU Wien Bibliothek.

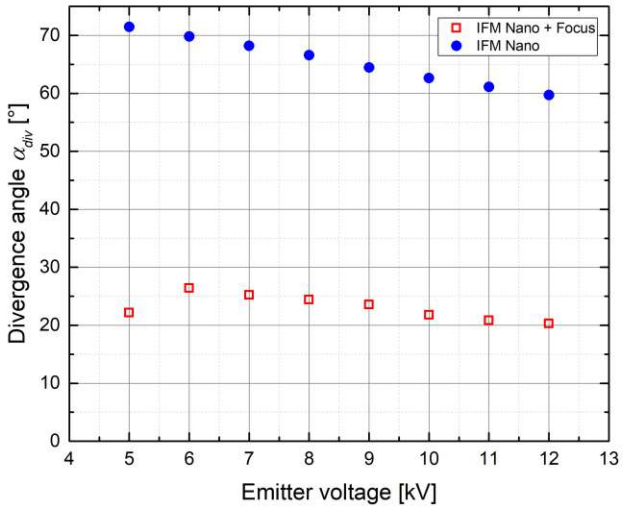

Figure 4.14: Divergence half-angle α_{div} as a function of the emitter voltage V_{em} at constant emitter current $I_{\mathrm{em}} = 3.5\,\mathrm{mA}$ for IFM Nano Thruster with and without attached focus module.

The red data points in Figure 4.16 (right) are intended to show that the entire thrust range can be covered by using only two HV supplies. Here the extractor voltage was equal to the protection electrode voltage ($V_{\mathrm{ex}} = V_{\mathrm{pe}} = -6\,\mathrm{kV}$). The thrust was changed by changing the emitter voltage ($V_{\mathrm{em}} = V_{\mathrm{fe}}$) from 5 to 12 kV in steps of 1 kV. Thereby, the produced thrust is in the upper specific pulse range of an IFM Nano Thruster.

Die approbierte gedruckte Originalversion dieser Dissertation ist an der TU Wien Bibliothek verfügbar.
The approved original version of this doctoral thesis is available in print at TU Wien Bibliothek.

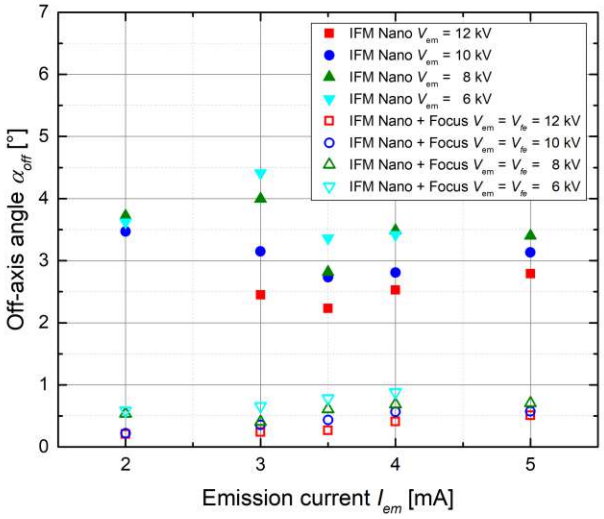

Figure 4.15: Off-axis angle α_{off} as function of the emitter current I_{em} for different emitter voltages V_{em} for IFM Nano Thruster with and without attached focus module.

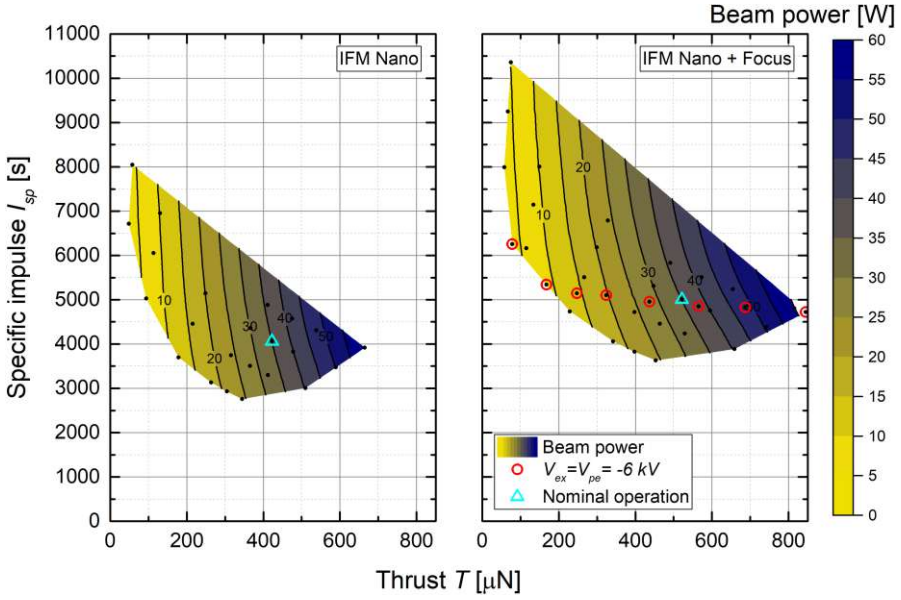

Figure 4.16: IFM Nano Thruster laboratory model performance map without (left) and with attached focus module (right).

Die approbierte gedruckte Originalversion dieser Dissertation ist an der TU Wien Bibliothek verfügbar.
The approved original version of this doctoral thesis is available in print at TU Wien Bibliothek.

4.5 Conclusion

An evolutionary focus module for the IFM Nano Thruster was developed, which is consistent with the modular design due to its compact dimensions of $100 \times 100\,\mathrm{mm}$ and its flexible interchangeability. The module was developed using a verified ion trajectory simulation model. Since the simulation model considers the space charge of the emitting ions, a compact focus design could be developed. With this the height of the IFM Nano Thruster with attached focus module is increased by only 42 mm and by an additional weight of less than 300 g.
Experimental beam diagnostics measurements were carried out to investigate the beam characteristics and performance of an IFM Nano Thruster laboratory model with and without attached focus module. The module achieves up to 30 % higher performance, i.e. thrust and specific impulse, with the same available power. In addition, it was demonstrated that the already available two high voltage supplies are sufficient to cover a thrust range up to $800\,\mu\mathrm{N}$ in the upper specific impulse range. This means that the available IFM Nano Thruster electronics can be reused also with attached focus module. Furthermore, it was observed that by using the focus module the beam divergence can be reduced by $41 \pm 2.3\,^\circ$ to an angle of less than $20\,^\circ$. This allows the IFM Nano Thruster to be competitive with other electrical propulsion systems that can generate highly focused beams, such as gridded ion thrusters. In addition, the thrust vector misalignment from the geometric centre axis was measured, which was for all measurements with focus module below $0.9\,^\circ$. This compensates, for example, the varying emission levels of individual needles or alignment inaccuracies during the assembly. It was also shown that the ion trajectory focusing is effective for all IFM Nano Thruster operating points. With these performance and beam characteristics, the IFM Nano Thruster is a promising candidate for scientific missions, such as NGGM. Here it is suitable for both required propulsion systems, as main propulsion in a clustered version for drag compensation and as single module for fine attitude control. In the future, the newly developed focus module will be tested for its longevity before it is passed on for commercialisation. Furthermore, the IFM Nano Thruster neutralisers will be integrated at two facing corners of the focus module.

4.6 Acknowledgments

This chapter is the result of research projects funded by the European Space Agency (ESA) under the contract 4000127152/19NL/HB and the Austrian Research Promotion Agency (FFG) under the contract 874844.

Die approbierte gedruckte Originalversion dieser Dissertation ist an der TU Wien Bibliothek verfügbar.
The approved original version of this doctoral thesis is available in print at TU Wien Bibliothek.
TU Bibliothek Your knowledge hub WIEN

5 Conclusion and outlook

At the beginning of this work, an IFM Nano Thruster laboratory model was experimentally characterised in high detail. This includes direct thrust measurements using a torsion thrust balance and beam diagnostics analyses using a system of Faraday cups and a retarding potential analyser. Based on the measured spatial ion current density and kinetic energy distribution, beam properties could be determined, like divergence angle, thrust vector alignment and indirect thrust. A novel FEEP simulation model was developed using COMSOL Multiphysics, including the ion emission from a nm-sized tip and the computation of its trajectories to the diagnostics system in 1 m distance. The simulation model was setup based on empirical equations that could be established from the experimental results.
With the simulation model, the ion beam of an entire IFM Nano Thruster was simulated three-dimensional for all thruster operation points. Due to its excellent agreement with the experiment, the simulation model was used to optimise the beam properties of the IFM Nano Thruster by developing an electrostatic focus system. The optimised thruster was manufactured and experimentally characterised. It resulted in an optimisation of the thrust efficiency of 30 % and a reduction of the beam divergence from 60 ° to 20 °, as well as a thrust vector stability improvement from $< 5\,^\circ$ degrees to $< 0.9\,^\circ$ degrees. The results obtained were exactly in line with the predictions of the simulation model.
The performance of an IFM Nano Thruster laboratory model without and with attached newly developed focus module was characterised for all operation points. A next step to bring the focus module to commercialisation would be further optimisation for space qualification, such as lifetime test, vibration and shock test and detailed performance characterisation. Since the developed focus electrode is particularly distinguished by its modularity, performance tests in a clustered configuration could be carried out.
Moreover, in the future, the simulation model could be used to develop further FEEP thruster designs to be compliant with certain mission requirements. For example, the model could be the basis for developing a fine positioning thruster for the Next Generation Gravity Mission (NGGM) [75]. Thereby, the nominal thrust has to be increased from 350 μN up to 500 μN, the beam divergence angle reduced from 60 ° to 30 ° and a thrust vector stability of $< 0.1\,^\circ$ needs to be achieved [99]. The developed focus module is already partly compliant with these requirements and can be further optimised under the use of the developed ion trajectory simulation model. In addition, multiply thrusters could be clustered, whereby the results of the above mentioned clustered lifetime test could deliver inputs. Not only achieving the thrust vector stability of $< 0.1\,^\circ$ will be a challenge, but also the ability to resolve it with the available beam diagnostics system. Therefore, a stationary array consisting of $n \times n$ digital Faraday cups could be developed to resolve the thrust vector variation with a measurement frequency > 10 Hz.

Die approbierte gedruckte Originalversion dieser Dissertation ist an der TU Wien Bibliothek verfügbar.
The approved original version of this doctoral thesis is available in print at TU Wien Bibliothek.
TU Bibliothek Your knowledge hub WIEN

In the electric propulsion area, scalability plays a particularly important role. For this purpose, the simulation model could be used to scale a FEEP thruster geometry arbitrarily to achieve a certain thrust. There would be a wide range of parameters that could be varied. For example, various thruster operation parameters, such as lower emitter voltages to reduce the power consumption. Furthermore, the emitter needles could be arranged hexagonally or linearly in rows. In order to increase the thrust value, the number of needles could be increased. With the increase in the number of needles, the emitted current would also raise, which would lead to a beam broadening due to the increasing space charge in front of the thruster. This influence could be analysed in detail by using the simulation model. When increasing the space charge, it is particularly necessary to counteract this by neutralisation. Neutralisation of spacecraft takes place through the emission of electrons. The implementation of electron trajectories would therefore be a possible further extension of the simulation model.
In addition to the emission of ions, droplets are also emitted by a FEEP thruster. For the future it is planned to investigate the spatial distribution of indium droplets, using a quartz crystal micro balance. These experimental observations could provide a basis for the implementation of droplets in the simulation model.
It can be concluded that the model offers a wide range of possible applications and will play a major role in the future development of the FEEP technology.

Die approbierte gedruckte Originalversion dieser Dissertation ist an der TU Wien Bibliothek verfügbar.
The approved original version of this doctoral thesis is available in print at TU Wien Bibliothek.
TU Bibliothek Your knowledge hub WIEN

Bibliography

[1] J. Orloff, M. Utlaut, L. Swanson, High Resolution Focused Ion Beams FIB and its Applications, Springer, 2003. doi:10.1007/978-1-4615-0765-9.

[2] G. Taylor, Disintegration of Water Drops in an Electric Field, Proc. R. Soc. London (280 (1964) 383). doi:10.1098/rspa.1964.0151.

[3] A. E. Bell, L. W. Swanson, Mechanisms of liquid metal ion source operation, Nucl. Instrum. Methods Phys. Res. (10 (1985) 783-787). doi:10.1016/0168-583X(85)90107-7.

[4] R. Gomer, On the mechanism of liquid metal electron and ion sources, Appl. Phys. A: Mater. Sci. Process. (19 (1979) 365). doi:10.1007/BF00930099.

[5] D. R. Kingham, L. W. Swanson, Shape of a Liquid Metal Ion Source, Appl. Phys. A: Mater. Sci. Process. (34 (1984) 123). doi:10.1007/BF00614764.

[6] N. N. Ljepojevic, R. G. Forbes, A comparison of the numerical and analytical treatments of a liquid-metal ion source, Surf. Sci. (266 (1992) 170). doi:10.1016/0039-6028(92)91017-6.

[7] B. Praprotnik, W. Driesel, C. Dietzsch, H. Niedrig, HV-TEM in-situ investigations of the tip shape of indium liquid metal ion emitter, Surf. Sci. (314 (1994) 353-364). doi:10.1016/0039-6028(94)90237-2.

[8] G. L. R. Mair, R. G. Forbes, An analytical calculation of LMIS cusp length, Surf. Sci. (266 (1992) 180-184). doi:10.1016/0039-6028(92)91018-7.

[9] R. G. Forbes, N. N. Ljepojevic, Calculation of the shape of the liquid cone in a liquid-metal ion source, Surf. Sci. (246 (1991) 113-117). doi:10.1016/0039-6028(91)90401-D.

[10] G. L. R. Mair, R. G. Forbes, Analytical determination of the dimensions and evolution with current of the ion-emitting jet in liquid-metal ion sources, J. Phys. D: Appl. Phys. (24 (1991) 2217-2221). doi:10.1088/0022-3727/24/12/014.

[11] R. I. Hornsey, A unified description of liquid metal ion source energy distribution, J. Phys. Colloq. (50 (1989) C8-197-C8-202). doi:10.1051/jphyscol:1989834.

[12] W. Knauer, Analysis of Energy Broadening in Electron and Ion Beams, Optik (54 (1979) 211-234).

Die approbierte gedruckte Originalversion dieser Dissertation ist an der TU Wien Bibliothek verfügbar.
The approved original version of this doctoral thesis is available in print at TU Wien Bibliothek.
TU Bibliothek Your knowledge hub WIEN

[13] G. L. R. Mair, Beam-energy distribution measurements of liquid gallium field-ion sources, J. Phys. D: Appl. Phys. (16 (1983) L209). doi:10.1088/0022-3727/16/10/006.

[14] C. Bartiol, A review of the past and present research on ion field emission, in: ESTEC Field Emission Day, no. ESA-SP-119, 1977, pp. 1–9.

[15] F. G. Rüdenauer, W. Steiger, H. Studnicka, P. Pollinger, Mass and energy spectra of a capillary-type indium liquid-metal ion source, Int. J. Mass Spectrom. Ion Processes 77 (1) (1987) 63–74. doi:10.1016/0168-1176(87)83024-0.

[16] R. Schmidt, H. Arends, A. Pedersen, M. Fehringer, F. Rüdenauer, W. Steiger, B. T. Narheim, R. Svenes, K. Kvernsveen, K. Tsuruda, H. Hayakawa, M. Nakamura, W. Riedler, K. Torkar, A novel medium-energy ion emitter for active spacecraft potential control, Rev.of Sci. Instrum. 64 (8) (1993) 2293–2297. doi:10.1063/1.1143924.

[17] K. Tsuruda, H. Hayakawa, M. Nakamura, T. Okada, A. Matsuoka, F. S. Mozer, R. Schmidt, Electric Field Measurements on the GEOTAIL Satellite, J. Geomag. Geoelec. 46 (8) (1994) 693–711. doi:10.5636/jgg.46.693.

[18] K. Torkar, W. Riedler, M. Fehringer, F. Rüdenauer, C. P. Escoubet, H. Arends, B. T. Narheim, K. Svenes, M. P. McCarthy, G. K. Parks, R. P. Lin, H. Rème, Spacecraft potential control aboard Equator-S as a test for Cluster-II, Ann. Geophys. 17 (12) (1999) 1582–1591. doi:10.1007/s00585-999-1582-3.

[19] K. Torkar, H. Arends, W. Baumjohann, C. P. Escoubet, A. Fazakerley, M. Fehringer, G. Fremuth, H. Jeszenszky, G. Laky, B. T. Narheim, W. Riedler, F. Rüdenauer, W. Steiger, K. Svenes, H. Zhao, Spacecraft potential control for Double Star, Ann. Geophys. 23 (8) (2005) 2813–2823. doi:10.5194/angeo-23-2813-2005.

[20] K. Torkar, R. Nakamura, M. Tajmar, C. Scharlemann, H. Jeszenszky, G. Laky, G. Fremuth, C. P. Escoubet, K. Svenes, Active Spacecraft Potential Control Investigation, Space Sci. Rev. 199 (1-4) (2014) 515–544. doi:10.1007/s11214-014-0049-3.

[21] N. S. Mühlich, H. Jeszenszky, J. F. G. Fremuth, J. Gerger, F. Plesescu, M. Steller, B. Seifert, R. Nakamura, F. Cipriani, Development and Coupling Test of Active Spacecraft Potential Control - Next Generation (ASPOC-NG), submitted to Rev. Sci. Instrum.

[22] M. Fehringer, F. Rüdenauer, W. Steiger, Space-Proven Indium Liquid Metal Field Ion Emitters for Ion Microthruster Applications, in: 33rd JPC, no. AIAA 97-3057, Seattle, 1997.

[23] M. Fehringer, F. Rüdenauer, W. Steiger, Indium liquid-metal ion sources as micronewton thrusters, in: AIP Conf. Proc., 1998. doi:10.1063/1.57413.

Die approbierte gedruckte Originalversion dieser Dissertation ist an der TU Wien Bibliothek verfügbar.
The approved original version of this doctoral thesis is available in print at TU Wien Bibliothek.
TU Bibliothek Your knowledge hub WIEN

[24] A. Genovese, W. Steiger, M. Tajmar, Indium FEEP Microthruster: Experimental Characterization in the 1-100 μN Range, in: 37th JPC, no. AIAA 2001-3788, 2001.

[25] A. Genovese, M. Tajmar, W. Steiger, F. Rüdenauer, Indium FEEP Endurance Test: Preliminary Results, in: 27th IEPC, no. IEPC-01-289, 2001.

[26] M. Tajmar, W. Steiger, A. Genovese, Indium FEEP Thruster Beam Diagnostics, Analysis and Simulation, in: 37th JPC, 2001.

[27] C. Scharlemann, A. Genovese, N. Buldrini, R. Schnitzer, M. Tajmar, H. Früholz, R. Killinger, Status of the Indium FEEP Micropropulsion Subsystem Development for LISA Pathfinder, in: 30th IEPC, no. IEPC-2007-122, 2007.

[28] C. Scharlemann, A. Genovese, N. Buldrini, R. Schnitzer, M. Tajmar, H. Früholz, R. Killinger, Development and Test of an Indium FEEP Micropropulsion Subsystem for LISA Pathfinder, in: 43rd JPC, American Institute of Aeronautics and Astronautics, 2007. doi:10.2514/6.2007-5251.

[29] C. Scharlemann, M. Tajmar, A. Genovese, N. Buldrini, R. Schnitzer, In-FEEP Qualification Test Program for LISA Pathfinder, in: 44th JPC, American Institute of Aeronautics and Astronautics, 2008. doi:10.2514/6.2008-4825.

[30] C. Scharlemann, A. Genovese, R. Schnitzer, N. Buldrini, P. Sattler, M. Tajmar, R. Killinger, H. Früholz, Test results of the qualification tests for the In-FEEP technology for LISA PF, in: 31st IEPC, no. IEPC-2009-050, 2009.

[31] C. Scharlemann, N. Buldrini, R. Killinger, M. Jentsch, A. Polli, L. Ceruti, L. Serafini, D. DiCara, D. Nicolini, Qualifciation test series of the indium needle FEEP micro-propulsion system for LISA Pathfinder, Acta Astronaut. 69 (9-10) (2011) 822–832. doi:10.1016/j.actaastro.2011.05.037.

[32] C. Scharlemann, N. Buldrini, R. Killinger, D. DiCara, Test of a novel FEEP emitter with LISA PF hardware, in: 33rd IEPC, 2013.

[33] I. Vasiljevich, M. Tajmar, N. Buldrini, A. Genovese, K. Marhold, Development of a Focus Electrode for an Indium FEEP Thruster, in: 41st JPC, AIAA, 2005. doi:10.2514/6.2005-4384.

[34] N. Buldrini, A. Genovese, M. Tajmar, In-FEEP Cluster for LISA Pathfinder, in: 29th IEPC, no. IEPC-2005-224, 2005.

[35] I. Vasiljevich, M. Tajmar, W. Grienauer, F. Plesescu, N. Buldrini, J. G. del Amo, B. Carnicero-Dominguez, M. Betto, Development of an Indium mN-FEEP Thruster, in: 44th JPC, no. AIAA 2008-4534, 2008.

[36] I. Vasiljevich, Design, Development and Testing of a Highly Integrated and Upscalable FEEP-Multi-emitter using Indium as Propellant, Ph.D. thesis, TU Wien (2010).

Die approbierte gedruckte Originalversion dieser Dissertation ist an der TU Wien Bibliothek verfügbar.
The approved original version of this doctoral thesis is available in print at TU Wien Bibliothek.
TU Bibliothek Your knowledge hub WIEN

[37] M. Tajmar, C. Scharlemann, A. Genovese, N. Buldrini, W. Steiger, I. Vasiljevich, Liquid-metal-ion source development for space propulsion at ARC, Ultramicroscopy 109 (5) (2009) 442–446. doi:10.1016/j.ultramic.2008.10.009.

[38] A. Reissner, N. Buldrini, B. Seifert, F. Plesescu, C. Scharlemann, J. González del Amo, mN-FEEP Thruster Module Design and Preliminary Performance Testing, in: 33rd IEPC, no. IEPC-2013-G, 2013.

[39] A. Reissner, N. Buldrini, B. Seifert, T. Hörbe, F. Plesescu, C. Scharlemann, The IFM Nano Thruster - Introducing very high δv Capabilities for Nanosats and Cubesats, in: 52nd JPC, 2016.

[40] D. Krejci, A. Reissner, B. Seifert, D. Jelem, T. Hörbe, F. Plesescu, P. Friedhoff, S. Lai, Demonstration of the IFM nano feep thruster in low earth orbit, in: 4S Symposium, Sorrento, Italy, 2018.

[41] B. Seifert, N. Buldrini, T. Hörbe, F. Plesescu, A. Reissner, D. Krejci, P. Friedhoff, S. Lai, In-Orbit Demonstration of the Indium-FEEP IFM Nano Thruster, in: 6th SPC, Seville, Spain, 2018.

[42] Micropropulsion, in: Space Microsystems and Micro/nano Satellites, Elsevier, 2018, pp. 295–339. doi:10.1016/b978-0-12-812672-1.00008-4.

[43] N. S. Mühlich, B. Seifert, F. Aumayr, IFM Nano Thruster performance studied by experiments and numerical simulations, J. Phys. D: Appl. Phys. 54 (2021) 095203. doi:10.1088/1361-6463/abc84c.

[44] D. Bock, P. Laufer, F. Paries, M. Kopnarski, M. Tajmar, Plume characterization of NanoFEEP thrusters with a plasma diagnostics facility using carbon-velvet probes, in: 35th IEPC, no. IEPC-2017-471, 2017.

[45] N. S. Mühlich, J. Gerger, B. Seifert, F. Aumayr, Performance improvements of IFM Nano Thruster with highly focused ion beam generated with a compact electrostatic lens module, under review at Acta Astronaut.

[46] ENPULSION GmbH, ENPUSLION NANO Product Datasheet, Tech. Rep. ENP2018-001 (2018).
URL https://www.enpulsion.com/

[47] D. Rafalskyi, J. M. Martínez, L. Habl, E. Z. Rossi, P. Proynov, A. Boré, T. Baret, A. Poyet, T. Lafleur, S. Dudin, A. Aanesland, In-orbit demonstration of an iodine electric propulsion system, Nature 599 (7885) (2021) 411–415. doi:10.1038/s41586-021-04015-y.

[48] ThrustMe, NPT30-I2-1U Product Datasheet, Tech. rep. (2021).
URL https://www.thrustme.fr/

Die approbierte gedruckte Originalversion dieser Dissertation ist an der TU Wien Bibliothek verfügbar.
The approved original version of this doctoral thesis is available in print at TU Wien Bibliothek.
TU Bibliothek Your knowledge hub WIEN

[49] N. Bellomo, M. Magarotto, M. Manente, F. Trezzolani, R. Mantellato, L. Cappellini, D. Paulon, A. Selmo, D. Scalzi, M. Minute, M. Duzzi, A. Barbato, A. Schiavon, S. D. Fede, N. Souhair, P. D. Carlo, F. Barato, F. Milza, E. Toson, D. Pavarin, Design and In-orbit Demonstration of REGULUS, an Iodine electric propulsion system, CEAS Space J. 14 (1) (2021) 79–90. doi:10.1007/s12567-021-00374-4.

[50] T4i Technology for Propulsion and Innovation S.r.l., REGULUS Electrical Propulsion system for Micro-satellites Product Datasheet, Tech. Rep. IT04B02040289 (2022).
URL https://www.t4innovation.com/

[51] A. Kramer, P. Bangert, K. Schilling, UWE-4: First Electric Propulsion on a 1U CubeSat—In-Orbit Experiments and Characterization, Aerospace 7 (7) (2020) 98. doi:10.3390/aerospace7070098.

[52] Morpheus Space Inc. (May 2022). [link].
URL morpheus-space.com

[53] N. S. Mühlich, J. Gerger, B. Seifert, F. Aumayr, Simultaneously measured direct and indirect thrust of a FEEP thruster using novel thrust balance and beam diagnostics, Acta Astronaut. 197 (2022) 107–114. doi:10.1016/j.actaastro.2022.05.009.

[54] S. Keerl, D. Jelem, N. S. Mühlich, W. Engel, J. Fries, E. Ceribas, R.-J. Koopmans, B. Seifert, Two-dimensional plasma plume density characterisation of the IFM Nano Thruster, in: 36th IEPC, no. IEPC-2019-566, 2019.

[55] N. S. Mühlich, S. Keerl, W. Engel, E. Ceribas, R.-J. Koopmans, Retarding Potential Analyser Development for Low Density FEEP Thruster Beam Diagnostics, in: 36th IEPC, no. IEPC-2019-445, 2019.

[56] M. Tajmar, K. Marhold, S. Kropatschek, F. Rudolf, Advanced 3D Plasma Diagnostic for the Indium FEEP Microthruster, in: 39th JPC, American Institute of Aeronautics and Astronautics, 2003. doi:10.2514/6.2003-4569.

[57] N. S. Mühlich, B. Seifert, F. Aumayr, Verification of simulation model based on beam diagnostics measurements of the IFM Nano Thruster, in: 72nd IAC, no. IAC-21-C4.6.14, 2021.

[58] N. S. Mühlich, B. Seifert, E. Ceribas, J. Gerger, F. Aumayr, High-Precision Digital Faraday Cups for FEEP Thrusters, under review at JINST (JINST-061P-0422).

[59] N. S. Mühlich, J. Gerger, B. Seifert, F. Aumayr, Performance Prediction of New FEEP Thruster Design Verified with Direct and Indirect Thrust Measurements, in: 8th SPC, no. SP2022-54, 2022.

[60] N. S. Mühlich, J. Gerger, B. Seifert, F. Aumayr, Highly focused ion beam of a FEEP thruster generated with a compact electrostatic lens system, in: 37th IEPC, 2022.

Die approbierte gedruckte Originalversion dieser Dissertation ist an der TU Wien Bibliothek verfügbar.
The approved original version of this doctoral thesis is available in print at TU Wien Bibliothek.
TU Bibliothek Your knowledge hub WIEN

[61] J. González del Amo, G. Saccoccia, ESA Electric Propulsion Activities, in: 32nd IEPC, no. IEPC-2011-329, 2011.

[62] D. Krejci, V. Hugonnaud, T. Schönherr, B. Little, A. Reissner, B. Seifert, Q. Koch, E. Bosch-Borràs, J. González del Amo, Full Performance Mapping of the IFM Nano Thruster, Including Direct Thrust Measurements, JoSS.

[63] M. Tajmar, A. Genovese, W. Steiger, Indium Field Emission Electric Propulsion Microthruster Experimental Characterization, J. Propul. Power (20 (2004) 2). doi:10.2514/1.9247.

[64] I. Vasiljevich, M. Tajmar, The beam divergence of an indium LMIS at a distance of 50μm as determined by plasma diagnostic measurements, Ultramicroscopy 111 (8) (2011) 969–972. doi:10.1016/j.ultramic.2011.01.040.

[65] B. S. Sommers, J. E. Foster, C. N. Davis, E. Viges, Preliminary Characterization of Ion Energy Spectra Acquired from High Current Hollow Cathodes, in: 33rd IEPC, no. IEPC-2013-437, 2013.

[66] D. M. Goebel, I. Katz, Fundamentals of Electric Propulsion: Ion and Hall Thrusters, Jet Propulsion Laboratory California Institute of Technology, 2008.

[67] P. D. Prewett, G. L. R. Mair, Focused Ion Beams from Liquid Metal Ion Sources, no. 18 (1992) 377, Wiley, 1992. doi:10.1002/sia.740180511.

[68] P. Joyes, J. Van De Walle, C. Colliex, About the stability and structure of metallic clusters produced by a LMIS, Ultramicroscopy (20 (1986) 65-70). doi:10.1016/0304-3991(86)90170-1.

[69] W. Driesel, C. Dietzsch, H. Niedrig, B. Praprotnik, HV TEM in situ investigations of the tip shape of a gallium liquid-metal ion/electron emitter, Ultramicroscopy (57 (1995) 45-58). doi:10.1016/0304-3991(94)00165-J.

[70] D. Jelem, Development of a performance model for a Field Emission Electric Propulsion system, Master's thesis, FHWN (2016).

[71] COMSOL Multiphsysics, Particle Tracing Module Users Guide version 5.4 (2018).

[72] W. Knauer, Energy Broadening in Field Emitted Electron and Ion Beams, Optik (59 (1981) 335-354).

[73] S. Papadopoulos, D. Barr, W. Brown, A. Wagner, The energy spread of ions from gold liquid metal ion sources as a function of source parameters, J. Phys. Colloq. (45 (1984) C9-217).

[74] L. W. Swanson, G. A. Schwind, A. E. Bell, J. E. Brady, Emission characteristics of gallium and bismuth liquid metal field ion sources, J. Vac. Sci. Technol. (16 (1979) 1864). doi:10.1116/1.570314.

Die approbierte gedruckte Originalversion dieser Dissertation ist an der TU Wien Bibliothek verfügbar.
The approved original version of this doctoral thesis is available in print at TU Wien Bibliothek.
TU Bibliothek Your knowledge hub WIEN

[75] L. Massotti, J. G. del Amo, P. Silvestrin, D. Krejci, A. Reissner, B. Seifert, The Next Generation Gravity Mission and the qualification of the indium-fed mN-FEEP thruster, CEAS Space J. 14 (1) (2021) 109–124. doi:10.1007/s12567-021-00386-0.

[76] A. Schwertheim, E. R. Azevedo, G. Liu, E. B. Borràs, L. Bianchi, A. Knoll, Inter-laboratory validation of a hanging pendulum thrust balance for electric propulsion testing, Rev. Sci. Instrum. 92 (3) (2021) 034502. doi:10.1063/5.0037100.

[77] A. Neumann, J. Simon, J. Schmidt, Thrust measurement and thrust balance development at DLR's electric propulsion test facility, EPJ Techn. Instrum. 8 (1). doi:10.1140/epjti/s40485-021-00074-7.

[78] Z. Zhang, G. Hang, J. Qi, Z. Zhang, Z. Zhang, J. Liu, W. Yang, H. Tang, Design and fabrication of a full elastic sub-micron-Newton scale thrust measurement system for plasma micro thrusters, Plasma Sci. Techn. 23 (10) (2021) 104004. doi:10.1088/2058-6272/ac1ac3.

[79] M. Kößling, M. Monette, M. Weikert, M. Tajmar, The SpaceDrive project - Thrust balance development and new measurements of the Mach-Effect and EMDrive Thrusters, Acta Astronaut. 161 (2019) 139–152. doi:10.1016/j.actaastro.2019.05.020.

[80] S. Xu, Z. Zhang, Z. Zhang, W. Yang, H. Tang, W. Y. L. Ling, Time-frequency-domain method for thrust noise characteristics of electric thrusters, Acta Astronaut. 188 (2021) 308–325. doi:10.1016/j.actaastro.2021.07.033.

[81] D. G. Courtney, S. Dandavino, H. Shea, Comparing Direct and Indirect Thrust Measurements from Passively Fed Ionic Electrospray Thrusters, J. Propul. Power 32 (2) (2016) 392–407. doi:10.2514/1.b35836.

[82] D. Krejci, F. Mier-Hicks, R. Thomas, T. Haag, P. Lozano, Emission Characteristics of Passively Fed Electrospray Microthrusters with Propellant Reservoirs, J. Spacecr Rockets 54 (2) (2017) 447–458. doi:10.2514/1.a33531.

[83] B. Seifert, A. Reissner, N. Buldrini, F. Plesescu, Development and Verification of a μN Thrust Balance for High Voltage Electric Propulsion Systems, in: 33rd IEPC, no. IEPC-2013-N, 2013.

[84] D. Krejci, B. Seifert, C. Scharlemann, Endurance testing of a pulsed plasma thruster for nanosatellites, Acta Astronaut. 91 (2013) 187–193. doi:10.1016/j.actaastro.2013.06.012.

[85] J. E. Polk, A. Pancotti, T. Haag, S. King, M. Walker, J. Blakely, J. Ziemer, Recommended Practice for Thrust Measurement in Electric Propulsion Testing, J. Propul. Power 33 (3) (2017) 539–555. doi:10.2514/1.b35564.

Die approbierte gedruckte Originalversion dieser Dissertation ist an der TU Wien Bibliothek verfügbar.
The approved original version of this doctoral thesis is available in print at TU Wien Bibliothek.
TU Bibliothek Your knowledge hub WIEN

[86] B. van Reijen, S. Weis, A. Lazurenko, J. Haderspeck, A. Genovese, P. Holtmann, K. Ruf, N. Püttmann, High Precision Thrust Vector Determination through Full Hemispherical RPA Measurements assisted by Angular Mapping of Ion Energy Charge State Distribution, in: 33rd IEPC, 2013.

[87] F. S. Gulczinski, A. D. Gallimore, Near-Field Ion Energy and Species Measurements of a 5-kW Hall Thruster, J. Propul. Power 17 (2) (2001) 418–427. doi:10.2514/2.5758.

[88] F. G. Hey, Micro Newton Thruster Development, Springer Fachmedien Wiesbaden, 2018. doi:10.1007/978-3-658-21209-4.

[89] B. Seifert, A. Reissner, N. Buldrini, T. Hörbe, F. Plesescu, A. Bulit, E. Bosch Borras, Verification of the FOTEC μN Thrust Balance at the ESA Propulsion Lab, in: 34th IEPC, no. IEPC-2015-258 / ISTS-2015-b-258, 2015.

[90] V. Hugonnaud, S. Mazouffre, D. Krejci, Faraday cup sizing for electric propulsion ion beam study: Case of a field-emission-electric propulsion thruster, Rev. Sci. Instrum. 92 (8) (2021) 084502. doi:10.1063/5.0060931.

[91] ENPULSION GmbH (Feb. 2022). [link].
URL https://www.enpulsion.com/

[92] D. Lev, R. M. Myers, K. M. Lemmer, J. Kolbeck, H. Koizumi, K. Polzin, The technological and commercial expansion of electric propulsion, Acta Astronaut. 159 (2019) 213–227. doi:10.1016/j.actaastro.2019.03.058.

[93] T. Morris, M. Forget, C. Malardier-Jugroot, M. Jugroot, Multi-Scale Investigation of a Colloid Micro-Propulsion System, Plasma Processes Polym. 8 (6) (2011) 478–489. doi:10.1002/ppap.201100003.

[94] G. Cai, H. Zheng, L. Liu, X. Ren, B. He, Three-dimensional particle simulation of ion thruster plume impingement, Acta Astronaut. 151 (2018) 645–654. doi:10.1016/j.actaastro.2018.07.007.

[95] S. Cesare, M. Aguirre, A. Allasio, B. Leone, L. Massotti, D. Muzi, P. Silvestrin, The measurement of Earth's gravity field after the GOCE mission, Acta Astronaut. 67 (7-8) (2010) 702–712. doi:10.1016/j.actaastro.2010.06.021.

[96] M. Szilagyi, Electron and Ion Optics, Springer US, 1988. doi:10.1007/978-1-4613-0923-9.

[97] M. Tajmar, Influence of Taylor cone size on droplet generation in an indium liquid metal ion source, Appl. Phys. A: Mater. Sci. Process. (81, 1447-1450 (2005)). doi:10.1007/s00339-005-3207-3.

[98] D. Jelem, private communication (2017).

Die approbierte gedruckte Originalversion dieser Dissertation ist an der TU Wien Bibliothek verfügbar.
The approved original version of this doctoral thesis is available in print at TU Wien Bibliothek.
TU Bibliothek Your knowledge hub WIEN

[99] L. Bettiol, Internal Technical Note - Requirements Compliance Matrix - Thales NGGM Phase A, techreport FTC2022-007-01-00, FOTEC Forschungs- und Technologietransfer GmbH (Mar. 2022).

Die approbierte gedruckte Originalversion dieser Dissertation ist an der TU Wien Bibliothek verfügbar.
The approved original version of this doctoral thesis is available in print at TU Wien Bibliothek.
TU Bibliothek Your knowledge hub WIEN

Die approbierte gedruckte Originalversion dieser Dissertation ist an der TU Wien Bibliothek verfügbar.
The approved original version of this doctoral thesis is available in print at TU Wien Bibliothek.

List of Abbreviations

AFC	Analogue Faraday Cup
ARC	Austrian Research Centre Seibersdorf
ASPOC	Active Spacecraft Potential Control
CAD	Computer-Aided Design
COTS	Commercial Off-The-Shelf
DFC	Digital Faraday Cup
EFD-iE	Electric Field Detector - ion Emitter
EM	Emitter
EP	Electric Propulsion
ESA	European Space Agency
FC	Faraday Cup
FEEP	Field Emission Electric Propulsion
FOTEC	FOTEC Forschungs- und Technologietransfer GmbH
F/T	Feed-through
FWHM	Full Width at Half Maximum
GOCE	Gravity Field and Steady-State Ocean Circulation Explorer
HEMPT	High Efficiency Multistage Plasma Thruster
HET	Hall Effect Thruster
IFM	Indium FEEP Multiemitter
IOD	In Orbit Demonstration
IWF	Institut für Weltraumforschung
LEO	Low Earth Orbit
LIFET	Large Indium FEEP Test Facility
LISA	Laser Interferometer Space Antenna
LMIS	Liquid Metal Ion Source
MMS	Magnetospheric Multiscale Mission
NGGM	Next Generation Gravity Mission
PCB	Printed Circuit Board
PID	Proportional-Integral-Derivative
PTR	Power-to-Thrust Ratio
RPA	Retarding Potential Analyser
SMART-2	LISA Pathfinder
VCA	Voice Coil Actuator

Die approbierte gedruckte Originalversion dieser Dissertation ist an der TU Wien Bibliothek verfügbar.
The approved original version of this doctoral thesis is available in print at TU Wien Bibliothek.

Die approbierte gedruckte Originalversion dieser Dissertation ist an der TU Wien Bibliothek verfügbar.
The approved original version of this doctoral thesis is available in print at TU Wien Bibliothek.

Nomenclature

α	Multiply charged species term
α_{div}	Half-cone divergence angle
α_{off}	Off-axis angle / thrust vector misalignment
Δx_{c}	Shift of energy distribution centre
ΔE	Full width at half maximum of Gaussian distribution
γ	Divergence efficiency
η_{ν}	Acceleration efficiency
η_{m}	Mass efficiency
ϕ	Horizontal angles (diagnostics arm position)
θ_{T}	Taylor cone half angle
θ	Vertical angle (location of Faraday cups)
ρ	Density distribution of initialised ions
B	Magnetic flux in VCA permanent magnetic field
b	VCA offset
f	VCA conversion factor
I_{em}	Emitter current
I_{ex}	Extractor current
I_{fe}	Focus electrode current
I_{sp}	Specific impulse
I_{tot}	Total beam current
l	Taylor cone jet length
k	VCA gain-factor
r_{cap}	Taylor cone jet curvature radius
r_{jet}	Taylor cone jet radius
r_{tip}	Needle tip radius
T	Thrust
V_{em}	Emitter voltage
V_{ex}	Extractor voltage
V_{fe}	Focus electrode voltage
V_{pe}	Protection electrode voltage
V_{ret}	Retarding voltage

Die approbierte gedruckte Originalversion dieser Dissertation ist an der TU Wien Bibliothek verfügbar.
The approved original version of this doctoral thesis is available in print at TU Wien Bibliothek.

Die approbierte gedruckte Originalversion dieser Dissertation ist an der TU Wien Bibliothek verfügbar.
The approved original version of this doctoral thesis is available in print at TU Wien Bibliothek.

List of Figures

2.1 IFM Nano Thruster with its main components. 20
2.2 Schematic drawing of a Taylor cone. 21
2.3 Movable beam diagnostics arm equipped with 23 Faraday cups and an RPA with resulting mesh. 23
2.4 RPA measurement for 1 of 28 needles firing. 24
2.5 Ion current density measurement for 1 of 28 needles firing. 25
2.6 Ion trajectory simulation model, including thruster geometry and detector sphere to analyse beam properties. 26
2.7 SEM picture of utilised porous tungsten needle, compared to the modelled needle with Taylor cone and jet. 27
2.8 Mesh structure of needle and Taylor cone. 28
2.9 Experimental ion energy distribution of single needle at different emitter voltages. 29
2.10 Potential distribution of the RPA retarding electrode. 31
2.11 Measured and simulated beam profile of one needle at $V_{em} = 6\,kV$. 32
2.12 Measured and simulated beam profile of one needle at $V_{em} = 2\,kV$. 32
2.13 Measured and simulated angular ion current density distribution for one needle at different emitter voltages. 33
2.14 Measured and simulated single needle divergence angle as a function of emitter voltage for different emitter currents. 34
2.15 Coulomb potential caused by the beam particles in front of the Taylor cone. 35
2.16 Ion current density distribution for 27 of 28 emitting needles. 36
2.17 Measured and simulated angular ion current density distribution for 27 of 28 needles at different emitter voltages. 36

3.1 Drawing of an IFM Nano Thruster with indicated main components. . . . 40
3.2 Schematic drawing of the used voice coil actuator. 42
3.3 Combined test setup including IFM Nano Thruster on mN-thrust balance and beam diagnostics arm. 44
3.4 Top view sketch of combined setup with IFM Nano Thruster on thrust balance and beam diagnostics. 45
3.5 IFM Nano Thruster schematic drawing. 45
3.6 Schematic drawing of the novel mN-thrust balance. 46
3.7 Schematic drawing of a digital Faraday cup. 47
3.8 VCA calibration curve with linear fit-function. 49
3.9 VCA verification during installation on mN-thrust balance. 50

Die approbierte gedruckte Originalversion dieser Dissertation ist an der TU Wien Bibliothek verfügbar.
The approved original version of this doctoral thesis is available in print at TU Wien Bibliothek.
TU Bibliothek Your knowledge hub WIEN

3.10 Direct thrust measurement at constant emitter current and stepwise variation of emitter voltage. . . . 51
3.11 Example of beam profiles at different thruster emission currents. . . . 52
3.12 Example of beam profile stability over time. . . . 52
3.13 Measured divergence angle for different thruster emission currents. . . . 53
3.14 Deviation of integrated total current from emitted current. . . . 54
3.15 Comparison of direct and indirect thrust measurements for different emitter voltages. . . . 55
3.16 Comparison of direct and indirect thrust measurements for different emitter currents. . . . 55

4.1 Evolution of FEEP thruster systems. . . . 58
4.2 IFM Nano Thruster electrode geometry and working principle. . . . 59
4.3 Test setup including IFM Nano Thruster with focus module and beam diagnostics arm. . . . 61
4.5 Experimental divergence half-angle of three different emitters; derived first linear calibration for simulation model based on EM1 and second exponential calibration based on EM2 and EM3. . . . 64
4.6 IFM Nano Thruster electrode geometry with attached focus module. . . . 65
4.7 Simulated ion trajectories with and without focus module. . . . 66
4.8 Picture of IFM Nano Thruster with and without focus module. . . . 66
4.9 Measured current at focus electrode during voltage sweep at the protection electrode for different focus electrode voltages. . . . 67
4.10 Required extractor voltage to achieve a certain emitter current for different emitter electrode voltages with and without focus module. . . . 68
4.11 Beam profile of IFM Nano Thruster with and without focus module. . . . 69
4.12 Angular ion current density distribution at horizontal cut through beam profile with and without focus module. . . . 70
4.13 Divergence half-angle as a function of the emitter current for different emitter voltages with and without focus module. . . . 71
4.14 Divergence half-angle as a function of the emitter voltage with and without focus module. . . . 72
4.15 Off-axis angle as function of the emitter current for different emitter voltages with and without focus module. . . . 73
4.16 IFM Nano Thruster laboratory model performance map without and with attached focus module. . . . 73

Die approbierte gedruckte Originalversion dieser Dissertation ist an der TU Wien Bibliothek verfügbar.
The approved original version of this doctoral thesis is available in print at TU Wien Bibliothek.
TU Bibliothek Your knowledge hub WIEN

List of Tables

1.1 Recent in orbit demonstrated electric micro propulsion thrusters. 13
1.2 Performance of IFM Nano Thruster laboratory model without and with attached focus module. 16

2.1 Experimental and numerical parameters of the simulation model. 28
2.2 Experimental Gaussian fit results for different emitter voltages. 30
2.3 Experimental Gaussian fit results for different emission currents per needle. 30

3.1 mN-thrust balance key specifications. 46
3.2 Digital Faraday cup system key specifications. 47

4.1 Experimentally determined single needle beam profiles of three different emitters. 63

Die approbierte gedruckte Originalversion dieser Dissertation ist an der TU Wien Bibliothek verfügbar.
The approved original version of this doctoral thesis is available in print at TU Wien Bibliothek.
TU Bibliothek Your knowledge hub WIEN

Die approbierte gedruckte Originalversion dieser Dissertation ist an der TU Wien Bibliothek verfügbar.
The approved original version of this doctoral thesis is available in print at TU Wien Bibliothek.

Danksagung

Zuallererst möchte ich Prof. Dr. Friedrich Aumayr herzlich für die Betreuung meiner Doktorarbeit danken. Er hat mir wichtige fachliche Tipps und Lebensweisheiten mitgegeben und mich stets in die richtige Richtung gelenkt. Prof. Dr. Hans Leiter danke ich, dass er sich als Gutachter dieser Arbeit bereiterklärt hat und dass er mir während meiner Masterarbeit bei *Airbus Safran Launchers* (heute *ArianeGroup*) den Mut gegeben hat, eine Promotion anzustreben. Auch Prof. Dr. Martin Tajmar danke ich für die Übernahme des Gutachtens und die anregenden Gespräche auf diversen Konferenzen.
Helmut Loibl und Bernhard Seifert danke ich für die Ermöglichung Promotion und Arbeit in Einklang zu bringen. Außerdem möchte ich mich bei David Krejci und Ivanhoe Vasiljevich bedanken, da sie mir durch ihre Unterstützung ermöglicht haben meine wissenschaftlichen Artikel in hoher Qualität zu publizieren.
Johanna Fries danke ich für die weitreichenden Gespräche beim Mittagessen und die erstklassige Zusammenarbeit. Auch Werner Engel danke ich ausdrücklich für seine Unterstützung, da er immer ein offenes Ohr hatte. Bei Joachim Gerger möchte ich mich für den wissenschaftlichen Austausch zum Verständnis der Schubmesswaage und für die iterative Zusammenarbeit bei der Entwicklung des Fokusmoduls bedanken. Außerdem hat Nembo Buldrini mit seiner langjährigen Erfahrung mit FEEP Triebwerken, mit wichtigen Erkenntnissen bedeutend zur Entwicklung des Fokusmoduls beigetragen. Florin Plesescu danke ich für die Beratung zur technischen Umsetzung des Fokusmoduls und die Fertigung lupenreiner Emitter. Zudem möchte ich mich bei Dusan Cabelka für seine CAD Zeichnungen und hochwertigen Renderings bedanken. Emre Ceribas und Thomas Hörbe haben mir, durch die Entwicklung einer erstklassigen Elektronik, die Aufnahme von hochauflösenden Daten ermöglicht. Laura Bettiol danke ich für die Verfügungstellung der Anforderungen, die Strahldiagnostik und das Fokusmodul erfüllen sollten. Besonders möchte ich mich bei der *Engineering Technolgies*-Gruppe der FOTEC bedanken: Michael Happl, Christian Matkovits und Martin Braunstorfer haben sowohl für die digitalen Faraday cups als auch für das Fokusmodul tadellose Teile gefertigt. Darüber hinaus bedanke ich mich bei der gesamten *Aerospace Engineering*-Gruppe der FOTEC für die hervorragende Zusammenarbeit.
Mein größter Dank geht jedoch an meinen Freund Robert Henrich, der mir auch bei den schwersten Tiefpunkten währen dieser Zeit zur Seite stand. Ohne sein Zureden und seine Unterstützung hätte ich meine Ziele nicht erreichen können. Ein besonderer Dank geht auch an meine Familie und Freunde, die mir gute Ratschläge mitgegeben und mich unterstützt haben.
Diese Arbeit wurde zu 50 % von der FOTEC Forschungs- und Technologietransfer GmbH und zu 50 % von der Österreichische Forschungsförderungsgesellschaft FFG finanziert.

Die approbierte gedruckte Originalversion dieser Dissertation ist an der TU Wien Bibliothek verfügbar.
The approved original version of this doctoral thesis is available in print at TU Wien Bibliothek.
TU Bibliothek Your knowledge hub WIEN

Die approbierte gedruckte Originalversion dieser Dissertation ist an der TU Wien Bibliothek verfügbar.
The approved original version of this doctoral thesis is available in print at TU Wien Bibliothek.

Affidavit

I declare in lieu of oath, that I wrote this thesis and performed the associated research myself, using only literature cited in this volume. If text passages from sources are used literally, they are marked as such. I confirm that this work is original and has not been submitted elsewhere for any examination, nor is it currently under consideration for a thesis elsewhere. I acknowledge that the submitted work will be checked electronically-technically using suitable and state-of-the-art means (plagiarism detection software). On the one hand, this ensures that the submitted work was prepared according to the high-quality standards within the applicable rules to ensure good scientific practice "'Code of Conduct"' at the TU Wien. On the other hand, a comparison with other student theses avoids violations of my personal copyright.

Vienna, August 2022

(Unterschrift)

Die approbierte gedruckte Originalversion dieser Dissertation ist an der TU Wien Bibliothek verfügbar.
The approved original version of this doctoral thesis is available in print at TU Wien Bibliothek.